

FORUM HOLZBAU INTERNATIONAL

25th International Wood Construction Conference (IHF)

Master Colloquium

Volume III December 5, 2019

Practical experience – Practical application

BETH BIEL
THER ROSENHEIM
UNIVERSITÄT HELSINKI
TU MUNICHEN
UNIVERSITY OF TORONTO
TU WIEN

Content MASTER COLLOQUIUM

Thursday, December 5 2019

Donaukanal 61 Wood and the Public in the City	03
<i>Sebastian Rapposch, Graz Technical University, Graz, Austria</i>	
Placemaking: A Case Study of Minimal-Impact Building in the Great Bear Rainforest	17
<i>Gordon Clayton, Rosenheim Technical University of Applied Sciences, Germany Campbell River, British Columbia, Canada</i>	
Vibrations in residential timber floors - A comparison between the current and the revised Eurocode 5	23
<i>Whokko Schirén and Trixie Swahn, Department of Building Technology, Linnaeus University, Växjö, Sweden</i>	
Experimental full-scale testing of a multistory timber frame building concerning dynamic properties	35
<i>Urs Oberbach, Institute for Timber Construction, Structures and Architecture / Bern University of Applied Sciences, Biel/Bienne, Switzerland</i>	
Design Study of Two Variants of a Pedestrian and Cyclist Bridge in Timber-Composite Design as a Construction Replacement Option for the City of Koblenz	45
<i>Paul Dreifke, University of Applied Sciences Koblenz, Koblenz, Germany</i>	
Calculation model for adhesive-bonded cross-laminated timber concrete composite elements	55
<i>Georg Erlinger, University of Applied Sciences Upper Austria, Wels, Austria Christoph Hackspiel, Camillo Sitte Bautechnikum Wien, Wien, Austria FH-Prof. DI Dr. Karin Nachbagauer, University of Applied Sciences Upper Austria, Wels, Austria</i>	
Investigation of lateral torsional buckling of timber beams subjected to combined bending and axial compression	69
<i>Nico Köppel, Janusch Töppler and Prof. Dr.-Ing. Ulrike Kuhlmann, Institute of Structural Design, University of Stuttgart, Stuttgart, Germany</i>	
Mechanical behaviour of beech glued laminated timber columns subjected to compression loading	85
<i>Monika Zeilhofer, Technical University Munich, Chair of Wood Science, Professorship of Wood Technology, Munich, Germany</i>	

Publisher:	FORUM HOLZBAU Bahnhofplatz 1, 2502 Biel/Bienne, Switzerland T +41 32 327 20 00
Machining and typesetting:	FORUM HOLZBAU, Katja Rossel, Simone Burri und Katharina Uebersax
Printing:	EBERL PRINT Kirchplatz 6, 87509 Immenstad, Germany T +49 8323 802 200
Edition:	200 Ex.

© 2019 by FORUM HOLZBAU, Biel/Bienne, Schweiz
ISBN 978-3-906226-28-6

www.forum-holzbau.com | www.forum-holzkarriere.com

Donaukanal 61

Wood and the Public in the City

Sebastian Rapposch
Graz Technical University
Graz, Austria



Donaukanal 61

Wood and the Public in the City

1. Introduction

The thesis Donaukanal 61 deals with the development and design of a hybrid wooden high-rise building at the Donaukanal in Vienna, putting special emphasis on wood and the public in connection with the architectural as well as social density of the surrounding intra-urban location.

This practical part of the thesis is based on theoretical research dealing with the term of sustainability, the history and status quo of multi-story timber construction systems as well as fire safety and the differences in national legislature concerning high-rise timber buildings.

In relation to the Donaukanal's high social and cultural diversity and density, the program of the proposed project is composed of different public and semi-public functions connected with (social) housing. This social and public functionality represents a decisive aspect of the project as a counterpart to the current dominance of non-public office, administration and hotel high-rises.

Despite the technological expertise and the unique potential of sustainability, multi-story timber construction systems still face a high amount of prejudices. To counter this and establish wood as a neutral and unprejudiced building material, it is necessary to bring timber construction especially to the city and the intra-urban space, which represents the dense center of our society. Moreover, it was not the aim to create architecture which defines itself by being made from wood but to produce *good* architecture which uses wood as a *neutral* construction material. With partly uncommon approaches and solutions the thesis Donaukanal 61 tries to contribute to these important developments.

2. Context

The project is located on the left bank of the Donaukanal at the crossing of the Obere Donaustraße 61 / Herminengasse. The surrounding area is formed from Gründerzeit buildings with a simple façade design in combination with newer buildings, mainly from the 1990s. The prominent character of the building site results from its location at the important urban edge of the Donaukanal, whose promenade is extremely busy with bars, cafés and restaurants in this area. In front of the building site there is also the Otto Wagner Schützenhaus, which is an important example of the Vienna Secession Style. In addition, the project is located on the same axis as the 74-meter-tall Ringturm, completed in 1955.

3. Design Goals

The Donaukanal represents not only a prominent historical and cultural but also socially dynamic and diverse intraurban axis of Vienna. As a result of its topographic character it also serves as an important architectural edge, corresponding well with high-rise buildings. However, the functionalities of the current high-rise buildings constitute a contrast to the Donaukanal's social and architectural diversity, as they are limited to non-public office, administration and hotel uses.

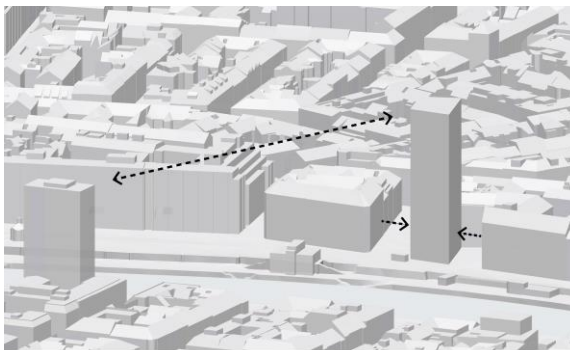
In contrast to that and in relation to the Donaukanal's high socio-cultural diversity and density, the program of the proposed project is composed of different public and semi-public functions connected with (social) housing. This social and public functionality represents a decisive aspect of the project as a counterpart to this dominance of non-public uses of the surrounding high-rise buildings.

Of course, it is also necessary to critically consider the high building density in the area. Therefore, the project's public character is strongly connected or rather defined by this urban density. As far as building laws are concerned, the thesis is based on the assumption, that the neighboring parties would waive part of their rights in favor of the added public value.

It is evident that the project's financial funding represents a strong contrast to the current real estate and investment market. It is rather the thesis' aim to provide an unconventional impulse as to where public authorities could guide project developments.

4. Design

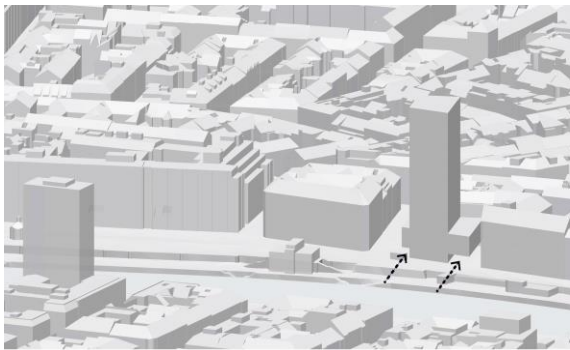
The project's design is, in a first step, based on distancing itself from the neighboring building façades and the building height's development according to the height of the Ringturm, in whose prominent axes the project is situated. At the same time this creates an opening of the urban perimeter block's introversion, which dominates the surrounding urban structure. Following the prominent hovering cantilever defines the inner and outer public space, but a small gap underlines the opening of the closed building façade along the Donaukanal. Moreover, a patio-like opening in the cantilever enables natural lighting of the interior and exterior. The project's two basic elements, the cantilever and the high-rise, are not separated from each other, but connected by the building's interior.



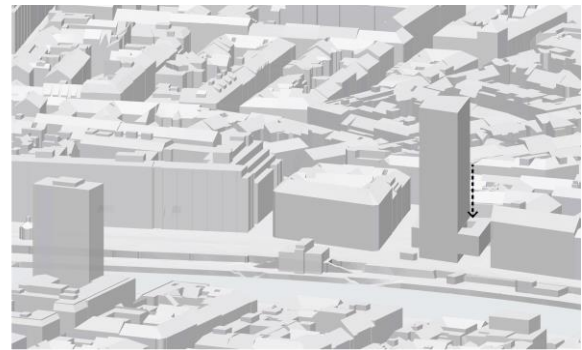
Axis Ringturm | Distancing



Contra urban perimeter Block | Opening the Inversion



Hovering cantilever | Definition of the public space



Atrium | Natural lighting for interior and exterior space

Figure 1: Design Concept

5. Organisation

The project's functions are organized in three zones (public, semipublic and private), which are connected to each other and correspond to the project's design. The different functional spaces are independent, but at the same time not strictly separated from each other, mixed uses are possible and intended.

- level 0 – level 2: public (forum, café/bar, art gallery, library)
- level 3 – level 4: semipublic (kindergarten)
- level 5 – level 20: private (housing)

In order to ensure independent use, the access and infrastructure are separated according to the zones. The northern infrastructure core with his two entries belongs to the semi-public and private area of the apartments, kindergarten and shared workspace, whereas the front core with its entries is part of the public area.

The two-storied forum, located in the center of the building, represents the heart of the public area. It has a strong connection to the public space outside, which opens to the

Donaukanal, but is at the same time sheltered by the hovering cantilever. Being a true public space, it is open to the public at any time and totally free in use. It can be used for markets, concerts, discussions as well as any kind of performances or festivities, but at the same time it also serves as a simple public place to spend time and meet.

The forum is multi-functional and has a gallery, which can be used as a separated area. The ground floor also hosts a café / bar, kitchen facilities for catering, toilets and a cloak room are located on level -1.

The public art gallery on level 1 is situated in the hovering cantilever, which has two-sided natural lighting and works as a multi-functional gallery space. Moreover, level 1 contains the semipublic area of the shared workspace. It offers work and rental space especially for the building's residents and extends to level 2.

There, the open library forms another part of the public space. Its book stockroom is located in the center of the building on top of the forum, whereas the work and reading spaces are situated in the cantilever.

On level 3 and 4 the semipublic kindergarten is located. Its two floors are both organized in two hips with a wide and two-sided open cloak area and facility rooms on the northern side. The group rooms have a functional storage/toilet module and are flexible in their size. Moreover, on level 3 there is a kitchen and dining space, as well as the wide outside playground on top of the cantilever.

Central aspects of the housing layout are flexibility and neutrality of use. The flats are organized in two hips with five flats of different sizes on each floor. The layout with an inner bathroom/storage room axes and a multi-functional internal corridor allows a flexible expansion of the rooms between the dwelling units. This tackles a highly topical issue due to the increasing flexibility of lifestyles and the shortage of inner-city housing. The second possible access on the façade side also allows the opening of the strict room layout and underlines the neutrality of use of the individual rooms themselves. The continuous surrounding balcony also contributes to this and at the same time provides shading during summer months. Exterior sliding elements made of expanded metal ensure additional shading and provide privacy.

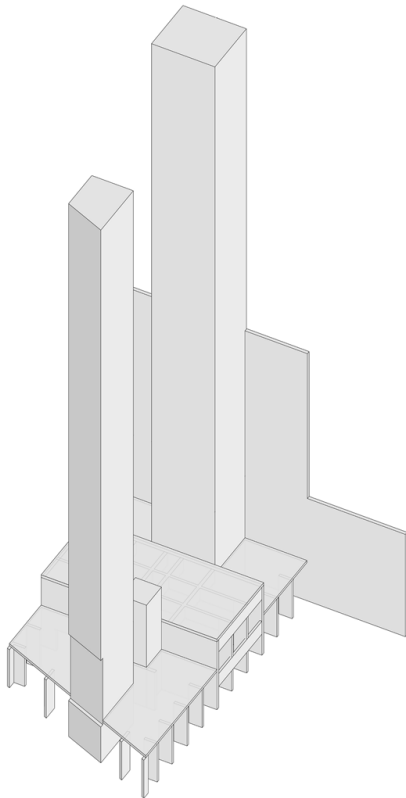
6. Construction

The project's construction system represents an integral part of the design itself. The system consists of a hybrid structure of two concrete cores and a concrete ground floor in connection with CLT ceilings and glulam pillars. The prominent cantilever is realized using LVL lattice trusses.

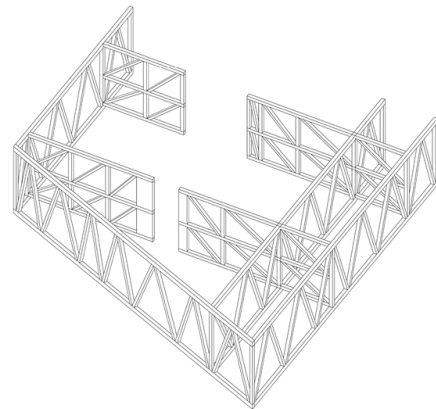
The vertical loads are transferred by the glulam pillars, whose positions are defined by one strict construction grid for the whole building. The CLT ceilings are supported by those glulam pillars punctually and without beams as single-span and two-span with cantilever or three-span two-way slabs. Their shifted layout and their shear connection make them a statically useable slab, which transfers the horizontal loads into the concrete cores. The punctual connection between slab and pillar is made with a special steel detail, which allows not only for a lateral pressure-free load transfer, but also for an easy and fast assembly. Of course, it is necessary to mention the Brock Commons – Tallwood House from Acton Ostry Architects and Hermann Kaufmann in Vancouver, Canada as reference for this system.

The prominent cantilever is realized using a system of two-story timber lattice trusses. Their position refers to the general pillar grid which allows a straight load transfer through the whole building. The connection detail is based on the standard detail, allowing for a lateral pressure-free load transfer through the upper and lower chords and fire protection for the detail's steel parts. Because of its higher strength values the lattice trusses and the pillars on level 1 and 2 are realized in laminated veneer lumber (LVL).

Besides the two infrastructure cores and the ground floor, also the forum is realized in concrete. Its ceiling consists of a concrete girder grid, which optimizes the use of material and transfers the load of the three pillar axes above.



Concrete | Level 0 | Cores | Firewall



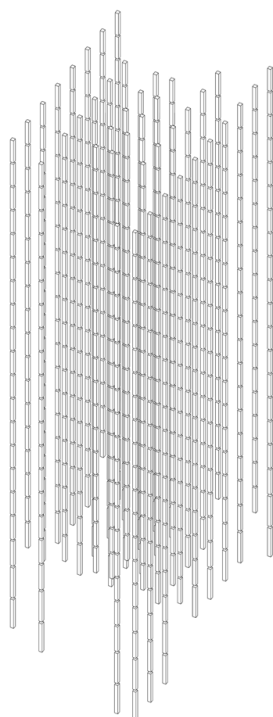
Cantilever | LVL lattice truss

7. Materials

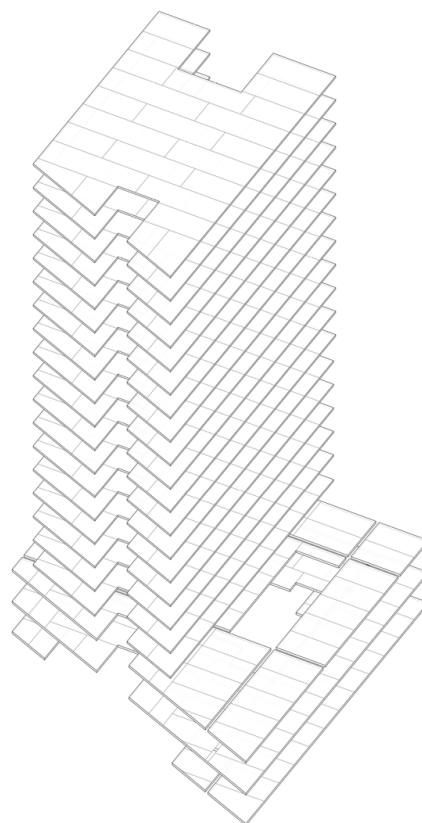
The used materials and appearance of the façade follows a clear division into three sections, the contrasts of which could also be described with the characteristic of a *Cadavre Exquis*. While the ground floor, contrary to its massiveness, appears as a light glass cube, the façade image of the cantilever is clearly dominated by the timber framework. The two-layered façade of the residential and kindergarten area consists of the sliding shading elements out of expanded metal on the outer level and the large windows in alternation with pre-grayed plywood façade panels. This results in a dynamic and transparent appearance that reflects the urban density of the environment.

The plywood façade panels by their planar structure also clearly distance themselves from the traditional wood façade image associated with rural areas.

Within the flats and the kindergarten, the cross laminated timber ceilings and glulam beams are left visible, only the supports in the corridor areas and wet rooms are covered with drywalls for reasons of building physics and to reduce the fire load in these areas.



Glulam | Pillars



CLT | Ceilings

Figure 2: Construction Concept

8. Fire Safety

The project's fire safety concept is directly connected to the design itself and based on following aspects:

- small fire sections and short escape routes for a fast evacuation in case of fire
- staircase cores in concrete, evacuation routes free of flammable materials
- load-bearing and non-covered timber elements (CLT ceilings, glulam pillars, LVL lattice trusses) in REI 90 (bigger profiles)
- pillars in public corridors are covered with drywalls for reduced fire load
- fire sprinkler systems in the whole building in order to compensate the flammable load-bearing building elements and to stop the spread of fire as fast as possible
- continuous floor screed as a fire- and smoke-proof horizontal barrier
- accurate connection details with covering of all steel parts
- balcony ceilings with fire-proof bottom side (fibre reinforced concrete panels) as barrier against the spread of fire over the façade
- good and easy access for fire brigades to the critical public areas of the cantilever



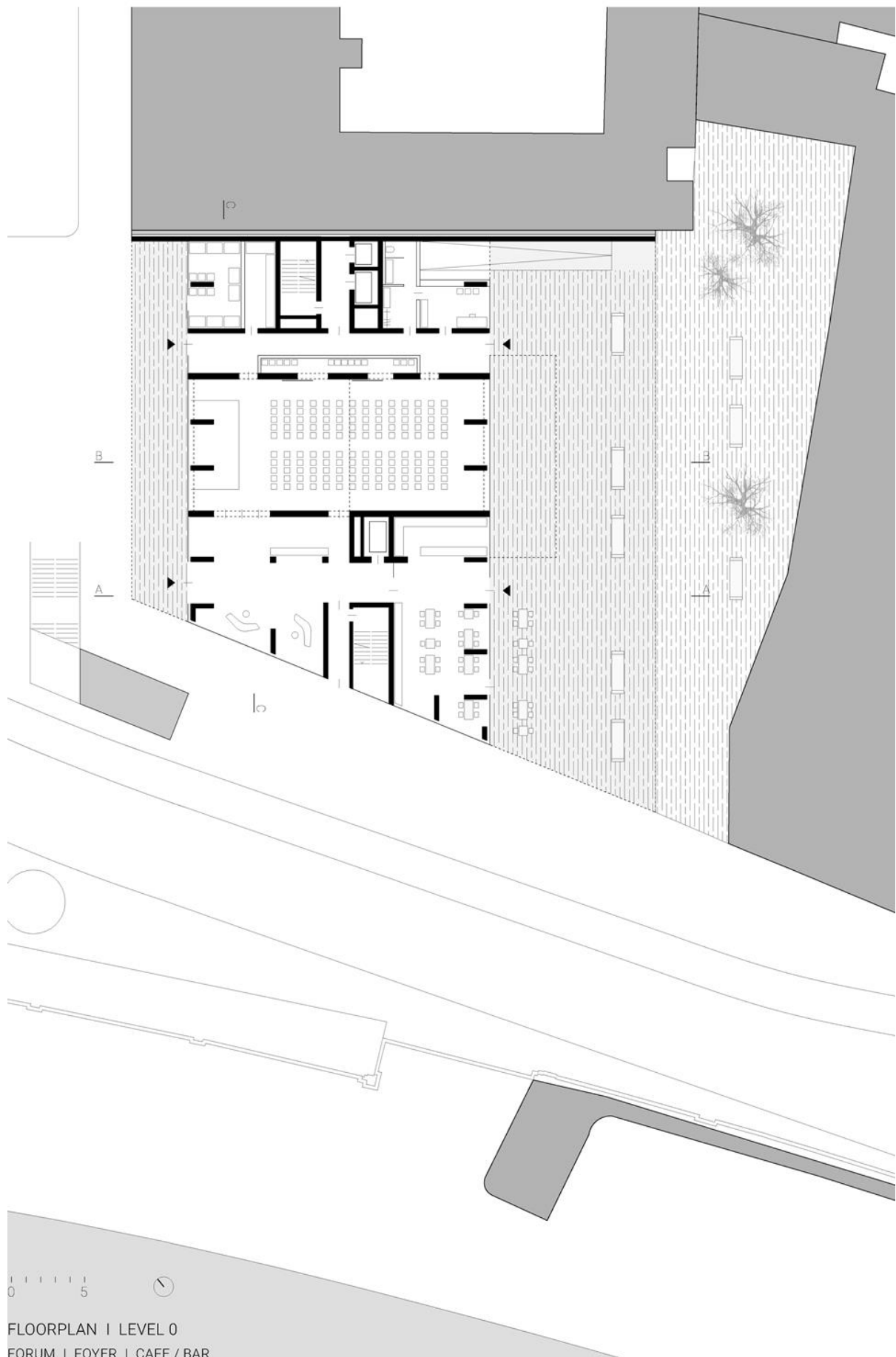
ELEVATION SOUTHWEST

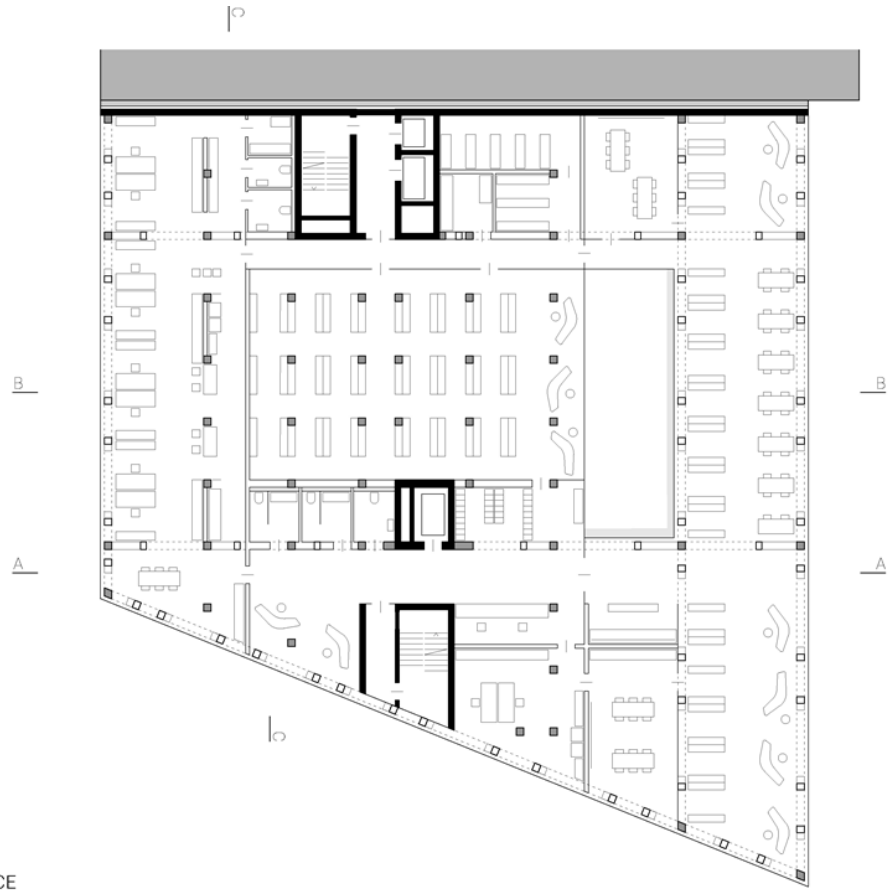
0 50



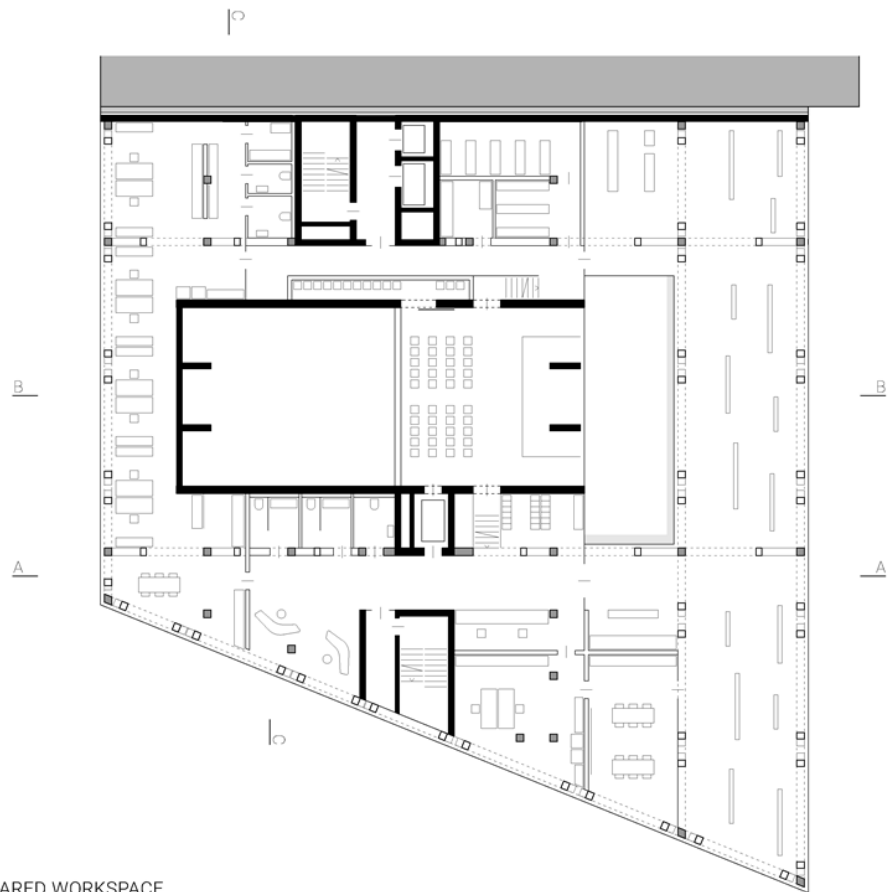
SITEPLAN

0 50





FLOORPLAN | LEVEL 2
LIBRARY | SHARED WORKSPACE

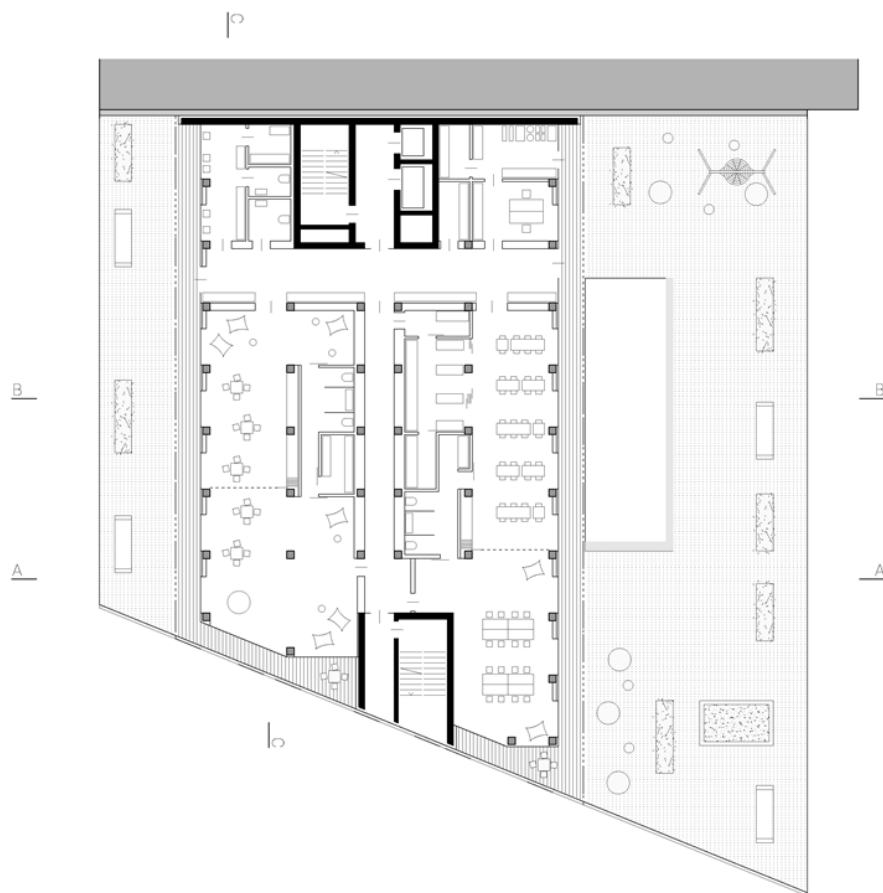


FLOORPLAN | LEVEL 1
FORUM | ART GALLERY | SHARED WORKSPACE





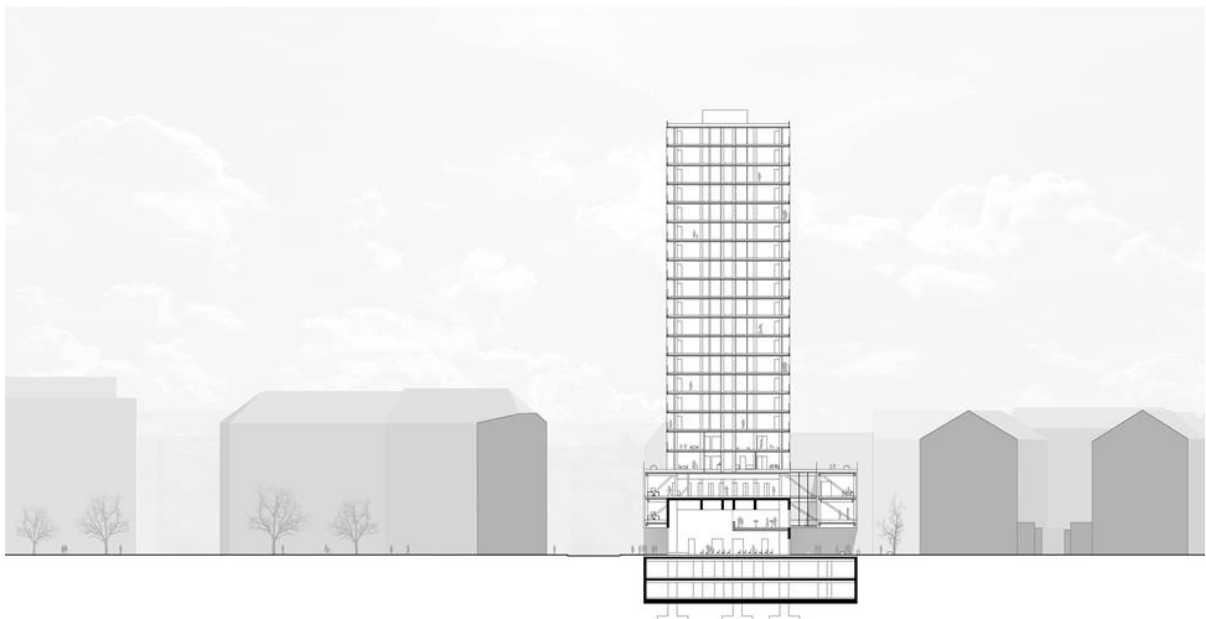
FLOORPLAN | LEVEL 8-20
HOUSING



FLOORPLAN | LEVEL 3
KINDERGARTEN

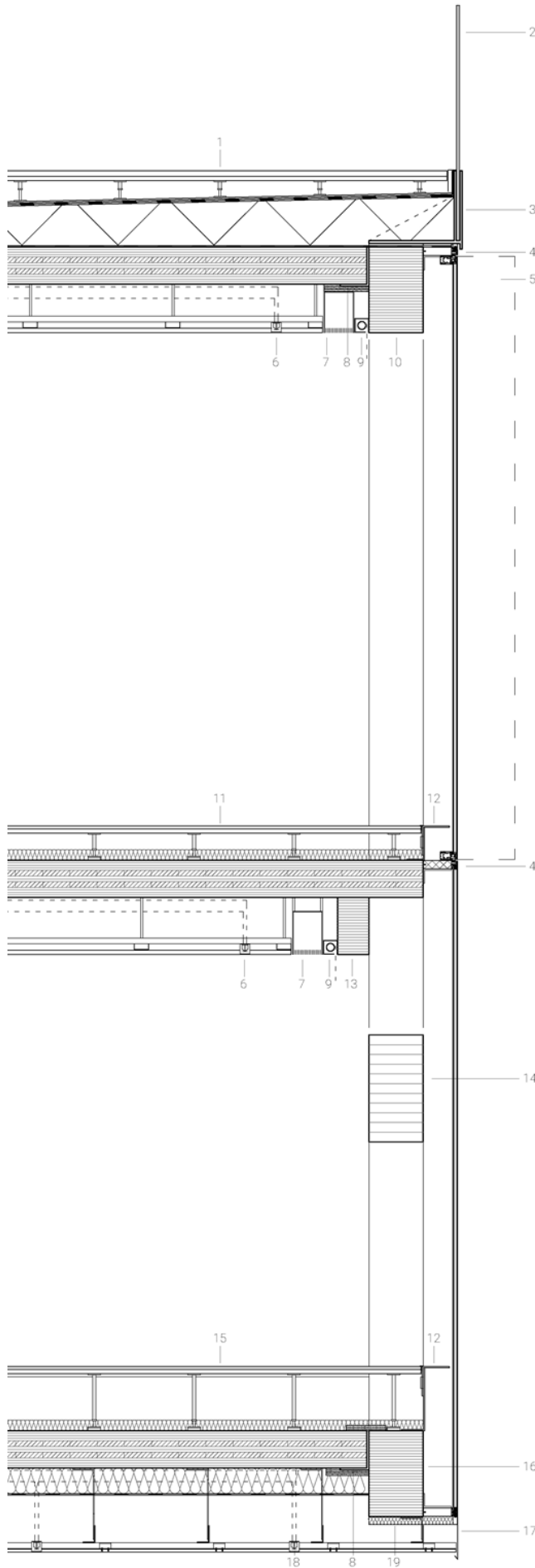


SECTION CC



SECTION BB

0 | | | | 50



FACADE SECTION

- 1 Tartanplatten 40 mm
Trägerplatten 30 mm
Stellfüße 80-370 mm
Bautenschutzmatte 10 mm
Bitum. Abdichtung, 2-lagig 15 mm
Gefälledämmung, XPS 60-350 mm
Abdichtung
Brettsper Holzdecke, 7ss DL 260 mm
Abgehängte Decke 310 mm
Gipsfaser Akustikplatten 30 mm
- 2 Absturzsicherung VSG
- 3 Stahlkonsole, verzinkt RAL 9006
Einspannung Absturzsicherung
Montage auf Elastomer-Dämmstreifen
- 4 Pfosten-Riegel-Fassade
(Structural-Glazing)
Brandschutz-Isolierverglasung
Riegel brandschutzgedämmt
- 5 Parallel-Ausstellfenster,
gegen Brandüberschlag
geschossweise versetzt
- 6 Sprinklervollschutz, Vernebelung
- 7 Mechan. Be-/ Entlüftung
- 8 Stahlwinkel, Auflager Decken
Kapselung 45 mm
3 x Gipsfaserfeuerschutzplatten
- 9 Blendschutzrollo
- 10 Obergurt Furnierschichtholz Buche
380 x 600 mm
- 11 Parkettboden 25 mm
Trägerplatte 30 mm
Stellfüße 190 mm
(auf Trittschalldämmstreifen)
dazw. Mineralwolle 50 mm
Brettsper Holzdecke, 7ss DL 260 mm
Abgehängte Decke 370 mm
Gipsfaser Akustikplatten 30 mm
- 12 Stahl-Abschlusswinkel, öffnenbar
- 13 Nebenträger Furnierschichtholz Buche
220 x 400 mm
- 14 Strebe Furnierschichtholz Buche
320 x 380 mm
- 15 Parkettboden 25 mm
Trägerplatte 30 mm
Stellfüße 400 mm
(auf Trittschalldämmstreifen)
dazw. Mineralwolle 50 mm
Brettsper Holzdecke, 7ss DL 260 mm
Stahl-UK, verzinkt 570 mm
dazw. Mineralwolle 160 mm
Winddichtung
Glasfaserbetonplatten 15 mm
- 16 Untergurt Furnierschichtholz Buche
380 x 600 mm
- 17 Stahlblech verzinkt, RAL 9006
mit Tropfnase
- 18 Sprinklervollschutz, Vernebelung
glykolbefüllt
- 19 Dämmstreifen 60 mm





Placemaking: A Case Study of Minimal-Impact Building in the Great Bear Rainforest

Gordon Clayton
Rosenheim Technical University of Applied Sciences
Campbell River, British Columbia, Canada



Placemaking:

A Case Study of Minimal-Impact Building in the Great Bear Rainforest

The task: design a high-performance building to fit naturally into the temperate coastal rainforest. It should meet and adapt to the needs of a diverse community. Make it recyclable. Do not disturb the ecosystem where possible.

While these may seem like separate tasks, they are intrinsically linked. Assessing the current and future needs of a community belongs to the field of sociology. The preservation and rehabilitation of forest ecosystems the work of an ecologist. Making material choices based on their sustainability is not the modus operandi of builders in our region.

Here we observe the benefit of using a case study as a testing grounds for these complex interactions. It allows for a personal and in-situ assessment of design, materiality and feasibility. The project's initiators went out of their way to respect the longstanding local tradition of fostering community engagement in determining the best use of the case study property. Their parameters for the housing initiative were that it be highly energy-efficient and maximize the use of local and regional resources where feasible. This case study represents one approach to the task set out above. It describes the methods and reasoning used to thoughtfully shape a pristine piece of land to fit the needs of the community- indeed to make a place.

1. Case Study Challenge

British Columbia's rural communities are in a state of transition. As natural resource sectors such as forestry, mining, paper production and the fishing industry restructure, local benefits from those sources are dwindling, leading to reduced employment opportunities and shrinking populations. As in many other rural and remote coastal communities across B.C., recent increases in real-estate values, paired with a demand for seasonal vacation properties has impacted the cost of living on Quadra Island.

With an aging population, a need for affordable housing and a lack of sustainable year-round industry, Quadra Island finds itself at an important juncture of its development and future sustainability; long-time residents observe a need for newcomers to be part of their community, made possible through affordable housing options. They realize a need for a different type of housing so that in their less independent years, they can remain a part of their community and enjoy a less auto-centric lifestyle. One of the central challenges of the case study is how to introduce higher-density yet palatable housing solutions to this community. While design may not singularly solve all the above problems, when seen in conjunction with regulatory changes and economic drivers such as new industry, it can provide a framework to help alleviate the key concerns of the community.

A look through *Infrastructure Canada's* "Investing in Canada" Plan Project Map illustrates the overwhelming demand for adequate safe housing and a call for more sustainable communities across B.C.'s rural regions. This is an especially relevant and topical issue to areas like remote coastal settlements, island communities, isolated interior towns and many of B.C.'s indigenous communities where there is a demonstrated need for healthier, safer, and more energy-efficient buildings.

While prefabricated building assemblies present an opportunity to tackle some of these challenges head-on, they suffer regionally from a poor image; many prefabricated homes and buildings from previous eras provided affordable housing but did not address thermal performance, building longevity, sustainability or architectural aesthetic.

2. Case Study Goals

This case study and its suggestions manoeuvre outside the typical context of urban housing proposals. The project is framed within the rural context, a locale where energy efficiency and sustainable practice typically do not have a strong presence. As an alternative to the large-area land ownership practices of many rural regions, this thesis proposes a more sustainable and compact mixed-use building typology that meets the needs of, and fosters a diversifying community while elevating the standards of rural housing. Inherent to the design is the agility and scalability of the construction to be applied in different contexts, while adapting to local materials and practices.

The principal goals of the case study are therefore:

1. **Design an energy-efficient multi-unit residential building using as many regional resources as is feasible,**
2. **Design the building to be constructed and assembled easily by local tradespeople with a high degree of prefabrication,**
3. **Design the buildings to be sustainable, fully recyclable, and to have a minimal impact on the building site.**

In addition to those mentioned above, certain secondary goals are inherent to the case study:

- the creation of added-value to the community through engagement, employment, and accessibility,
- the production of higher quality construction at par with standard construction costs, and
- creating and fostering a place-led approach to urban (rural) planning

Finally, an emphasis on a new form of rural housing cooperative seeks to address issues of social isolation through a diverse range of demographics, where the elderly can live beside young families, and chance encounters are a regular part of daily activities; the *Mehrgenerationshaus* is a well-established social structure in the DACH region.

3. Case Study Structure

In order to develop an informed design for the project in question, a review of the regional guidelines on development was completed. Existing guidelines, by-laws, building codes and Quadra Island's official community plan were referenced to check for compliance and to ensure that the proposed building form and density were plausible.

Quadra Island has a tradition of community involvement in decision-making. Through multiple workshops and community engagement events, a catalogue of rural planning recommendations was developed together with the project's initiators, an advisory group, and the community as a whole. The purpose of forming an advisory group was to aid in decision-making, for the group members to provide feedback in their respective fields of expertise, and to function as a sort of checks and balances. The group included governmental agencies as well as experts from the architectural, construction and engineering industries. A review of the literature and media published from community engagement events was completed, and the information used to determine a key building typology for the property; a multi-unit residential building assembled from pre-fabricated components, scalable in all dimensions.

To address the commercial viability and health of the standing timber on the 11 ha. case study property, a LiDAR-based analysis of the forest was completed to provide the information required for a long-term synergy of a privately-owned forest and the proposed mixed-use housing initiative. By measuring the crown height, density and species of the standing timber, a site plan could be made that ensures the property will maintain its rainforest optic for generations to come. Using these aerial LiDAR scans, a best-possible

location for the future building ensemble was determined. Urban (rural) planning considerations such as access to, and movement on and about the property, building services, and privacy spheres were developed. A discussion of this approach is described in a section called "**Synergy of Forestry and Housing**".

The following section, "**Leitmotif: Wood**" presents arguments as to how wood as a building material, when used sensibly, can assist in reaching the principal and secondary goals of the case study. Details of building material selection and how to maximize added-value for the region bring the section full-circle.

"**Strategies and Components**" introduces adaptations made to regional wood construction methods to increase the performance of the building envelope and thereby the comfort of building occupants, all the while increasing efficiency and work safety in its construction. Strategies for building envelope construction and assembly, water conservation, integration of building services, and fire protection are presented. A catalogue of building assemblies, components and their contributions to building physics can be found in the case study's **Building Element Catalogue**. Collectively, these sections provide arguments for using regional and sustainable materials, strategies for using said materials to fulfill the case study goals, and present the proposed building assemblies and their performance parameters.

The rural planning proposal is presented visually in "**The Design**". There, the results of the place-led approach described above are distilled and examined through larger-scale site plans. Study Build's vision for a "**modern forest Bauernhof**" was created using several buildings of differing heights but with similar form and identical construction details. Physical models were built to determine optimal spatial relationships between the structures. A set of floorplans was created to demonstrate the highly configurable nature of the building, depending on the target demographic; Floorplans are included for aging-in-place, for those with limited mobility, for young families, or seasonal housing for employees of local eco-tourism operations.

Having defined a key building typology, a building design and an optimal location, detail work on the building assemblies was undertaken. To test the feasibility of the details a 1:1 scale model of an exterior building corner was built to test the construction concept and to better understand and further simplify the construction details. The section "**Building Plans**" provides the necessary information required by carpenters and other tradespeople to construct the building as designed. Emphasis is put on the integrity of the building envelope and the diversity of floor plans possible within a strict building raster.

"**Energy Results and Discussion**" presents the calculated energy consumption of the proposed building and determines whether the building can feasibly reach the ambitious Passivhaus standard. A discussion as to balancing building efficiency with building longevity takes place. Using the Passivhaus Planning calculations, the thermal performance and comfort criteria of the building were calculated and found to be within the specifications set out by the Passivhaus Institute.

4. Conclusion + Future Work

The first goal of designing an energy-efficient housing initiative using as many regional resources as is feasible was realized. In terms of energy efficiency, the building reaches a Passivhaus standard, despite extensive shade conditions. When realized, this building will be the first Passivhaus in the region. In terms of the use of regional resources, the construction of the building was designed to utilize as much dimensional lumber as possible, in industry-standard dimensions, so that local sawyers can supply building materials when possible. By using standard-sized lumber, the use of recycled wood is also facilitated in many of the assemblies.

The second thesis goal of designing a construction to be built and assembled easily by local tradespeople, with a high degree of prefabrication, has been reached. By adapting regional carpentry practices and using materials familiar to local tradespeople, there should be no problem with acceptance and workability of the design. The prefabrication of wall, roof and floor assemblies, complete with conduit, building services and connecting elements has been achieved where feasible. A limiting factor here is the transport of assemblies to the building site and lifting capabilities. Using the building platform as a temporary work platform is a prefabrication strategy discussed in the relevant section.

The final thesis goal of designing the buildings to be sustainable, fully recyclable and to have a minimal impact on the building site were overarching criteria that affected every design decision throughout the evolution of the case study. The project's social sustainability is achieved through the intense community engagement, by targeting the social demographics most in need of housing, and informing the design according to their individual needs. The project's environmental sustainability, a strict criterion from the start, is guaranteed in terms of the buildings construction. The urban design, with its minimal visual impact and vehicle-free design exemplifies the light-touch principle, and protection of existing ecosystems is paramount in the project siting and development.

The recyclability of the construction informs the material decisions and assembly order. The use of synthetic or bonded materials is kept to an absolute minimum, to ensure the building can be separated easily into its constituent parts at the end of its lifecycle and be re-used or recycled.

The impact on the building site is reduced through the use of ground screw foundations-also part of the recycling concept. The ground screws eliminate the use of concrete and the amount of excavating work necessary. By choosing to work with sections of the land requiring site repair, the land as a whole becomes more attractive and valued by the community.

Throughout the case study and public engagement process, areas for further research related to the case study have presented themselves:

- Design of a large-scale lumber kiln with heat recovery for a rural island community,
- Design of a permanent manufacturing facility for the building components presented in the case study,
- A cost analysis of the presented construction method compared to conventional construction methods,
- A Life Cycle Analysis of the proposed construction,
- An off-grid variant of the construction for use in the eco-tourism industry along B.C.'s coast,
- An adaptation of the proposed construction to be transported by helicopter (weight restrictions, pick-point engineering and logistics),
- A float-home variant of the proposed construction
- Sequential expansion of the proposed buildings in-situ using additional assemblies

With the introduction of new, more stringent energetic standards to the Canadian building code, there is a growing discourse around the sustainability and energetic standards of our building stock but also a significant knowledge gap in the corresponding building physics required to build successfully. To address this knowledge gap, a concerted effort must be made at the classroom level at the vocational and polytechnic institutions to bring both experienced and apprentice carpenters up to speed, because it is ultimately these tradespeople who will be construction and assembling these structures.

Vibrations in residential timber floors – A comparison between the current and the revised Eurocode 5

Whokko Schirén
Department of Building Technology,
Linnaeus University
Växjö, Sweden



Trixie Swahn
Department of Building Technology,
Linnaeus University
Växjö, Sweden



Vibrations in residential timber floors – A comparison between the current and the revised Eurocode 5

1. Introduction

Floor structures could, in very general terms, be divided into heavy and light-weight floor structures. Traditional building methods with concrete as the main building material result in heavy floor structures while light-weight floor structures could be made out of steel, light-weight concrete or timber [1]. The development of lighter floor structures is driven by the aim to be more efficient and use less materials, as well as to use materials which are considered environmentally friendly, such as timber. Due to an increased awareness of sustainability aspects, the interest for building even higher wooden buildings is increasing, and today, about one tenth of new multi-family houses built in Sweden are built out of timber [2].

All light-weight floor structures are prone to unwanted vibrations [3] and humans are vibration sensitive beings, programmed to take notice of noise and vibrations as possible sources of danger [1, 4, 5]. People in motion often tolerate greater vibrations than people who are still [6]. Vibrations where the source is obvious, for example when the vibration originates from the own apartment, result in a lower disturbance than vibrations from less obvious sources from neighbouring apartments [1]. A vibration which decrease fast is perceived as less disturbing than a prolonged vibration [1, 7]. The human body is especially susceptible to vibrations between 4–8 Hz as this is frequencies at which the body's organs could start to resonate [8]. Thus, special focus in the design for vibrations in residential floors is laid on this range of frequencies.

The Eurocode series provides support when designing buildings and encompasses a set of design methods provided by the European Committee for Standardisation (CEN). The Eurocode is divided into general chapters and chapters for specific building materials. Eurocode 5, EC5, specifically contains design methods for timber constructions. It includes a chapter on vibrations in floor structures, [9], which is currently under revision. A draft for a revised design method for vibrations was presented in April 2019 and is investigated in this paper.

Today the building industry uses the current Eurocode 5, cEC5, when designing buildings. Changing from the current to a revised standard might change the classification of floor systems and thus, could lead to increased costs for the building industry. It is of utmost importance to the building industry to prepare for corresponding changes of standardisation.

Herein, the performance of floor structures, commonly used in Sweden today, are investigated based on the criteria provided in the draft for a revised design method for vibrations in Eurocode 5, and compared to the current version of the code. Both more traditional floor structures consisting of joists covered by sheathing, and less traditional floor structures with CLT as a main building material, are included in the study.

The study focuses exclusively on non-acoustic structural vibrations in timber floors. The design calculations were performed in the Serviceability Limit State (SLS) in accordance with the cEC5 and rEC5.

Three limited parametric studies with length, mass, modal mass, centre to centre distances and support conditions as variables, have been conducted in order to assess the sensitivity of the design method and to highlight corresponding influence parameters for the classification of floor systems.

2. Material and methods

2.1. Investigated floor systems

The design of the six floor structures investigated in this study are presented in Table 1. Due to the fastening methods used between the different layers in the floor structures, composite action is assumed in all floors.

Floor A and B are lightweight joist floors with joists covered by particle board sheathing. In Floor A the joists are made of structural timber and in B of Laminated Veneer Lumber (LVL). These floor structures are normally used in single-family houses. The floors span over two bays where the first span is 4.3 m and the second 3.9 m, which makes the total floor length 8.2 m. The floor width is 10.8 m. The non-rigid beam supporting the floors between the bays is an IPE 200 steel beam with a maximum span of 3.5 m.

Floor C is a glulam and LVL floor structure used in a building system with glulam columns and beams. The building system is often used in taller and larger buildings with more than two storeys and it is able to handle up to 8 m of free span. The floor is most common in multi-family houses or office buildings. The floor is simply supported and single spanning with a floor element width of 1.9 m and a floor length of 5.0 m.

Floor D is a composite floor with lightweight I-joists consisting of flanges of structural timber, C30, and a web of OSB/3. The gypsum boards in the ceiling are connected to the battens via steel profiles, Gyproc AP, developed to optimise the sound insulation. The floor is simply supported and single spanning with a floor length of 5.2 m and a width of 12 m.

Floor E consist of a five-layer CLT slab with a joist system on top. The joist system is made out of lightweight steel joists with damping elements for an efficient sound insulation. The joist system come in different heights and the sound insulation increases with the height of the joists, in this case the height is 190 mm. The floor is a double-spanning floor, the longer span is 5.5 m and the shorter span 3.9 m, which gives a total length of 9.4 m. The floor width is 11 m.

Floor F is a CLT floor with a layer of gypsum screed on top of the CLT. The floor consist of a five-layer CLT slab with a thickness of 150 mm, a layer of macadam, a layer gypsum screed and a parquet flooring. The macadam and the gypsum screed make the floor heavier. The floor system spans over two bays, the first span is 3.9 m and the second 5.5 m, which makes the total floor length 9.4 m. The floor width is 11 m.

2.2. Design according to the current Eurocode 5 method

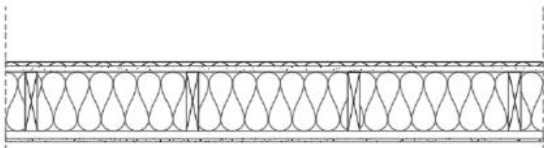
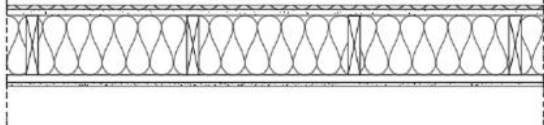
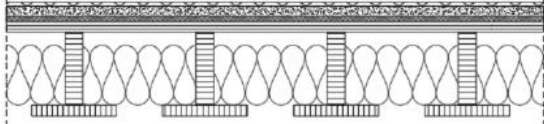
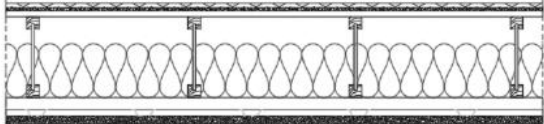
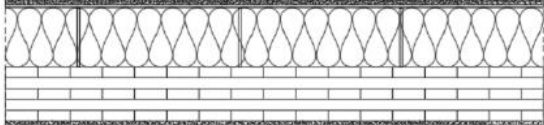
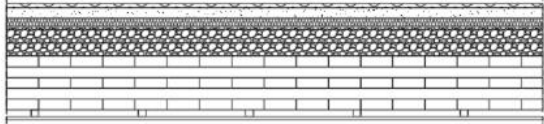
The chapter on vibrations in timber floors in the cEC5 gives guidance on the design of timber floors with a fundamental frequency of 8 to 40 Hz. The cEC5 uses two criteria, the point load deflection and the unit impulse velocity response [9]. The design process is presented in Figure 1 and includes equations for the natural frequency of the floor, f_1 , number of first order modes below 40 Hz, n_{40} , and the impulse velocity response, v . Point load deflection is calculated based on the structural system of the single- or multiple-span floor and corresponding boundary conditions.

The variables used for the cEC5 are the fundamental frequency, f_1 , in Hz, spanning length of the floor, l , in the direction of the load bearing beams in m, spanning width, b , in the transverse direction to the load bearing beams in m, mass of the floor, m , per unit area in kg/m^2 , the bending stiffness of the floor, $(EI)_l$, in the direction of the beams and the bending stiffness of the floor, $(EI)_b$, in the direction transverse to the load bearing direction, both in Nm^2/m . The point load deflection, w , divided by a load of 1 kN, F , should be lower than or equal to the limiting value, $a = 1.5 \text{ mm}/\text{kN}$, given in the national annex [10]. The unit impulse velocity response v should be smaller than or equal to $b^{f_1 \zeta - 1}$ where b is given by the national annex [10] and ζ is the unitless modal damping ratio.

2.3. Design according to the revised Eurocode 5 method

In the rEC5, floor performance levels are introduced. The levels range from I to VII where I is the best floor performance level, VI is the worst still acceptable floor performance level and level VII is unacceptable. The floor performance level is determined by the stiffness criterion, w_{1kN} , and the response factor, R , see Table 2. If the floor performance level is below VII for both the stiffness criterion and the acceleration or velocity criterion then the floor is considered acceptable. The process for the draft design method for vibrations in timber floors is presented in Figure 2. It includes calculation of the natural frequency of the floor, which needs to be higher than 4.5 Hz, for the method to be applicable. In a first step however, the stiffness criterion of the floor is evaluated. The equations given in Figure 2 exemplifies calculation of the deflection of a single span beam under a point load.

Table 1: Cross section of the investigated floor systems A-F.

Floor A		15 mm PARQUET FLOOR 22 mm FLOOR PARTICLE BOARD (FPB) 220x45 mm STRUCTURAL TIMBER C24 cc600 220 mm STONEWOOL 28x95 mm BATTENS cc400 13 mm GYPSUM BOARD
Floor B		15 mm PARQUET FLOOR 22 mm FLOOR PARTICLE BOARD (FPB) 220x45 mm KERTO BEAMS cc600 220 mm STONEWOOL 28x95 mm BATTENS cc400 13 mm GYPSUM BOARD
Floor C		14 mm PARQUET FLOOR 40 mm CONCRETE 17 mm INSULATION 63 mm LAMINATED VENEER LUMBER BOARD 270x63 mm GLULAM WEB 42x315 mm GLULAM FLANGE
Floor D		15 mm PARQUET FLOOR 13 mm FLOOR GYPSUM BOARD 22 mm FLOOR PARTICLE BOARD (FPB) 300 mm I-BEAM H300, c600 200 mm INSULATION 45x95 mm BATTENS CC400 25 mm GYPROC AP 2x15 mm GYPSUM BOARD (GF)
Floor E		15 mm PARQUET FLOOR 2x13 mm GYPSUM BOARD 22 mm FLOOR PARTICLE BOARD (FPB) 10+190 mm JOIST 190 mm INSULATION 200 mm CLT-SLAB 15 mm GYPSUM BOARD
Floor F		15 mm PARQUET FLOOR 40 mm GYPSUM SCREED 30 mm SOUND INSULATION 110 mm MACADAM 150 mm CLT-SLAB 25x25 mm BATTENS cc400 13 mm GYPSUM BOARD

The variables used in the rEC5 are F , a point load of 1 kN, l and b_{ef} , the length and effective width of the floor, both in metres, the mass of the floor, m , in kg/m². The bending stiffness of the floor in the direction of the load bearing beams is $(EI)_L$ in Nm²/m. For the

fundamental frequency two multipliers are introduced, $k_{e,1}$ and $k_{e,2}$, which handle the cases single or double spanning floors respectively one- or two-way spanning floors.

When using the acceleration criterion, for $4.5 < f_1 \leq 8$ Hz, $\alpha = e^{-0.4f_1}$ is a Fourier coefficient, F_0 is a vertical load of 700 N coming from the person giving rise to the disturbance, ζ is the unitless modal damping ratio and M^* is the modal mass in kg. The modal mass is a measure for how much of the total floor mass contribute to the vibration of a specific mode and it depends on how many sides the floor structure is supported on.

For the velocity criterion, when $f_1 > 8$ Hz, I is the mean modal impulse depending on the walking frequency, f_w , and the fundamental frequency, f_1 . In the peak velocity response $V_{1,peak}$, K_{red} is a reduction factor, I is the mean modal impulse and M^* the modal mass in kg. The impulsive multiplier, K_{imp} , depend on the length, l , width, b , in m and the bending stiffnesses, $(EI)_L$, in the load bearing direction and, $(EI)_T$, in the direction transverse to the load bearing direction, both in Nm^2/m .

The limit of applicability for the rEC5 is that the fundamental frequency of the floor has to be 4.5 Hz or above. The deflection criterion in the cEC5 is kept for coherency, it changes name to the stiffness criterion and it is accompanied by two new criteria namely the acceleration criterion and the velocity criterion. The acceleration criterion is used for low-frequency floors with a fundamental frequency of 4.5 to 8 Hz, and the velocity criterion is used for high-frequency floors with a fundamental frequency above 8 Hz. Both the stiffness criterion and the acceleration or velocity criterion result in response factors, R . For a visible representation of the relation between the limiting values for the point load deflection, which affect the stiffness criterion, the R-factors, coming from the acceleration or velocity criterion, and the floor performance levels, see Figure 3.

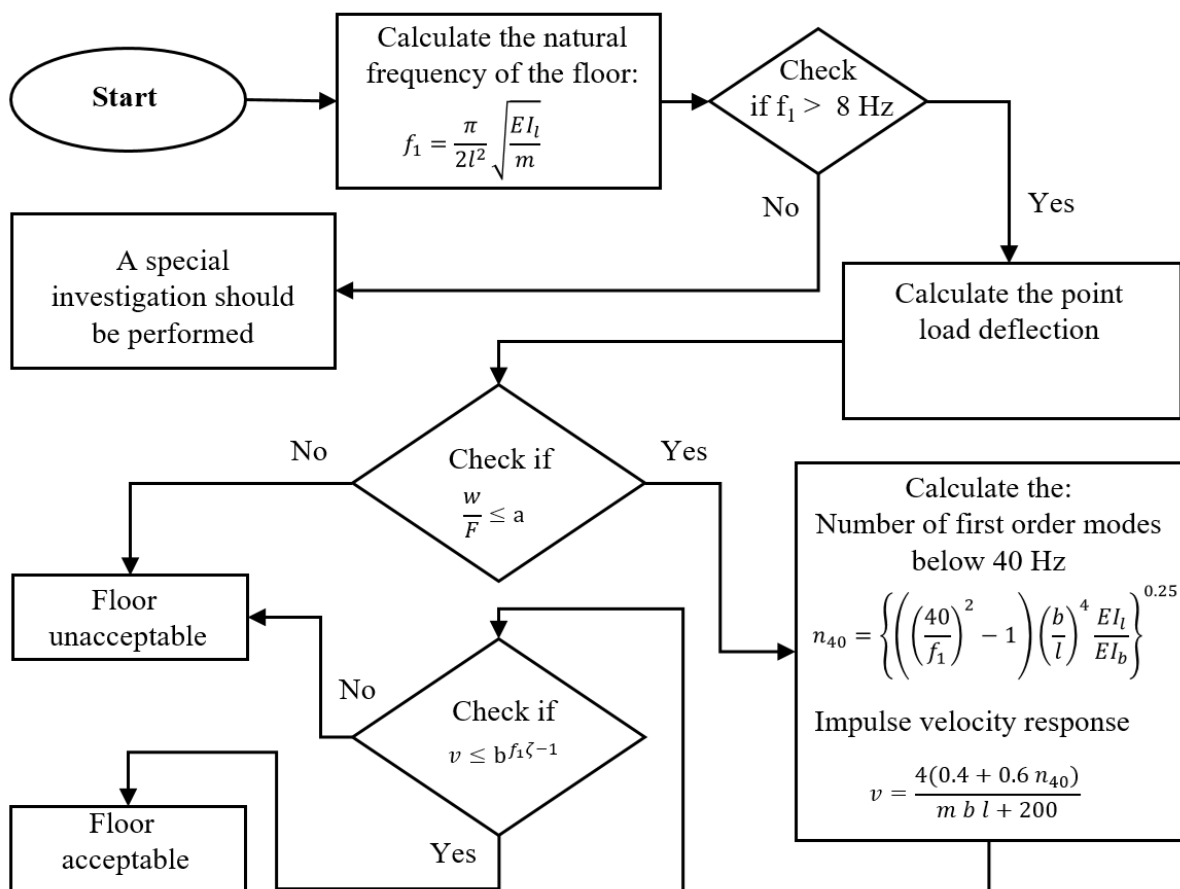


Figure 1: Illustration of the design process for timber floors according to the chapter on vibrations in the current Eurocode 5, cEC5.

Table 2: Floor vibration criteria of the classification system in the rEC5 [9].

Criteria	Floor performance levels						
	I	II	III	IV	V	VI	VII
Frequency f_1 [Hz] \geq	4.5						
Stiffness criteria							
w_{1kN} [mm] \leq	0.25	0.5	0.8	1.2	1.6	Unacceptable	
Response factor R	4	8	12	16	24	32	Unacceptable
Acceleration criteria							
when $f_1 < 8$ [Hz]							
a_{rms} [m/s ²] \leq	R × 0.005						
Velocity criteria							
when $f_1 \geq 8$ [Hz]							
v_{rms} [m/s] \leq	R × 0.0001						

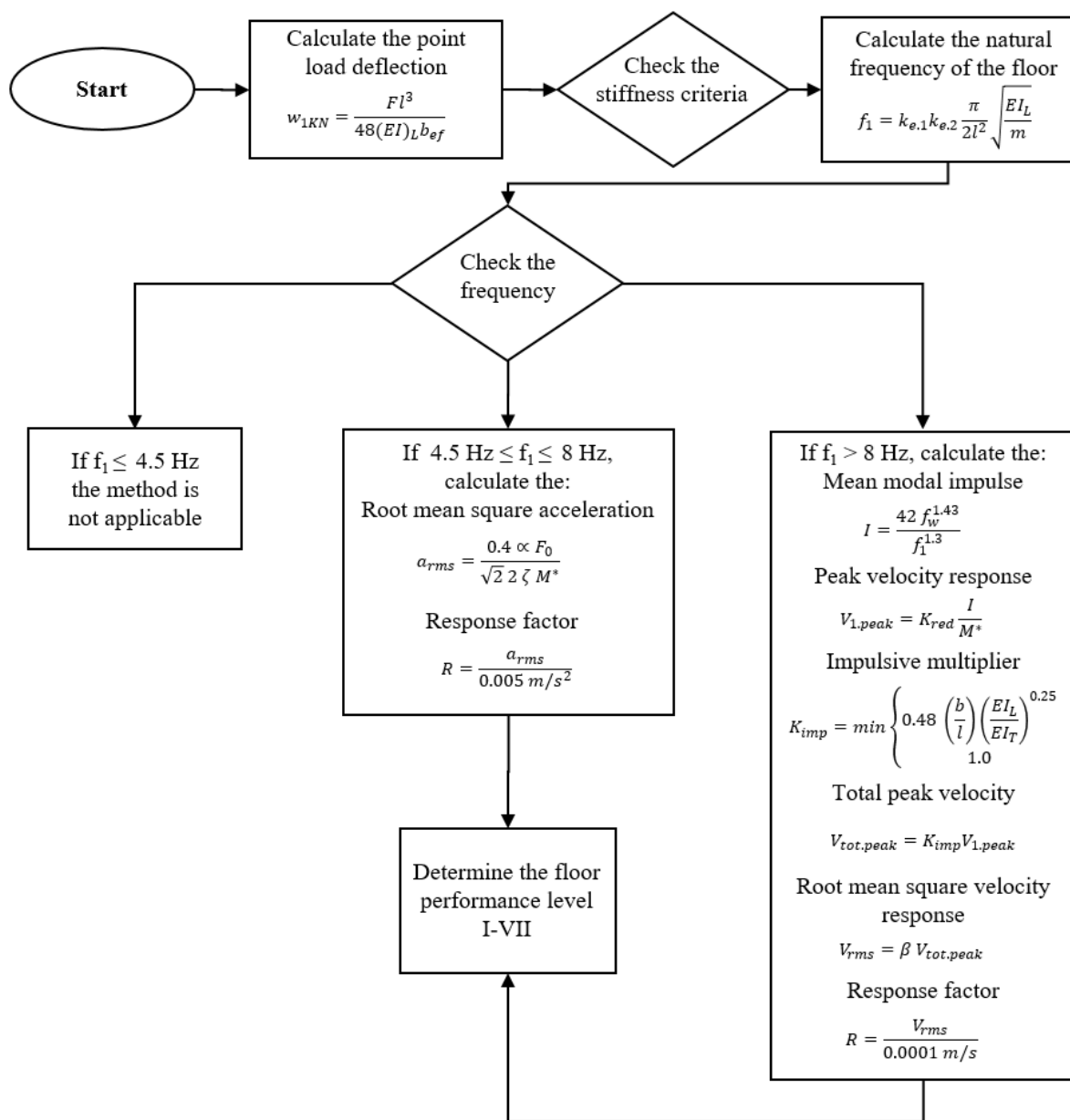


Figure 2: Illustration of the design process for timber floors according to the draft chapter on vibrations in the revised Eurocode 5, rEC5.

2.4. Parametric study – Effect of length, mass and modal mass on R-factors

Three parametric studies were performed, of which one is presented herein. In this parametric study, the length and mass per unit area were varied to study the effect of these variables on the R-factor. Calculations were made for the self-weight of the floor, m , i.e. the mass per square metre. In m_p the mass from partitions are added to the self-weight. The weight from imposed loads could be added in two ways, according to EKS 10, the Swedish national annex to the Eurocodes, 30 % of the imposed loads should be added to the mass [10] and according to rEC5 only 10 % of the imposed loads should be added. Calculations have been carried out for both cases, that is $m_{i0.3}$ and $m_{i0.1}$. Calculations have also been done for a combination of loading from partitions and imposed loads, $m_{p,i0.3}$ and $m_{p,i0.1}$. The R-factors are also influenced by whether the floor structure is considered to be one- or two-way spanning as these cases lead to two different modal masses.

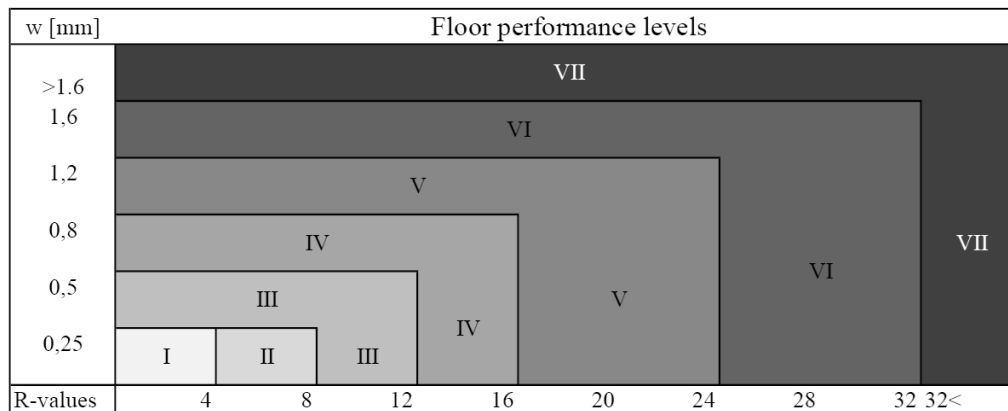


Figure 3: Relation between stiffness criteria, floor performance level and response factors, R , in rEC5.

3. Results and discussion

3.1. Floor A – F

Results for the calculations are presented in Table 3 in accordance with cEC5 and rEC5. Regarding the cEC5, the unit impulse velocity response and the limit for the unit impulse velocity response are both given so that a comparison can be made. If the point load deflection is lower than 1.5 mm and if the unit impulse velocity response is lower than the limit for the unit impulse velocity response then the floor has passed the criteria of the current design method, cEC5.

When considering the rEC5, the root mean square acceleration response has been calculated for floor structures with a fundamental frequency of 4.5 to 8 Hz and for floors with a fundamental frequency above 8 Hz the root mean square velocity response is calculated. Based on the acceleration or velocity response the response factor, R , is obtained. For rEC5 a low response factor, R , obtained means that the floor has a better floor performance level, i.e. a floor performance level I is excellent and VII is unacceptable. Two floor performance levels has been calculated and presented for each floor. The first performance level is based on the stiffness criteria and the second is based on the acceleration or velocity criteria dependent on the fundamental frequency of the floor. The highest level obtained is taken as the floor performance level of the floor. If both performance levels obtained are below VII then the floor is acceptable according to the draft design method, rEC5.

A summary of the results for the six floor structures A-F is presented in Table 4. The calculation results for the point load deflection, w , the response factor, R , and the impulse velocity response, v , are given. The floor performance level R for the floor is taken from the worst case, i.e. the highest floor performance level in Table 2. If cEC5 cannot be applied to the floor then this is marked with N.A. which stands for not applicable.

Table 3: Results for A – F.

Floor A			Floor B		
	Design method			Design method	
	cEC5	rEC5		cEC5	rEC5
Fundamental frequency	16.4 Hz	15.2 Hz	Fundamental frequency	17.7 Hz	16.3 Hz
Point load deflection	1.03 mm	1.42 mm	Point load deflection	0.84 mm	1.22 mm
Unit impulse velocity response	21.9 mm/Ns ²		Unit impulse velocity response	20.9 mm/Ns ²	
Limit for unit impulse velocity response	45.4 mm/Ns ²		Limit for unit impulse velocity response	51.1 mm/Ns ²	
RMS acceleration response			RMS acceleration response		
RMS velocity response		6.58 mm	RMS velocity response		5.80 mm
Response factor		65.8	Response factor		58.0
Pass or fail	Pass		Pass or fail	Pass	
Performance level based on deflection		VI	Performance level based on deflection		VI
Performance level based on response factor		VII	Performance level based on response factor		VII
Floor C			Floor D		
	Design method			Design method	
	cEC5	rEC5		cEC5	rEC5
Fundamental frequency	23.9 Hz	23.9 Hz	Fundamental frequency	11.3 Hz	11.3 Hz
Point load deflection	0.11 mm	0.07 mm	Point load deflection	0.90 mm	1.18 mm
Unit impulse velocity response	2.6 mm/Ns ²		Unit impulse velocity response	11.5 mm/Ns ²	
Limit for unit impulse velocity response	271.2 mm/Ns ²		Limit for unit impulse velocity response	28.2 mm/Ns ²	
RMS acceleration response			RMS acceleration response		
RMS velocity response		0.38 mm	RMS velocity response		2.12 mm
Response factor		3.8	Response factor		21.2
Pass or fail	Pass		Pass or fail	Pass	
Performance level based on deflection		I	Performance level based on deflection		V
Performance level based on response factor		I	Performance level based on response factor		V
Floor E			Floor F		
	Design method			Design method	
	cEC5	rEC5		cEC5	rEC5
Fundamental frequency	11.0 Hz	13.4 Hz	Fundamental frequency	5.6 Hz	6.8 Hz
Point load deflection	0.09 mm	0.09 mm	Point load deflection		0.21 mm
Unit impulse velocity response	1.0 mm/Ns ²		Unit impulse velocity response		
Limit for unit impulse velocity response	35.5 mm/Ns ²		Limit for unit impulse velocity response		
RMS acceleration response			RMS acceleration response		42.0 mm
RMS velocity response		0.31 mm	RMS velocity response		
Response factor		3.1	Response factor		8.4
Pass or fail	Pass		Pass or fail	–	
Performance level based on deflection		I	Performance level based on deflection		I
Performance level based on response factor		I	Performance level based on response factor		III

From Table 4, it becomes obvious, that the draft revised method for the assessment of floor systems gives more differentiation of the performance. In most assessed floor structures, the stiffness criterion and the response factor, R , yielded similar classification, while it differed for floors A, B and F.

Of the six floor structures studied, five pass the current design criteria and four pass the criteria of the draft revised design method. Section 3.1, Table 4, shows that Floor C, D and E achieve the same floor performance level from both the stiffness criterion and the velocity criterion according to the draft revised design method. The other three floors, A, B and F, perform better according to the stiffness criterion than the acceleration or velocity criterion. Floor A and B get an acceptable floor performance level, level VI, according to the stiffness criterion but achieve level VII according to the velocity criterion. Floor F reaches level I based on the stiffness criterion and level III based on the acceleration criterion. According to the results, both Floor A and B would fail the criteria in the rEC5 and the cEC5 cannot be applied to Floor F as this floor has a fundamental frequency below 8 Hz.

Table 4: Summary of results for Floor A–F with respect to the criteria in cEC5 and rEC5.

Floor structure	Criteria in	Floor performance level
	cEC5 [w/ν]	rEC5 [w/R]
A	Pass/Pass	Level VI/VII
B	Pass/Pass	Level VI/VII
C	Pass/Pass	Level I/I
D	Pass/Pass	Level V/V
E	Pass/Pass	Level I/I
F	N.A. / N.A.	Level I/III

3.2. Parametric study – Effect of length, mass and modal mass on R-factors

The parametric study focused on the effect of length, mass and modal mass on the response factors, R . The variables were varied as described in Section 2.4. The combinations used gave rise to sixty response factors per floor, the results are presented in Table 6. The colour key for the parametric study is presented in grey scale, see Table 5. When the velocity criterion has been used the R -values are given with normal font and when the acceleration criterion has been used the R -factors are given in italic font. When the response value, R , is 32 and above the font is white and when the fundamental frequency is below 4.5 Hz the cell is left empty as none of the criteria are applicable.

A shorter span results in a lower response factor, R . For the velocity criterion, the lowest response factor was generally achieved for the shortest span, 3.5 m, and the largest mass, i.e. when partitions and 30 % of the imposed loads were included in the mass per unit area. To achieve a fundamental frequency below 8 Hz, which leads to using the acceleration criterion, spans of more than 3.5 m are necessary for most floors. The lowest response factor for the acceleration criterion was obtained for a combination of a low mass per unit area and the shortest span needed to trigger the acceleration criterion.

Table 5: Colour key for the point load deflection based on the revised design method, floors with performance level VII fail as the R -factor is above 32.

Performance Level	Velocity Criteria	Acceleration Criteria
I	0 to 4	<i>0 to 4</i>
II	4 to 8	<i>4 to 8</i>
III	8 to 12	<i>8 to 12</i>
IV	12 to 16	<i>12 to 16</i>
V	16 to 24	<i>16 to 24</i>
VI	24 to 32	<i>24 to 32</i>
VII	above 32	<i>above 32</i>

Assuming that the floor was supported on four sides, the modal mass becomes $M^* = mbl/4$, which result in a response factor R twice as large as if the floor had been assumed to be supported on only two sides.

The modal mass depends on the floor structures support conditions, whether the floor is supported on two or four sides. According to the results in Section 3.1, floors supported on two sides get twice as good response factors as floors supported on four sides. That is, according to the results, floors supported on four sides are more sensitive to vibrations than floors supported on only two sides, this seems counter intuitive.

Table 6: Summary of results from parametric study, response factor, *R*.

Floor A						
$M^*=mlb/2$	Mass [kg/m ²]	Response factors				
$m_{p,i,0.3}$	139,8	17,8	20,5	17,8		
$m_{p,i,0.1}$	99,0	19,1	22,3	15,1	42,9	
$m_{i,0.3}$	104,1	18,9	22,0	15,5	42,8	
$m_{i,0.1}$	63,3	20,4	24,5	31,2	41,7	
m_p	78,6	19,8	23,5	29,5	42,9	
<i>m</i>	42,9	21,1	26,2	34,4	37,1	80,0
$M^*=mlb/4$						
$m_{p,i,0.3}$	139,8	35,6	41,0	35,5		
$m_{p,i,0.1}$	99,0	38,2	44,6	30,2	85,8	
$m_{i,0.3}$	104,1	37,8	47,0	25,7	85,5	
$m_{i,0.1}$	63,3	40,9	49,1	62,5	83,5	
m_p	78,6	39,7	47,0	59,0	85,7	
<i>m</i>	42,9	42,3	52,4	68,8	74,1	160,0
Length [m]		3,5	4,0	5,0	6,5	8,0

Floor B						
$M^*=mlb/2$	Mass [kg/m ²]	Response factors				
$m_{p,i,0.3}$	142,3	15,9	18,4	13,4		
$m_{p,i,0.1}$	101,5	16,9	19,9	24,9	34,9	
$m_{i,0.3}$	106,6	16,7	19,7	24,6	35,0	
$m_{i,0.1}$	65,8	17,8	21,7	27,9	32,6	
m_p	81,1	17,4	20,8	26,5	34,2	
<i>m</i>	45,4	18,2	22,9	30,5	28,0	65,2
$M^*=mlb/4$						
$m_{p,i,0.3}$	142,3	31,7	36,8	26,7		
$m_{p,i,0.1}$	101,5	33,7	39,8	49,9	69,9	
$m_{i,0.3}$	106,6	34,8	39,4	49,2	70,0	
$m_{i,0.1}$	65,8	35,7	43,3	55,9	65,3	
m_p	81,1	34,8	41,7	52,9	68,4	
<i>m</i>	45,4	36,3	45,8	61,0	56,0	130,4
Length [m]		3,5	4,0	5,0	6,5	8,0

Floor C						
$M^*=mlb/2$	Mass [kg/m ²]	Response factors				
$m_{p,i,0.3}$	259,8	1,0	1,5	2,6	4,5	16,1
$m_{p,i,0.1}$	219,0	0,9	1,5	2,6	4,7	7,0
$m_{i,0.3}$	224,1	0,9	1,5	2,6	4,6	7,0
$m_{i,0.1}$	183,3	0,8	1,4	2,7	4,8	7,4
m_p	198,6	0,9	1,5	2,7	4,8	7,2
<i>m</i>	162,9	0,8	1,4	2,7	5,0	7,6
$M^*=mlb/4$						
$m_{p,i,0.3}$	259,8	2,0	3,0	5,2	8,9	32,3
$m_{p,i,0.1}$	219,0	1,8	3,0	5,3	9,3	14,0
$m_{i,0.3}$	224,1	1,9	3,0	5,3	9,3	13,9
$m_{i,0.1}$	183,3	1,7	2,9	5,4	9,7	14,7
m_p	198,6	1,8	2,9	5,3	9,5	14,4
<i>m</i>	162,9	1,5	2,8	5,4	9,9	15,2
Length [m]		3,5	4,0	5,0	6,5	8,0

Floor D						
$M^*=mlb/2$	Mass [kg/m ²]	Response factors				
$m_{p,i,0.3}$	183,6	11,7	13,6	16,8	28,6	
$m_{p,i,0.1}$	142,8	12,2	14,3	17,9	28,2	
$m_{i,0.3}$	147,9	12,1	14,2	17,8	28,3	
$m_{i,0.1}$	107,1	12,6	15,1	19,3	26,5	
m_p	122,4	12,5	14,8	18,7	27,4	
<i>m</i>	86,7	12,8	15,6	20,3	24,5	53,1
$M^*=mlb/4$						
$m_{p,i,0.3}$	183,6	23,4	27,1	33,5	57,1	
$m_{p,i,0.1}$	142,8	24,4	28,7	35,9	56,3	
$m_{i,0.3}$	147,9	24,3	28,4	35,5	56,5	
$m_{i,0.1}$	107,1	25,3	30,3	38,6	53,0	
m_p	122,4	24,9	29,5	37,4	54,9	
<i>m</i>	86,7	25,7	31,3	40,7	49,1	106,2
Length [m]		3,5	4,0	5,0	6,5	8,0

Floor E						
$M^*=mlb/2$	Mass [kg/m ²]	Response factors				
$m_{p,i,0.3}$	275,2	0,8	0,9	1,2	6,4	
$m_{p,i,0.1}$	234,4	0,8	0,9	1,2	6,1	12,5
$m_{i,0.3}$	239,5	0,8	0,9	1,2	6,1	
$m_{i,0.1}$	198,7	0,8	1,0	1,3	5,6	12,6
m_p	214,0	0,8	1,0	1,3	5,8	12,6
<i>m</i>	178,3	0,8	1,0	1,3	5,3	12,6
$M^*=mlb/4$						
$m_{p,i,0.3}$	275,2	1,5	1,8	2,4	12,8	
$m_{p,i,0.1}$	234,4	1,5	1,9	2,5	12,1	25,0
$m_{i,0.3}$	239,5	1,5	1,9	2,5	12,2	
$m_{i,0.1}$	198,7	1,6	1,9	2,6	11,3	25,3
m_p	214,0	1,6	1,9	2,5	11,7	25,2
<i>m</i>	178,3	1,6	2,0	2,6	10,6	25,2
Length [m]		3,5	4,0	5,0	6,5	8,0

Floor F						
$M^*=mlb/2$	Mass [kg/m ²]	Response factors				
$m_{p,i,0.3}$	387,3	1,3	1,5	5,1		
$m_{p,i,0.1}$	346,5	1,3	1,5	5,0		
$m_{i,0.3}$	351,6	1,3	1,5	5,0		
$m_{i,0.1}$	310,8	1,4	1,6	4,8		
m_p	326,1	1,3	1,5	4,9		
<i>m</i>	290,4	1,4	1,6	4,7		
$M^*=mlb/4$						
$m_{p,i,0.3}$	387,3	2,6	2,9	10,2		
$m_{p,i,0.1}$	346,5	2,6	3,0	9,9		
$m_{i,0.3}$	351,6	2,6	3,0	10,0		
$m_{i,0.1}$	310,8	2,7	3,1	9,6		
m_p	326,1	2,7	3,1	9,8		
<i>m</i>	290,4	2,7	3,2	9,4		
Length [m]		3,5	4,0	5,0	6,5	8,0

4. Conclusions and further research

The hypothesis of this work was that the introduction of the draft of the rEC5 might force some changes to the construction practice and that these changes may increase costs for the industry. Of the six floor systems currently used by companies in Sweden the two floors most commonly used in single-family houses, Floor A and B, only reached floor performance level VII, which is unacceptable according to rEC5. Thus, adaptations of these floor systems would be required in order to fulfil the design criteria in rEC5.

The parametric study showed that Floor A and B achieved floor performance level V for a span of 3.5 metres when they were assumed to be supported on only two sides. If they were assumed to be supported on four sides, the floor performance level would become unacceptable. Floor F is an example of a floor structure which cannot be designed based on cEC5, when considering the floor performance levels in rEC5 it performs exceptionally well.

It can be concluded that changes may have to be implemented for the common Floors A and B to have acceptable performance when a revision of EC5 is introduced and these changes could result in increased costs for the timber construction industry. A broader study including more floor structures should be conducted in order to assess the need of adaptations of further common floor structures in case rEC5 would be introduced.

In the parametric study primarily one discovery seemed contradictory. Floors supported on four sides got worse response factors than floors supported on two sides. This finding should be further assessed for a decision on the suitability of the proposed draft design method. Since the present work was finalised the revision work has continued with national comments and their implementation. A draft version two has been finalised in late October 2019.

5. References

- [1] T. Toratti and T. Asko, «Classification of Human Induced Floor Vibrations», *Building Acoustics*, 13(3): 211-221, 2006.
- [2] S. Brege, T. Nord and L. Stehn, «Industieellt byggande i trä - nuläge och prognos mot 2015», Linköping University, Linköping, 2017, in Swedish.
- [3] K. Jarnerö, A. Brandt and A. Olsson, «Vibration properties of a timber floor assessed in laboratory and during construction.», *Engineering Structures*, 82: 44-54, 2015.
- [4] B. Zhang, B. Rasmussen, A. Jorissen and A. Harte, «Comparison of vibrational comfort assessment criteria for design of timber floors among the European countries», *Engineering Structures*, 52: 592-607, 2013.
- [5] M. Basner, W. Babisch, A. Davis, M. Brink, C. Clark, S. Janssen and S. Stansfeld, «Auditory and Non-Auditory Effects of Noise on Health», *The Lancet*, 383: 1325-1332, 2014.
- [6] S. Ohlsson, «Floor vibrations and human discomfort», Chalmers University of Technology, Division of Steel and Timber Structures, 1982.
- [7] A. Brandt, K. Jarnerö and A. Olsson, «In situ testing of timber floor vibration properties», in proceedings of the World Conference on Timber Structures, *WCTE 2010*, 2010.
- [8] J. Weckendorf, T. Toratti, I. Smith and T. Tannert, «Vibration serviceability performance of timber floors», *European Journal of Wood and Wood Products*, 74(3): 353-367, 2016.
- [9] EN 1995-1-1:2004, «Eurocode 5: Design of timber structures - Part 1-1: General - Common rules and rules for buildings», 2004.
- [10] Boverket, «Boverkets konstruktionsregler - EKS10 - BFS 2011:10», Boverket, Stockholm, 2016, in Swedish.

Experimental full-scale testing of a multistory timber frame building concerning dynamic properties

Urs Oberbach
Institute for Timber Construction,
Structures and Architecture,
Bern University of Applied Sciences
Biel/Bienne, Switzerland



Experimental full-scale testing of a multistory timber frame building concerning dynamic properties

1. Introduction

Since 2003 the Swiss codes demand to carry out an earthquake verification for building structures. The dynamic loads, that occur in a structure during an earthquake or dynamic excitation are not depending on the choice of a certain load, but on the dynamic response of the structure. Therefore, its dynamic behavior must be known, and the engineer usually chooses a fundamental period T_1 that he thinks fits best between various methods of calculation. One can obtain fundamental periods that differ a lot and so earthquake forces may differ to factor 5 or more for the same structure. In addition, especially in wood construction with wide spread material properties, the underestimation of material stiffness lead to higher forces.

The fundamental period, which is the longest period of a structure, is the time in which a building makes one free oscillation. The stiffness and the mass of the building are influencing the fundamental period. In fact, every building, as its never infinitely stiff, is oscillating even if people don't recognize. Interference of soil and building frequencies is crucial behavior while amplitudes get summed up.

As investigations have shown, timber frame shear walls are significantly stiffer than calculated with available means and codes. Dynamic properties of timber frame walls are difficult to predict, research in this domain is mandatory. Nevertheless, the engineer must choose one fundamental period for the building design. If its short and a period on the spectral plateau is chosen, high design forces will occur and a lot of anchorage pieces result, however if it is chosen long, seismic forces are little, its more economic, but this softness must be guaranteed once build.



Figure 1: Experimental plant with 4 story building and racks for cable tensioning system.

In Chamoson, Canton of Valais the building is erected and tested during summer 2019. On the floorplan it is 5,04 m x 3,86 m. The idea is to make a full-scale static and dynamic testing of a timber frame building during different stages. Therefore, the building is investigated during the erecting phase, but before in the laboratory to compare results from numerical analysis, laboratory results and the reality «as built».

There are two shorter walls in Y direction without openings and two longer walls in X direction with a window opening. According to the codes, the same stiffness for analysis must be used, because the shear length is identical.

Research has shown, that entire timber frame buildings [6], timber frame shear walls [5] and the staple connection between OSB and studs [2] have on one hand higher stiffness than calculations according to the code say, but on the other hand much higher stiffness in only very little excitation. Therefore, on-site measurement of fundamental period with ambient noise measurement (ANM) which is a non-destructive and relatively simple way to do the analysis will not give the same results than a free oscillation test. Deflection influences periods.

2. Specimen and material properties

The walls consist of studs of 160mm in GL24h intermediate studs in C24 and a 15 mm OSB/3 on the outside. The connection between these two parts are staples 1,53/50 mm. This configuration provides accessibility during the erection phase from the inside. OSB are trimmed 20 mm on all sides. This prohibits friction between two adjacent panels or shoring a panel while it rotates under shear load. 20 walls were produced, that corresponds to 5 stories. Four walls are tested monotonous in the laboratory, to know the wall behavior for the full-scale building test and compare these results.



Figure 2: Timber frame shear wall "C2" during test in the laboratory at BUAS.

2.1. Glulam

Before wall assembly, every piece of glulam has been checked for density, Young's modulus and wood moisture content. The pieces are then sorted by density and designed at the right place for the wall assembly. Pieces with highest densities are set in the ground floor and lower densities in the top stories. The knowledge of Young's modulus for each piece allows a precise numerical analysis.

Figure 3 shows the density results after sorting.

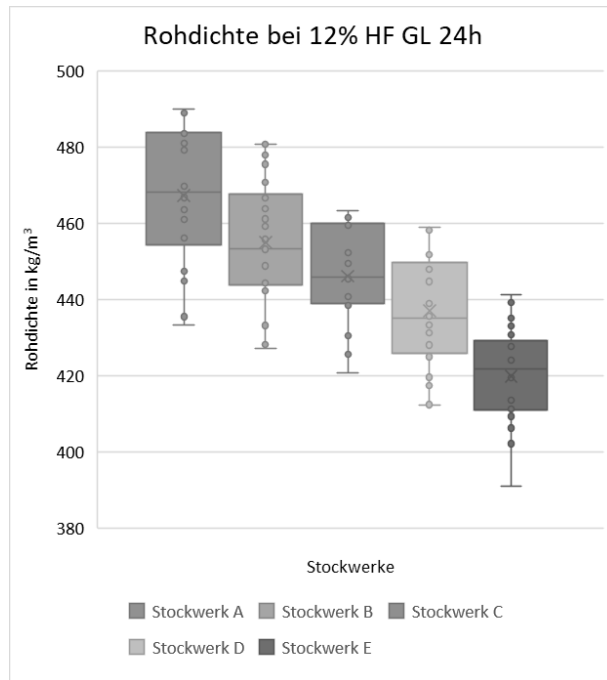


Figure 3: Density of glulam pieces corrected to 12% wood moisture content. Boxplot groups according to the story belonging.

2.2. OSB

OSB/3 15mm are checked for density, but no sorting is done. However, some specimens are set aside to investigate the shear modulus in grain direction and perpendicular to it. All boards used for the wall sheeting belong to one production cycle. Material properties should therefore be relatively homogeneous. The panels are size of 1,25 m x 2,70 m.

2.3. Staples

Properties of staples are determined by a preliminary analysis in this and other projects at Bern University of Applied Sciences. As a result, the slip modulus of staples is higher, than building codes predict. Especially in little excitation, the stiffness of these connections is significantly higher. Among other things, friction between OSB and studs may contribute to this increased stiffness.

For the tests to follow, influence on stiffness after several loading cycles must be assured. In other words, one must be sure that staple connections and so the walls have the same stiffness during the different testing stages, to compare the displacements and periods obtained. Results show, that 200 preloading cycles to the dimensioning value for staples ($F_{R,d} = 0,34$ kN/staple) has no influence of on slip modulus of the connection. Therefore, most of the tests are scaled to 67% of this force level with intention to not plastify or damage this connection in advance.

Influence of humidity to the stiffness of staple connections must also be considered. Tests were done to compare different full-scale test results. Temperature and air humidity are constantly logged on the building site and wood moisture content is checked after every testing day.

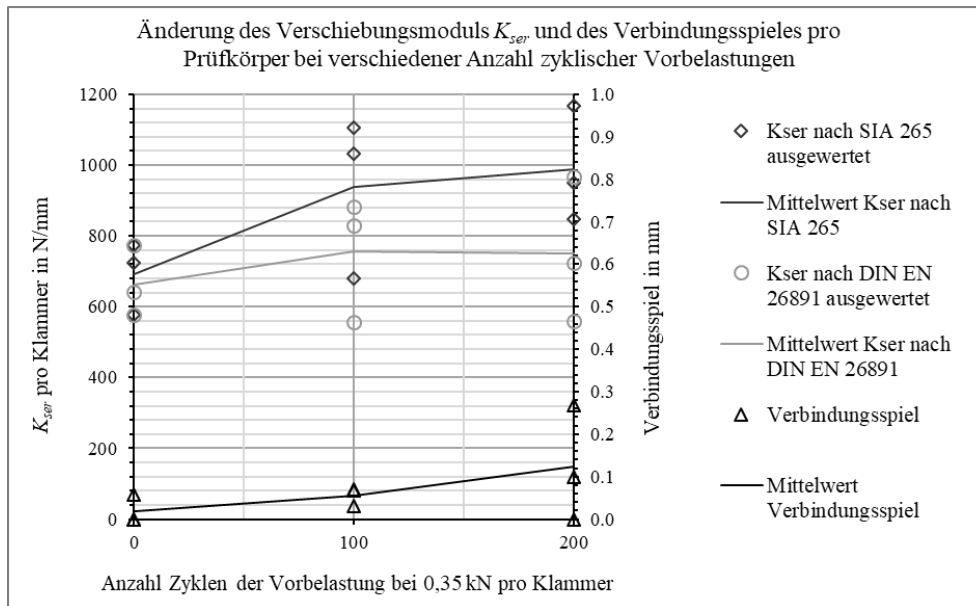


Figure 4: Variation of slip modulus of the stapled connection between OSB and glulam for different preloading situations. Depending on the evaluation method, slip modulus doesn't change or increases little [2].

2.4. Anchorage and story connection

Anchorage of vertical forces are executed by hold-downs. Between the foundation and the ground floor, there is a special steel anchorage piece, because of high tension forces of 550 kN. The connection of vertical forces between two stories is made with hold-downs type WHT740 XXL and threaded steel bars M24. All steel pieces are connected to the wood by screws LBS 5x70 predrilled with 3 mm. Main advantage is that there are only few different connector properties that must be known for the numerical simulation.

The shear connection from ground floor to foundation and between two stacked walls are done with classical wood screws 8x220 that go either in wood or in concrete (predrilled).



Figure 5: Action and reaction forces for two wall setups. On the left side: X-wall, right side: Y-wall.

2.5. Wall specimen

Each wall is preloaded in a cyclic test setup in the testing frame of the laboratory at Bern University of Applied Sciences in Biel. Three different force levels are defined, to 24%, 50% and 67% of the design value for staples by code SIA 265/1. These values correspond to the design value of exposure for staples by the annual wind, the wind with ten-year return period and the wind of fifty-year return period.

For calculation according to the code the walls in Y- and X-direction have the same stiffness, because sheeting at openings is not considered. X-walls have a shear length of $2 \cdot 1,25 \text{ m} = 2,5 \text{ m}$ and Y-walls a shear length of 2,5 m at one piece.

The graph below shows significant differences in stiffness between the X- and the Y- walls, but also stiffness variation due to the amplitude of loading.

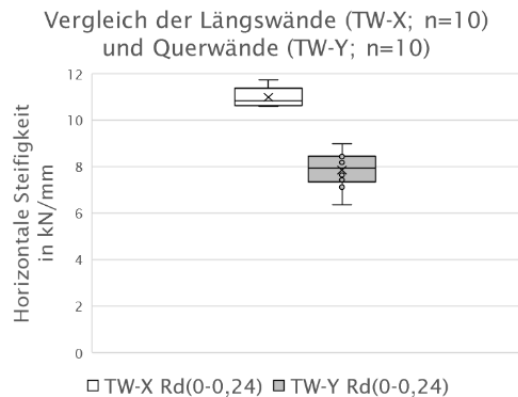


Figure 6: Comparison of horizontal stiffness between X- and Y-walls.

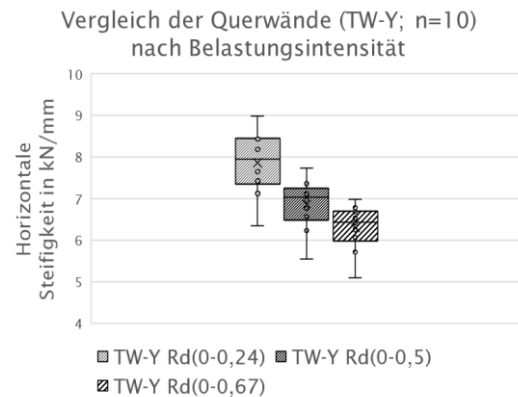


Figure 7: Comparison of horizontal stiffness for Y-walls with different loading intensities.

2.1. Floor slab

Floor slab composition is a wood beam construction of massive wood with a 25 mm OSB/3 on top for diaphragm effect. The panel is stapled to the beams and the joint between the panels is 20 mm.

Tension forces of the rope system are anchored with horizontal fixed hold-downs directly to the floor. In the middle of the floor there is an opening to access the different stories. It contains a little stair-case which is completely independent of the rest of the structure over the whole height of 10,80 m with enough space around, to let the building move.



Figure 8: Anchorage on floor slab to pull on the building.

2.2. Foundation

The foundation is a concrete plate of size 7 m x 10 m and 40-45cm thick. It is designed, to resist the pushover test of the building. Anchorage pieces are already set in place before pouring the concrete.



Figure 9: Pouring the concrete of the foundation. Anchorage pieces are already set.

2.3. Calculation model

The calculation is based on current codes with applying a ductile dimensioning to the structure. Thus, there must be a mechanism installed called hierarchy of resistances. Let's imagine a chain, and the chain will deform or break at the weakest chain link. Therefore, all other chain links must be stronger, to be sure, that the determined link to fail is the link which fails first and can dissipate the energy. In timber frame construction the weakest link, by the way highly ductile, can be attributed to the staple connection. But then all other parts, like the resistance of OSB, resistance of anchorage must be over dimensioned, thus higher.

The estimation of the fundamental period can be done by simple formulas as SIA 261.39 and leads mostly to short periods on the plateau of the soil acceleration response spectrum. Or bar models with replacement stiffness can be used to determine the answer of the building, which leads mostly to longer periods because of underestimation of material stiffness.

Numerical simulation for stiffness is done by using material properties from the building codes and the measured material properties to refine the calculation model where needed. Every wall, and every piece of wood or concrete that is set in place was measured with the balance shown in

Figure 11 to precisely know the masses for the simulation. The measurements on site are compared with an engineer's approach of mass estimation for load assumptions and for a mass determination with a complete 3D model.

2.4. Mass

In order to have some realistic building masses for dead-loads, 8 prefabricated concrete blocks are added on each floor slab. This is a mass of about 1,25 kN/m² that corresponds to screed and floor composition.

The structural dynamic behavior depends on stiffness and mass. A lot of energy is set in the wright acquisition of stiffness, but also masses must to be known for a precise analysis.



Figure 10: Prefabricated concrete blocks to simulate dead-load in a building.



Figure 11: Balance suspended on crane to weigh all pieces set in place.

3. Testing phase and measurement equipment



Figure 12: Evolution of the test building. During the erecting phase four different buildings were tested.

The testing phase began with material properties in January 2019. Then walls got assembled. After wall assembly they were tested in March at the laboratory.

In May the erection at the building site began. The tests were carried out after each added story. So, in fact 4 buildings were tested. For each building, first the Ambient Vibrations were recorded with accelerometers. Then the rope tensioning system was installed and tensioned. Displacement of free oscillations are recorded inside with displacement transducers which can measure the distance between the free-standing staircase and the floor slab on top of the building. The floor slab has an opening in the center of the building. From the outside an optical measurement system records the displacements at several positions on the building at once. This Digital Image Correlation (DIC) system allows to determine the deformations in and out of plane at each recorded surface. Hence, mode shape analysis, static and dynamic behavior of the building can be extracted. Due to high picture sampling rates frequency analysis is also possible.

However, frequency analysis will mainly be extracted from the accelerometers.

At the foundation anchorage pieces strain gauges were installed, primary to observe spatial effects, but it came out, that building frequency analysis is also possible with these devices, even if the anchorage pieces work only in tension.

The 4-storey building is exposed to free oscillations that exceed nearly by factor two the earthquake of the code for this building on this site.

Measurement equipment on site was all supplied by a solar system, because electrical energy was not accessible on site.

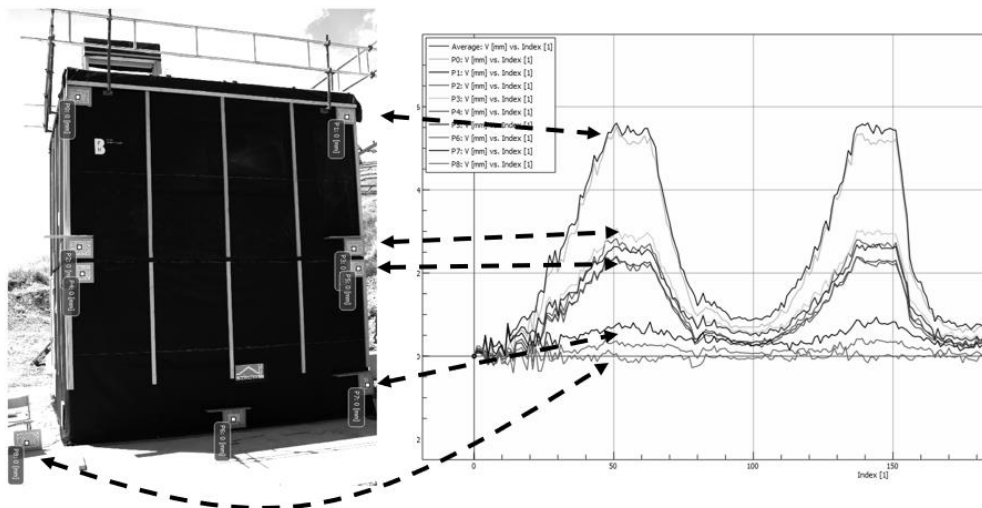


Figure 13: Symbolic DIC result for the two-story building in X direction. On the right graph on the ordinate is the horizontal relative displacement in X and the abscissae represents the pictures. The rope is tensioned several times on the building, before releasing the rope system.

At the end, a full-scale pushover test is executed as a monotonic test in field. Tension forces are so high, that the force and displacement graph for the static-nonlinear system is obtained to extract the yielding point of plastic deformation.

4. Investigation and objectives

The following questions should be answered at the end of the project:

- How can the fundamental period be determined for timber frame buildings?
- Is there a significant difference between the fundamental periods in X- and Y-direction of the building?
- What is the relationship of frequency between ANM and test by free oscillations?
- What is the relationship of damping between ANM and test by free oscillations?
- Are there spatial effects in the load bearing structure by neighboring walls?
- What are the mode shapes?
- Composition of deformation portions in timber frame shear walls and buildings?
- The torsional influence in a building with “perfect” symmetry?

5. Acknowledgements

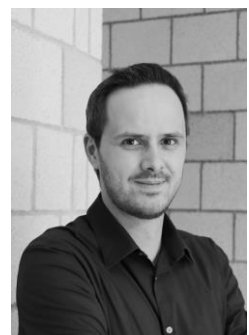
Thanks to all project partners and sponsors and especially to the Federal Office for the Environment FOEN, Coordination Centre for Earthquake Mitigation.

6. Literature

- [1] *Norm SIA 265 Holzbau*. Zürich: Schweizerischer Ingenieur- und Architekten Verein, 2012.
- [2] Preile, K. & Geiser, M. (2018) *Propriétés dynamiques des bâtiments à ossature bois, Rapport de travail AP2*. Biel, Schweiz.
- [3] *Norm ISO 21581 Timber structures – Static and cyclic load test methods for shear walls*. International Organisation for Standardisation, 2010.
- [4] Brunner, R. et al. (2010) *Technische Dokumentation der Lignum, Erdbebengerechte mehrgeschossige Holzbauten*. Zürich, Lignum.
- [5] Sadeghi A. et al. (2018). *OSB sheathed light-frame timber shear walls with strong anchorage subject to vertical load, bending moment, and monotonic lateral load*. Dübendorf, EMPA.
- [6] Steiger R. et al. (2016). *Ambient and forced vibration testing of a light-frame timber building – Conclusions regarding design of the lateral load resisting system*. In: Inter 49-15-1 (S.169-184)

Design Study of Two Variants of a Pedestrian and Cyclist Bridge in Timber-Composite Design as a Construction Replacement Option for the City of Koblenz

Paul Dreifke
University of Applied Sciences Koblenz
Koblenz, Germany



Design Study of Two Variants of a Pedestrian and Cyclist Bridge in Timber-Composite Design as a Construction Replacement Option for the City of Koblenz

1. Introduction

Timber-composite constructions are increasingly gaining ground in building construction and structural engineering due to their efficiency. This is demonstrated by several realized projects in building construction such as the "LCT One" in Bregenz and the multi-family house "e3" in Berlin. There are also several timber-concrete composite bridges such as the "Schiffarth bridge" in Rhein-Sieg district, two timber-concrete composite bridges in Schwäbisch-Gmünd, and the timber-concrete composite bridge in Winschoten. In the backdrop, the possibility of a replacement construction for a pedestrian and cyclist bridge in a timber-composite design is investigated in a real project by testing the feasibility of substituting concrete by granite. Using concrete as a load-bearing top layer demands a protective layer which has to be replaced regularly. This leads to high maintenance costs for the developer. Furthermore, the renewal of sealing level and road surface has a negative effect on the ecological life cycle balance. Using granite as load-bearing top layer intends to preserve the advantages of timber-concrete composite (TCC) structure and to reduce its disadvantages. Timber-concrete composite structures are generally superior to comparable solid or steel structures in terms of resource-efficient use of building materials. The timber-granite composite (TGC) offers even further optimization potential in this area. The inclusion of holistic considerations about lifespan is a firmly established procedure in building construction [1], which in future will also be applied within the field of infrastructure design. The exclusive consideration of the construction costs of engineering structures ignores their high maintenance costs. These leads to high costs for the developers over the service life.

However, using granite as a top layer is associated with various challenges. The granite slabs are fabricated in limited dimensions and need to be connected separately with timber beam. Depending on the type of fastening chosen for the slabs, the bond between the two construction materials granite and timber may be interrupted. This needs to be taken into account while calculating the internal forces and deformation by using an appropriate calculation method. Furthermore, for the durability of the overall construction the slab joints are to be designed in such a manner that water penetration can be ruled out.

2. Design and life cycle consideration

2.1. Structural design

The existing bridge (Fig. 1) which has to be replaced was constructed in 1970 as an elastic reinforced concrete frame clamped into the subsoil. Its free span is 27.5 metres with 2.40 meters as pavement width. It was required to integrate the existing abutments and previously developed structures into the new design, so the lines of the upper edge of the existing bridge had to be maintained.

Within these given basic conditions, various superstructure variants were designed and pre-dimensioned. The designs take into consideration that the superstructure is suitable for a timber-concrete composite construction as well as for a timber-granite composite construction. Therefore, the comparability of the two variants is achieved.

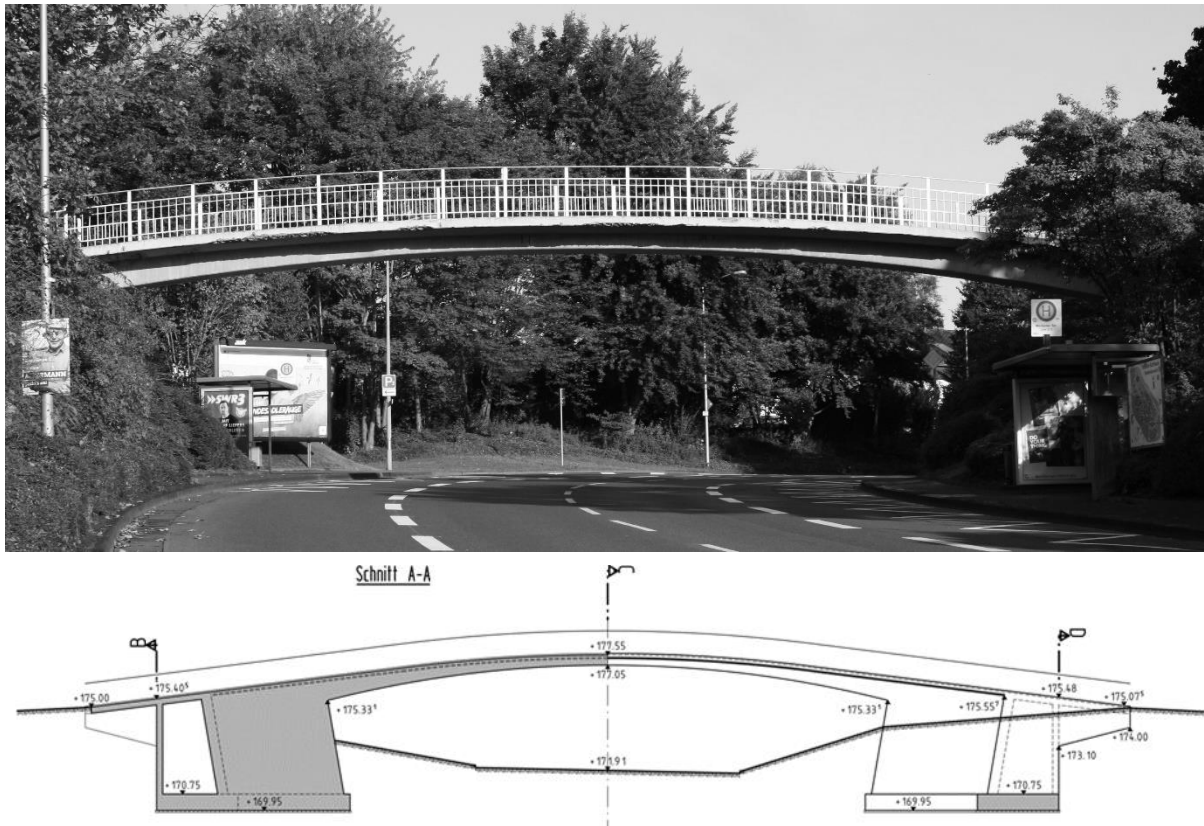


Figure 1: Existing concrete bridge across the Berliner Ring in Koblenz

As tensile forces induced into the planned composite walkway the tied arched bridge (Fig. 2a) was ruled out. Because the mineral top layer should always be under compressive stress. The large number of required joints could also have a negative effect on the durability of the overall structure. From a similar point of view, the variant with a perforated floor (Fig. 2b) was ruled out. These two variants were also rejected due to aesthetic considerations, especially as an arch at the top would not have fitted well into the surrounding area. The variants with a supporting structure of struts attached under the main girder (Fig. 2c), or as an arch (Fig. 2d) cause a continuous girder effect which is accompanied by negative moments in the main girder.

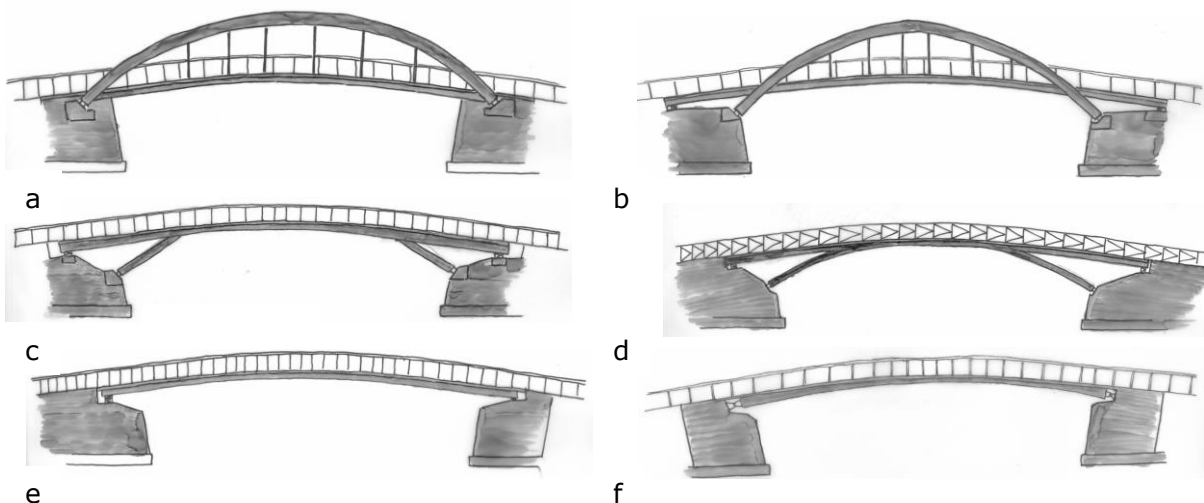


Figure 2: Different variants of the bridge design

These negative moments, in turn, lead to bending stress at certain points on the upper side of the mineral top layer that should be avoided. Furthermore, the position of the struts or arches is severely restricted by the clearance profile of the road which passes underneath the bridge so that an effective reduction of the span is not possible.

A beam-bridge design (Fig. 2e) would have required very high cross sections in order to comply with the deflection restrictions. The necessary cross sections for the beam bridge would have violated the boundary conditions of the design. Thus, the choice fell on a very flat arch construction as superstructure (Fig. 2f). Another advantage of the arched bridge is that additional compressive forces are activated by the arch from its dead load to ensure that the mineral top layer remains under compressive stress.

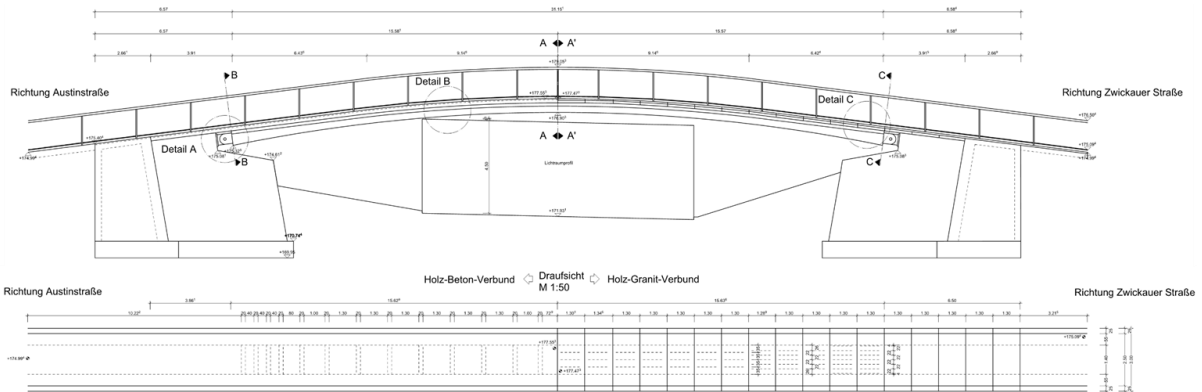


Figure 3: selected arch bridge design

For the chosen bridge's cross section, a bottom chord made of glued laminated timber was selected for both the timber-concrete and the timber-granite variant. Compared to concrete C30/37, which was used for the timber-concrete composite variant, the used granite has not only a higher strength but also a higher modulus of elasticity. Therefore, in the timber-granite variant the height of the top chord can be lower than in the timber-concrete variant, but without worsening the static properties of the overall structure. For the timber-concrete composite construction, notched connection with a staggered arrangement over length were chosen as connectors. For the timber-granite construction, expanded metal sheets glued into the timber and granite were used as fasteners. The number of fasteners were also staggered over the length according to the static requirements.

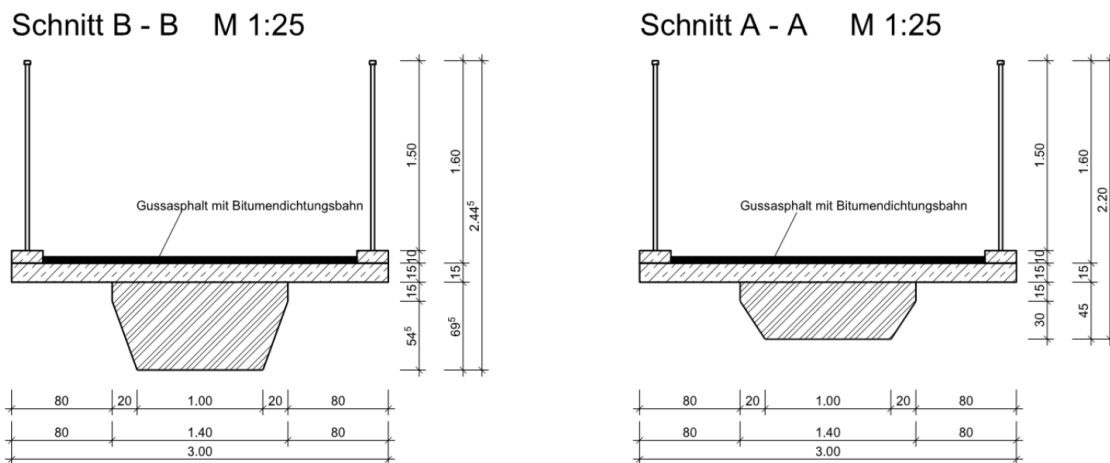


Figure 4: Cross section of the timber concrete composite bridge

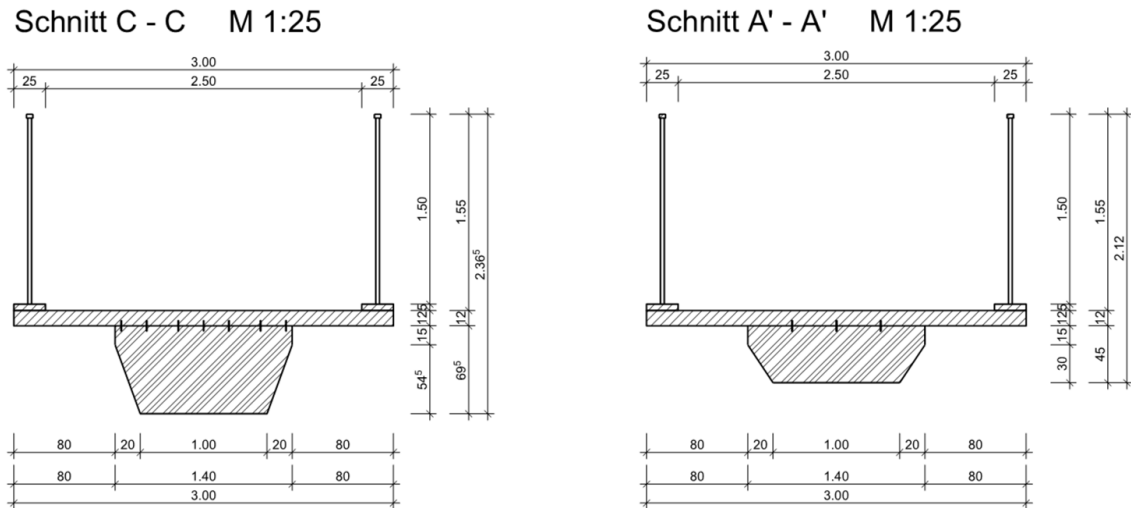


Figure 5: Cross section of the timber granite composite bridge

2.2. Life cycle consideration

The life cycle analysis for both variants is based on the assumption of a period of service of 80 years [2]. The main tasks consist of evaluating the economical as well as ecological costs of the structure holistically over the intended service life. A positive side effect of this consideration is that the running costs can be minimised during the service life. The reduction of usage cost through low maintenance and operating costs plays a major role as they can easily amount to twice the construction costs [3].

The estimated costs of both variants were comparable and move in the context of around 2400 €/m². The economic analysis assumes that the costs for the renewal of the bridge equipment as well as the tests are identical for both variants. However, for the timber-concrete composite variant, a 1.5 times renewal of surface layer and waterproofing is necessary over the service life of 80 years [4]. Considering this, the timber-concrete composite variant has higher maintenance costs as the timber-granite composite variant. For the ecological life cycle analysis, characteristic values are determined for the different service phases construction, operation, and demolition in order to be able to determine effects of the building on the environment. Based on the existing environmental product declarations, the two variants were compared only with regard to the construction and maintenance phases. For both variants a contribution to the storage of CO₂ could be proven due to the usage of timber and it turned out that both variants have similar environmental effects. Here, the timber-concrete composite variant performed slightly better during construction in the fields of energy consumption (PERT and PERTN) and Global Warming Potential (GWP) since a lot of energy is required for the mining, manufacturing, and transporting the slabs. If, however, the renewal of the roadway and the waterproofing over the service life is considered, the timber concrete composite variant loses a large part of the potential CO₂ storage. Furthermore, the consumption of non-renewable energy (PERTN) increases drastically (Fig. 6).

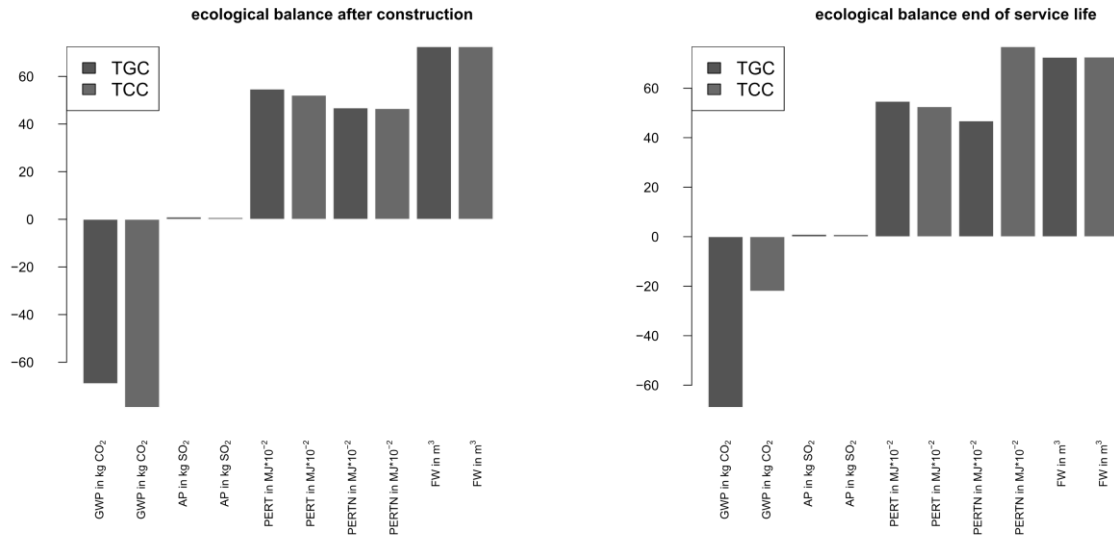


Figure 6: ecological comparison between construction phase and end of service life

3. Composite theory

3.1. General composite theory

In bridge construction, the number of cross sections that can be connected is limited to the bottom chord, usually a block girder made of glued laminated timber and the mineral based top chord. The degree of bonding achieved is limited by the lower barrier *no composite* and the upper barrier *rigid composite*. A *flexible composite* is created between these limits.

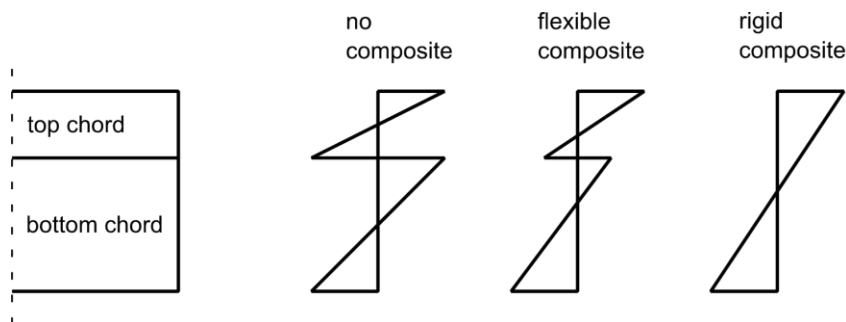


Figure 7: basic strain distributions of a two-part composite cross section

For timber-concrete composite structures in bridge construction, high stiffness of fasteners is decisive. Due to the larger span widths compared to slab structures in building construction, the fasteners need to transmit considerably higher shear forces while retaining a ductile failure. Furthermore, a high fastener stiffness leads to a high degree of bonding of the individual cross section and thus to a more effective use [5]. The aim is to utilize the minimum number of stiff load-bearing fasteners. This results in a discontinuous arrangement of the fasteners over the length of the composite girder with wider fastener spacings. The stiffness of the fasteners is also decisive for the cost effectiveness of a composite solution. To reduce costs in production and assembly as well as achieve a high degree of bonding it required to have as few stiff fasteners as possible.

3.2. Comparison of calculation methods

A discontinuous arrangement of fasteners bears the result that the calculation of the internal forces can no longer be carried out with the common “ γ -method” represented in EC 5. Framework solutions are established as an alternative to the calculation of yieldingly connected bending girders. They can be used to map both a continuous and a discontinuous bond in the joint. Depending on the model used, the effort for modelling the frameworks for the representation of discontinuous composite beams can increase considerably.

In order to handle this situation a possible truss model was developed by *Hartmann* and *Kneidel* [6]. In this truss model, the two chords are coupled with flexible diagonals which represent the medium stiffness of the composite. In order to force the same deformation of the chords, they are connected by pendulum rods.

Bergfelder [7] developed a further framework on the basis of a Vierendeel girder. The bond stiffness in the joint is represented in the framework by a flexible cantilever arm. The coupling of the cantilever arms to the top chord is done in a jointed connection to the top chord and to the bottom chord in a rigid connection.

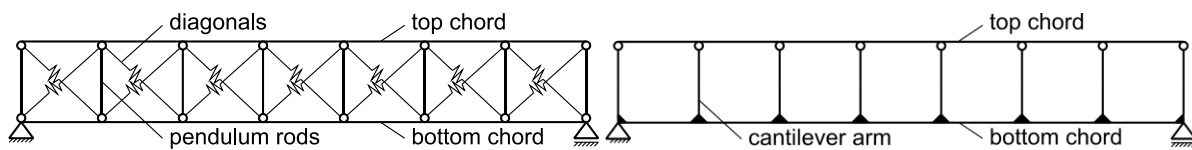


Figure 8: left: truss model, right: Vierendeel girder

Grosse, Hartnack, Lehmann and *Rautenstrauch* [8] developed a coupling bar system, the basic features of which resemble the Vierendeel girder according to *Bergfelder*. It divides the composite girder into chords with the properties of the individual cross sections and couples these by pendulum rods of infinite stiffness. In contrast to the Vierendeel girder model, cantilever arms with equivalent bending stiffness are placed at the points where the fasteners are attached to the chords and connected by a moment joint. A further framework solution was developed by *Kreuzinger* [9] that differs from the other three framework solutions in its approach to modelling. In contrast to the previous frameworks, the real beams are not represented, but the different stiffness components are assigned to different beams. This model is usually called shear analogy method.

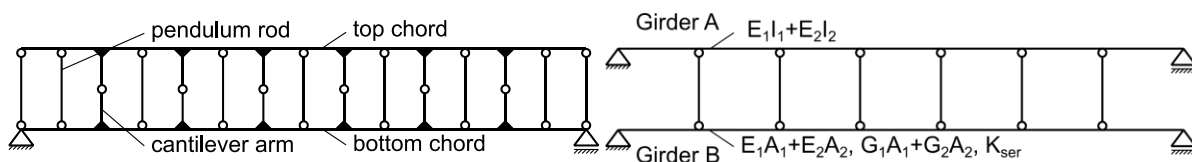


Figure 9: left: coupling bar system, right: model according to *Kreuzinger*

In order to estimate how much the distance between the coupling points influences the accuracy of the results and to check the model's basic suitability for a later calculation they were compared to each other in a parameter study. For the parameter study, a beam on two props with overhang was used as system. For this system, the exact results of the internal forces and deformations from different load cases exist as a solution to the differential equation of yieldingly connected bending girders. The model according to *Bergfelder* for small distances of the coupling points turned out to deliver a deviation of up to 32% at the determined internal forces from the exact result. The shear analogy method showed deviations of up to 9% regarding the internal forces. The framework solutions according to *Kneidel* and *Hartmann* as well as *Grosse et al.* showed only minor deviations of less than 5%.

For the later calculation of the two bridge variants, the coupling bar system according to Grosse et al. was selected since this framework solution represents the internal forces and connecting forces more clearly than the truss model. With this model, the internal forces and deformations were then determined for the timber-concrete composite and the timber-granite composite bridge. Both variants including the fasteners were verified in the ultimate limit state of load-bearing capacity and serviceability.

4. Summary and Outlook

A comparison of both variants shows, that if the service life is taken into account there are economic and ecological advantages in favour of the timber-granite composite construction. The renewal of the road surface of the timber-concrete variant leads to higher maintenance costs and worsens the ecological balance with regard to the CO₂ storage potential. In addition it leads to an increase in energy consumption over the lifetime of the timber-concrete composite bridge.

The static analysis of the two bridges shows that both variants are technically feasible. Furthermore, the timber-granite composite bridge achieved significantly higher stiffness in the final state and thus has a positive effect on the serviceability in the final state. That is due to the lack of creep deformation of the granite at hand. The increase in deformation compared to the initial condition of the timber-granite construction is only 14%. In comparison, the deformation of the timber-concrete construction increases by 80% in the final state. Future projects in the field of timber-granite composites need to investigate the actual behaviour when facing temperature fluctuations. Due to the internal static indeterminacy, the forced stresses from the temperature load might have a decisive influence on the utilisation of the cross sections. Furthermore, the concrete arrangement of the fasteners as well as the exact calculation and illustration of discontinuous composite structures need to be further investigated.

However, the achieved high load-bearing capacity and rigidity, low maintenance costs, and the positive ecological effects over the entire service life shows the superiority of the timber-granite bridge construction over a timber-concrete composite construction. This promises to make further research into the substitution of concrete by granite to be a rewarding endeavour.

5. Bibliography

- [1] T. Zinke, Nachhaltigkeit von Infrastrukturbauwerken, Ganzheitliche Bewertung von Autobahnbrücken unter besonderer Berücksichtigung externer Effekte, Karlsruher Institut für Technologie, 2016.
- [2] M. Gerold, «Lebenserwartung und Unterhaltungskosten von Holzbrücken - eine aktuelle Studie», 2005.
- [3] K. Geißler, Handbuch Brückenbau, Berlin : Ernst & Sohn Verlag, 2014.
- [4] F. Vollrath und H. Tathoff, Handbuch der Brückeninstandsetzung, Erkrath: Verlag Bau+Technik, 2002.
- [5] A. Simon, Analyse zum Trag- und Verformungsverhalten von Straßenbrücken in Holz-Beton-Verbundbauweise, Weimar: Fakultät Bauingenieurwesen, Bauhaus-Universität Weimar, 2008.
- [6] H. Hartmann und R. Kneidel, «Träger mit nachgiebigen Verbund», *Bauen mit Holz*, April 1995.
- [7] J. Bergfelder, «Näherungsverfahren zur Berechnung allgemeiner zusammengesetzter hölzerner Biegeträger mit elastischem Verbund», *Der Bauingenieur*, 1974.
- [8] M. Grosse, R. Hartnack, S. Lehmann und K. Rautenstrauch, «Modellierung von diskontinuierlich verbundenen Holz-Beton-Verbundkonstruktionen, Teil 1: Kurzzeittragverhalten», *Bautechnik*, 2003.
- [9] H. Kreuzinger, «Platten, Scheiben und Schalen, Ein Berechnungsmodell für gängige Statikprogramme», *Bauen mit Holz*, 1999.

Calculation model for adhesive-bonded cross-laminated timber concrete composite elements

Georg Erlinger
FH Oberösterreich
Wels, Austria



Christoph Hackspiel
Camillo Sitte Bautechnikum Wien
Wien, Austria



FH-Prof. DI Dr. Karin Nachbagauer
FH Oberösterreich
Wels, Austria



Calculation model for adhesive-bonded cross-laminated timber concrete composite elements

1. Abstract

In a timber-concrete composite the concrete takes over the pressure and the timber the tensile forces. The connection between the two materials often done by means of screws or notches, transmits the shear forces. This paper presents two calculation models for **adhesive**-bonded cross-laminated timber concrete composite elements. The first model accounts for the calculation of the ultimate limit state and the second one for the serviceability limit state. The basis of these two models is the γ -method. Climatic changes in temperature and the relative humidity of the environment are considered in the analysis of the long-term-behaviour.

The material parameters for concrete were taken from ÖNORM EN 1992-1-1. For the adhesive, tests were carried out to determine the exact shear modulus. The time depended behaviour of timber is described using a rheological model. Since the material behaviour of timber is highly influenced by the moisture content, its accurate calculation is of great importance. Therefore, the moisture content was determined with the implicit difference method using Fick's law.

To validate the ULS Model, composite elements were loaded until failure. The recalculation has shown, that although the load is overestimated, the system rigidity can be predicted relatively well.

For the validation of the SLS Model, three composite slabs were loaded over a period of one year. The comparison with the calculation model shows, that the deformation behaviour can be predicted as well.

2. Introduction

The bonding technology have been used in many sections of our general life since many centuries. Therefore, in an economic and static view it makes sense to produce bonded timber concrete composite (TCC) elements. In this paper, two calculation models for those elements are presented. This is intended to contribute to the development of TCC systems.

3. Calculation Approaches

In the following section the calculation approaches, material-models, and methods which are integrated in the calculation models are presented.

3.1. Gamma-Method

This method is the basis for both models and was developed by Möhler [1] for the calculation of timber beams made out of single cross-sections connected elastically. It can be used analogous for TCC elements. The requirements for the usage of the γ -method are as follows: [2]

- Simple supported beam
- Uniform cross section
- Smearred connection
- Sinusoidal load

The sinusoidal load is in total almost like a uniformly distributed load. Hence, the method can be used for uniformly distributed loads with a negligible error. The following equations are for the calculation of a TCC element consisting of five parts – two longitudinal-, one cross-slat, one adhesive layer and a concrete slab. To describe the resilient connection on the second layer, the γ -values are used. γ_1 is calculated with equation (1) and refers to the concrete section. The second layer is held mental, because of that the value of γ_2 is

one. A value of one means rigid connection, whereas a value of zero means no connection. As a result, both the resilience of the composite joint and the traverse position in the cross laminated timber can be represented. The value γ_3 is calculated with equation (2):

$$\gamma_1 = \left(1 + \frac{\pi^2 E_1 A_1}{l_{ref}^2} \cdot \frac{d_{1,2}}{b G_{R,12}} \right)^{-1} \quad (1)$$

$$\gamma_3 = \left(1 + \frac{\pi^2 E_3 A_3}{l_{ref}^2} \cdot \frac{d_{2,3}}{b G_{R,23}} \right)^{-1} \quad (2)$$

In these equations E_1 denotes the modulus of elasticity of the concrete and A_1 the corresponding concrete cross-sectional area. The area is calculated by multiplying the height d_1 by the width of the composite cross-section b , which is identical for all the layers. E_3 and A_3 refer to the longitudinal slat 3 of the CLT cross-section. The reference length l_{ref} corresponds to the span of a simple supported beam. The adhesive layer thickness is denoted by $d_{1,2}$ and the associated shear modulus by $G_{R,12}$.

Figure 1 shows the definition of the distances on the composite element. The layer 2 is the first layer of the CLT plate and the layer 3 is the bottom layer. Layer 2,3 represents the shear-soft transverse layer of the CLT.

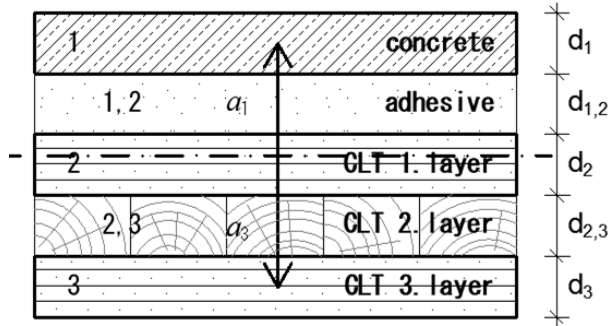


Figure 1: Assembly and definitions of a bonded timber-concrete element according to the Gamma-method.

The distances a_i are calculated with the equations (3), (4) and (5). [3]

$$a_2 = \frac{\gamma_1 \frac{E_1}{E_c} A_1 \left(\frac{d_1}{2} + d_{1,2} + \frac{d_2}{2} \right) - \gamma_3 \frac{E_3}{E_c} A_3 \left(\frac{d_2}{2} + d_{2,3} + \frac{d_3}{2} \right)}{\sum_{i=1}^3 \gamma_i \frac{E_i}{E_c} A_i} \quad (3)$$

$$a_1 = \left(\frac{d_1}{2} + d_{1,2} + \frac{d_2}{2} \right) - a_2 \quad (4)$$

$$a_3 = \left(\frac{d_2}{2} + d_{2,3} + \frac{d_3}{2} \right) + a_2 \quad (5)$$

E_c denotes the reference module, which can be chosen arbitrarily. It makes sense to equate the reference module with the modulus of elasticity of the CLT since the factor E_i/E_c in the CLT thus becomes one. In principle, the moment of inertia is calculated as for a homogeneous cross section, but the layers are weighted with the stiffness ratios and the Steiner content is additionally reduced with the gamma factor.

$$J_{eff} = \sum_{i=1}^3 \frac{E_i}{E_c} J_i + \sum_{i=1}^3 \gamma_i \frac{E_i}{E_c} A_i a_i^2 \quad (6)$$

3.2. Moisture distribution in timber

To calculate the moisture u in the timber, Fick's law was used for transient one-dimensional diffusion in the x -direction. [4]

$$\frac{\partial u}{\partial t} = \mathbf{D} \frac{\partial^2 u}{\partial x^2} \quad (7)$$

The preceding equation (7) can be derived from the mass flow q from [4]:

$$\mathbf{q} = -\mathbf{D} \cdot \nabla c \quad (8)$$

Where c is the concentration of water that can be assumed to be proportional to the moisture content u , and \mathbf{D} is the diffusion tensor. This tensor has only diagonal entries, namely the coefficients of diffusion between the individual layers. For the calculation of the coefficient of diffusion $D(u)$ there are several approaches. The approach to Hanhijärvi [4] for spruce wood depends only on the moisture content of the wood u and is calculated as:

$$D(u) = 8,0 \cdot 10^{-11} \cdot e^{4,0 u} \quad [m^2/s] \quad (9)$$

Since the coefficient of diffusion $D(u)$ is dependent on the wood moisture u , this has the effect that at a higher wood moisture leads to the increase in the diffusion of the wood. This causes a faster transport of moisture through the wood. Conversely, at a lower wood moisture the diffusion and the moisture transport speed are lower. The calculation of the moisture in the layers would be nonlinear, since the diffusion coefficient changes in each layer. However, the wood moisture changes only in small steps and $D(u)$ is a very small number. Therefore, the coefficient of diffusion can be assumed to be constant with a negligible error.

Equation (7) can be solved for $u = u(x, t)$ using the implicit difference method. In this case, the moisture $u(x_i, t_m)$ in each wood layer x_i is determined at each time t_m . Equation (7) is approximated by means of difference quotients as follows:

$$\begin{aligned} & \frac{u(x_i, t_{m+1}) - u(x_i, t_m)}{t_{m+1} - t_m} \\ &= D(u(x_{i-1,i}, t_{m+1})) \frac{u(x_{i-1}, t_{m+1}) - u(x_i, t_{m+1})}{(x_{i-1} - x_i)^2} \\ & - D(u(x_{i,i+1}, t_{m+1})) \frac{u(x_i, t_{m+1}) - u(x_{i+1}, t_{m+1})}{(x_i - x_{i+1})^2} \end{aligned} \quad (10)$$

Whereby the coefficient of diffusion of layer x_i on layer x_{i+1} at time t_{m+1} is abbreviated to $D(u(x_{i,i+1}, t_{m+1})) =: D_{i,m+1}$. For equidistant time and slice discretization, a simplified notation of

$t_{m+1} - t_m = \Delta t$ and $x_i - x_{i+1} = \Delta x$ and $d_{i,m+1} = \frac{D_{i,m+1} \Delta t}{(\Delta x)^2}$ are used to represent equation (10) as:

$$u_{i,m+1} - u_{i,m} = d_{i-1,m+1}(u_{i-1,m+1} - u_{i,m+1}) - d_{i,m+1}(u_{i,m+1} - u_{i+1,m+1}) \quad (11)$$

If we rearrange equation (11) so that all quantities at time t_{m+1} are on the same side of the equation, the result is:

$$u_{i,m+1} - d_{i-1,m+1}u_{i-1,m+1} + d_{i-1,m+1}u_{i,m+1} + d_{i,m+1}u_{i,m+1} - d_{i,m+1}u_{i+1,m+1} = u_{i,m} \quad (12)$$

This equation must hold for each layer x_i for $i = 1, 2, \dots, n-1$ and thus results in a linear equation system with the unknowns $u_{i,m+1}$ for $i = 1, 2, \dots, n-1$ at the time t_{m+1} . For the efficient solution of the linear system of equations, care must be taken that the correct sorting of the layers produces a tridiagonal matrix and is sparse. In addition, the following conditions must be considered for the right-hand side of the linear system of equations:

The moisture of the layer n is equal to the moisture in the layer $n-2$ due to symmetry conditions. At the edge of the board, the moisture content of the wood is equal to the compensation humidity u_{RH} , which depends on the environment.

In Figure 2, the half of a board cross-section is is shown for illustrative purposes. Details are described in the work of Fortuin [5] in chapter 4.1.

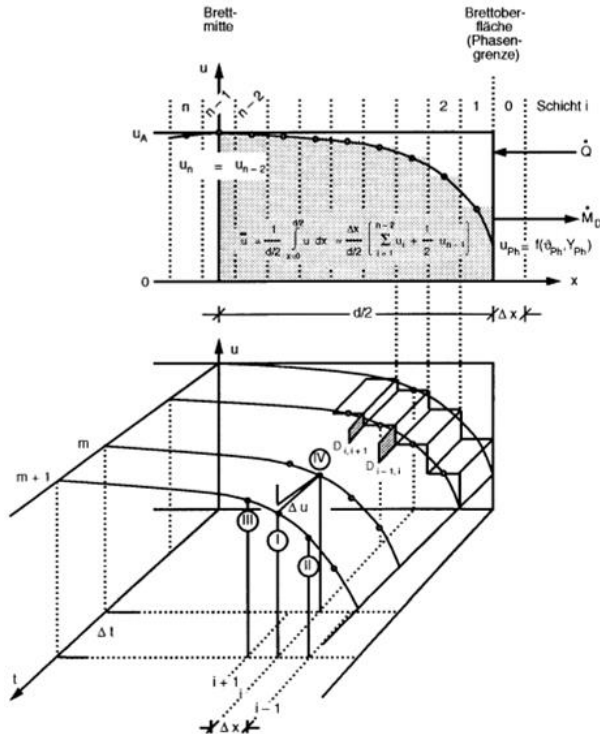


Figure 2: Moisture distribution in the wood cross-section with the implicit difference method [5]

3.3. Material-model for CLT

In this work the model of Eisenhut [6] was used for the modelling of the cross laminated timber. This corresponds to the material model according to Fortino [7] which was extended by the proportion of the thermal expansion α_T . Figure 3 shows the model.

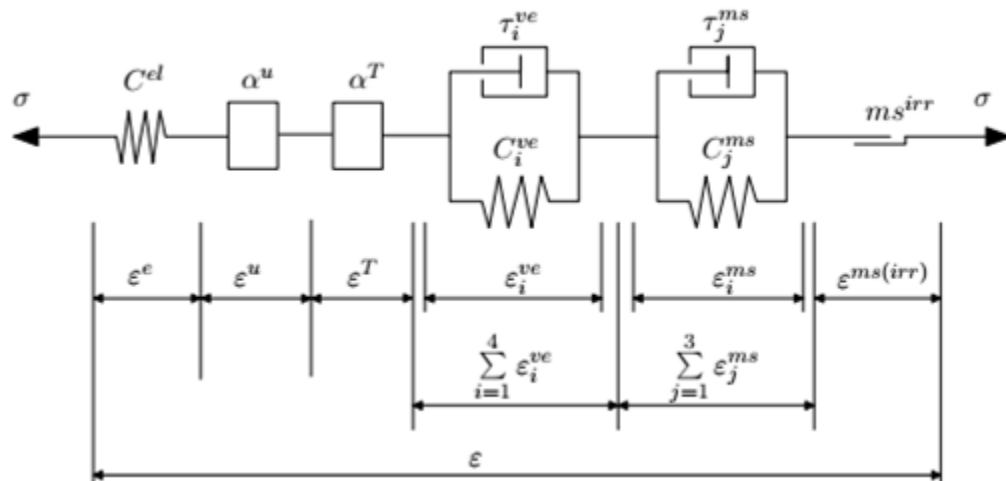


Figure 3: Material model by Fortino, extended by the temperature term α^T [6]

The total distortion is calculated using equation (13) and is dependent on the time t , the temperature T and the wood moisture u .

$$\varepsilon = \varepsilon^e + \varepsilon^u + \varepsilon^T + \sum_{i=1}^4 \varepsilon_i^{ve} + \sum_{j=1}^3 \varepsilon_j^{ms} + \varepsilon^{ms,irr} \quad (13)$$

with:

- ε^e elastic strains
- ε^u expansion due to moisture
- ε^T expansion due to temperature
- ε_i^{ve} viscoelastic strains
- ε_j^{ms} mechano-sorptive strains
- $\varepsilon^{ms,irr}$ irreversible mechano-sorptive strains

For the calculation of the individual terms refer to [6]. For the development of the long-term behaviour model, the viscoelastic and mechano-sorptive values of Fortino [7] and not of Eisenhut were used.

The creep number for the CLT is calculated to:

$$\varphi_{BSP,n-1} = \frac{\varepsilon(t)_{n-1}}{\varepsilon_0^e} - 1 \quad (14)$$

The elastic initial strain ε_0^e is calculated by dividing the stress by the modulus of elasticity at time $t = 0$. With an increase in load, the initial strain must be recalculated, as the stress also increases. The total strain is calculated using equation (13) and changes with time. Since the strains in the calculation model have some unrealistic outliers and these lead to rashes in the calculation, the creep was limited. The lower limit was set -0.1 and should allow the wood to increase the modulus of elasticity when, e.g., the ambient humidity decreases. At the top, the creep number was limited to 1.0 (see Wallner-Novak [3]).

4. Development of the calculation models

Both calculation models for the adhesive composite of CLT and concrete are based on the γ -method. However, this was modified for the ULS model in order to consider further influences. Figure 1 shows the structure of the adhesive TLC-concrete composite construction, which serves as the basis for both models. Similarly, the thickness of the individual layers is identical for both models. Table 1 shows the individual layer thicknesses, moduli of elasticity and intrinsic weights for the experiments. For the long-term behaviour tests, a C25/30 concrete and a spruce CLT of strength class C24 were used. The load-bearing tests, on the other hand, used a concrete C40/50 and a CLT of grade C30. The computational models were later validated with the experiments.

Table 1: Layer thicknesses, moduli of elasticity and dead weights for the model ULS and SLS

Layer	Thickness [mm]	Modulus of elasticity [N/mm ²]		Density [kN/m ³]	
		ULS	SLS	ULS	SLS
concrete	70	35,220	31,476	25	25
adhesive	3	67.2	67.2	-	-
1. CLT layer	40	11,000	12,000	4.2	4.6
2. CLT layer	40	370	400	4.2	4.6
3. CLT layer	40	11,000	12,000	4.2	4.6

4.1. Model – Ultimate Limit Strength

The model for the ultimate limit state is for calculating the stress in the individual layers. It also allows a prediction of the bending stiffness of the composite component, as well as an estimation of the maximum load.

4.1.1. Normal Stress

The normal stress in the single layers is calculated by equation (15) for the normal force component and equation (16) for the bending moment component.

$$\sigma_i = \frac{\gamma_i E_i a_i M}{E J_{eff}} \quad (15)$$

$$\sigma_{m,i} = \frac{0,5 E_i d_i M}{E J_{eff}} \quad (16)$$

The boundary stress per layer results from the addition of the two terms.

4.1.1. Shear Stress

The shear stress is calculated with the equation (17).

$$\tau_i = -\frac{V_z(x) S_y(z)}{J_{eff} b} \quad (17)$$

$V_z(x)$ describes the applied lateral force, J_{eff} the effective moment of inertia and $S_y(z)$ the static moment. The static moment depends on the layer which is considered in cross section and varies with the distance z of the single layer to the ideal overall centre of gravity.

4.2. Model – Serviceability Limit Strength

This chapter explains the creation of the SLS model and the effects of temperature, humidity, and time on the deflection of the composite component. The span of the specimen used to validate the model was 4.80 m and the additional load, in addition to its own weight, was 2.21 kN/m². There was no variable load, but additional load was applied later in the long-term study, increasing the overall load to 4.42 kN/m².

The total deformation of the composite section is calculated using equation (18). A positive value means a downward deflection and a negative value means an upward deflection. This is composed of the deformation according to self-weight w_G , additional load w_Q , shrinkage of the concrete w_S , swelling or shrinkage of the CLT slab w_{QS} , and according to the temperature differences between the two building materials wood and concrete w_T together.

$$w(t) = w_G + w_Q + w_S + w_{QS} + w_T \cdot 0,05 \quad (18)$$

The temperature deformation is multiplied by a factor of 0.05, since the parameter study has shown that the chosen approach reproduces the course of the vertical deformation well, but in a different order of magnitude. [8]

The deformation due to dead weight and additional load is determined by the same equation (19).

$$w_{G,Q} = \frac{5 q_{G,Q} l^4}{384 E J_{eff}} \quad (19)$$

4.2.1. Shrinkage and Creep of the Concrete

The deformation w_S due to shrinkage of the concrete is simulated via the equivalent force F_0 and is calculated according to equation (21). The equivalent force follows from the multiplication of the shrinkage strain ϵ_{cs} with the tensile stiffness EA of the concrete. If the equivalent force is multiplied by the distance a_1 (see equation (20)), the shrinkage moment M_S follows. The distance a describes the distance between the geometric centre of gravity of the concrete slab and the CLT slab.

$$a_1 = a \frac{EA_{BSP}}{EA_1 + EA_{BSP}} \quad (20)$$

$$w_S = \frac{M_S \cdot l^2}{8 \cdot E J_{eff}} \quad (21)$$

The creep of the concrete was determined by ÖNORM EN 1992-1-1 and affects only the modulus of elasticity of the concrete. The creep count is influenced by the temperature, time, and relative humidity of the environment.

4.2.2. Swelling and Shrinkage of CLT

The wood moisture content is calculated using equation (7) in each individual layer. This calculation was performed with the program Wolfram Mathematica 11.1. The CLT slab is hereby divided in total into 12 partial surfaces, whereby each partial surface is one centimetre thick. The layer 0 corresponds to the lower edge of the CLT slab and the layer 12 of the upper edge. For the calculation, however, the humidity was averaged for each layer of the CLT slab, since a varying modulus of elasticity is calculated for these layers. The averaging is done by reading the moisture at the boundaries between the CLT layers. The moisture in layer 1 corresponds to the equilibrium moisture content and depends on the ambient conditions. For layers 4, 8 and 12, the values are read from the Mathematica file. For this purpose, a function is set up according to the time as a function of the input variable - the difference of the equilibrium moisture Δu_{RH} (see Figure 4). The coefficient of diffusion according to Hanhijärvi was used at a constant wood moisture content of $u = 13\%$, which is shown in Figure 4 as greatly exaggerated due to better readability. Although this factor was calibrated on a spruce wood, it is also suitable for the pinewood used in the experiments. Since the density of the pine is slightly higher than that of the spruce, the factor should be slightly lower. However, the exact value of Hanhijärvi was used for the calculation model, because no corresponding values were found in the literature for pinewood. However, the associated error is small because the factors found in the literature for spruce are very different and have a low value.

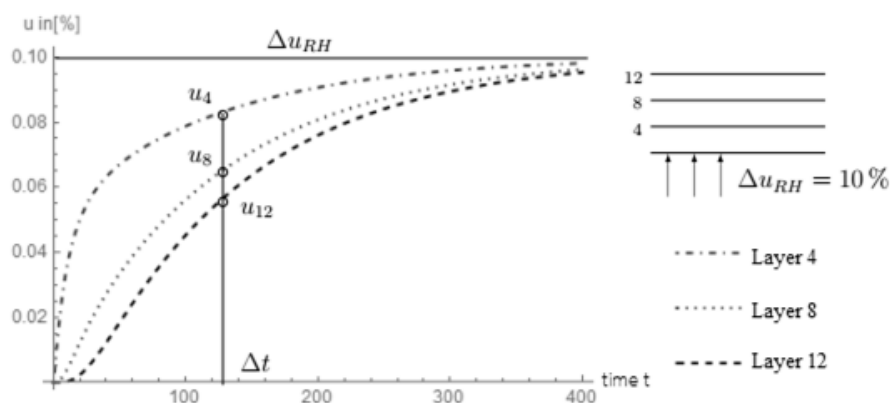


Figure 4: Moisture history in layer 4, 8 and 12 versus time with the increased diffusion factor by Hanhijärvi (difference of the balance moisture is 10%) [8]

The equilibrium moisture is used as the difference for the calculation. The wood moisture of the 12th layer for measurement $n-1$ is subtracted from the equilibrium moisture content for measurement n . As only the difference is used for the calculation of the function, the start vector with the constant humidity is set to zero. The schematic sequence is shown by way of example for the calculation of the wood moisture in Table 2.

Table 2: Schematic sequence of the moisture calculation. (1st index = layer, 2nd index = measurement)

Measurement	u_{RH}	Δu_{RH}	Δt	u_1	u_4	u_8	u_{12}	Calculation
0	13 %	0 %	0 h	13,0	13,0	13,0	13,0	$u = \text{konst.}$
1	15 %	2 %	1 h	13,8	13,3	13,0	13,0	$\Delta u_{RH} = u_{RH,1} - u_{12,0}$
2	16 %	3 %	8 h	14,5	14,0	13,1	13,0	$u_{4,2} = u_{4,1} - u_{4,Fkt}$
...
n	$u_{RH,n}$	Δu_n	Δt_n	$u_{1,n}$	$u_{4,n}$	$u_{8,n}$	$u_{12,n}$	

The difference of the equilibrium moisture Δu_{RH} in the second measurement gives a value of 3%. This follows from the calculation of $u_{RH} = 16\%$ minus the moisture in the twelfth layer at the first measurement ($u_{12;1} = 13\%$). In layers 4, 8 and 12, the moisture is read out at the time Δt in the function suitable for Δu_{RH} (see Table 2) and added to the value u_i of the previous measurement. Thus, the value $u_{4;2}$ of the second measurement is calculated from the sum of $u_{4;1}$ of the first measurement and the value u_4 at the time Δt

of the function for the fourth layer at the Δu_{RH} of the second measurement. The functions are stored in Excel with the values of the data points from Mathematica in the respective layers. The data was read into Excel for a time horizon of 720 hours (equivalent to one month).

For the swelling and shrinkage of the CLT slab, the moisture change in the respective longitudinal position is averaged and used to calculate the resulting strain ε_{QS} to:

$$\varepsilon_{QS} = \Delta u \cdot s \quad (22)$$

The shrinkage s of softwood in the longitudinal direction is 0.5% per % change in wood moisture Δu . The distortion ε_{QS} multiplied by the tensile stiffness of the respective layer EA_i gives the force $F_{QS,i}$ which arises as a result of swelling or shrinkage of the wood in the position of the CLT slab. The moment M_{QS} acting on the composite section is calculated from the sum of the forces $F_{s,i}$ multiplied by their distances a_i to the center of gravity of the concrete:

$$M_{QS} = \sum_{i=1}^2 F_{QS,i} \cdot a_i \quad (23)$$

Therein a_i describes the geometric distance between the centre of gravity of the layer i of the CLT plate to the centre of gravity of the concrete slab. The deflection due to the swelling or shrinkage of the CLT is calculated exactly the same as before the deflection due to shrinkage of the concrete (see equation (21), only the moment M_s is replaced by M_{QS}).

4.2.3. Temperature Change

A change in temperature leads to an expansion or compression of the concrete and the wood. Since these materials have different linear thermal expansion coefficients α_T ($\alpha_T^{concrete} = 12 \cdot 10^{-6} [K^{-1}]$; $\alpha_T^{timber} = 3,75 \cdot 10^{-6} [K^{-1}]$), there is a difference in expansion of the two building materials, and subsequently, to the deflection of the composite cross-section. As the temperature increases, the concrete expands more than the underlying CLT. As a result, the composite cross-section is bent upwards and there is a further reduction in the deflection. Similarly, a concrete slab heated at the top can be considered, which leads to the same effect. If, conversely, the temperature decreases, then the concrete shortens more than the CLT, which in turn leads to an increase in the deflection of the composite component. The separate strains of the individual building materials are calculated to:

$$\varepsilon_{T,i} = \alpha_{T,i} \cdot \Delta T \quad (24)$$

If a temperature increase occurs, the temperature change ΔT is positive. The difference in the thermal expansions between concrete and CLT is multiplied by the tensile strength of the concrete EA_1 :

$$F_T = (-\varepsilon_{T,1} + \varepsilon_{T,2}) \cdot EA_1 \quad (25)$$

Since an increase in the temperature leads to a greater expansion of the concrete than that of the CLT and an upward bend (negative deflection), the expansion of the concrete must be set negative. The expansion of the CLT is subtracted from the concrete expansion. By multiplying the distance a_1 (see equation (20)) by the force F_T , the moment due to the temperature change M_T is calculated. Finally, with moment M_T , the deflection is calculated as in equation (21).

5. Validation of the Calculation Models

In the following, the test results of the directly bonded specimens are compared with the calculation results of the two models. In the process, the deviations are discussed in more detail and approaches are reconsidered or, where necessary, analytically adapted.

5.1. Model – Ultimate Limit Strength

The ULS model is used to estimate the load bearing capacity of adhesive CLT-concrete composite elements. In order that the 4-point bending test can be reproduced accurately, the load in the computer program is gradually increased and the deformation in the centre of the plate is continuously calculated. The load is successively increased, and the stresses are evaluated in the layers until one of the maximum allowed stresses of the three materials is exceeded. These maximum allowed stress values correspond to the characteristic mean values of the building materials.

The recalculation of the experimental tests in Figure 5 shows that the CLT-concrete composite element is too rigid. However, since the input parameters are not known exactly, each are increased or decreased by 20%, while the other parameters remain at the initial value. A reduction of the modulus of elasticity of the CLT 20% already gives the course from the experiments very accurately. A change in the shear modulus of the adhesive or the CLT has only a minor effect on the overall rigidity of the construction and is not depicted in Figure 5.

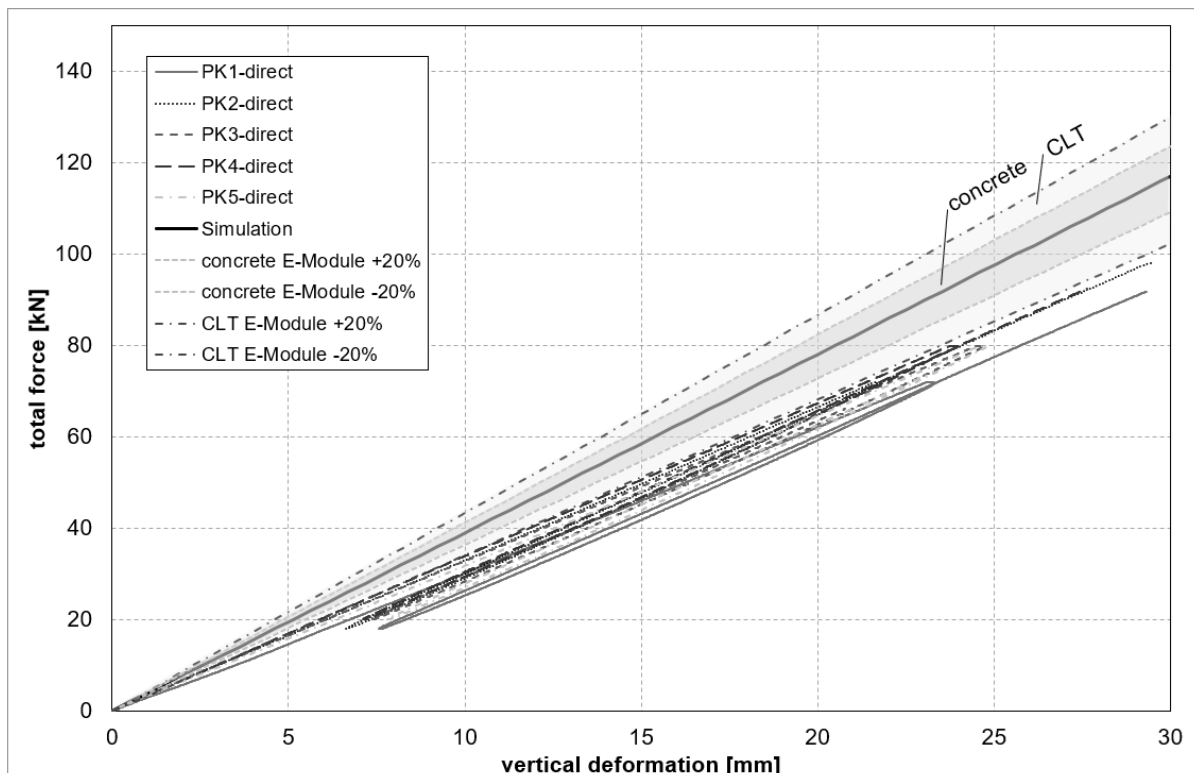


Figure 5: Comparison of results from the calculation model and the load-bearing test of directly bonded specimens

The comparison between the mathematical model and the test results of the directly bonded specimens in Figure 5 shows that the γ -method depicts the specimen too stiff. The difference in the deformations between the mean value from the tests (= 100%) and the simulation at 10% and 40% of the maximum load is on average 14%.

Thus, the calculation model with the gamma method is not as accurate because the loads are overestimated. This is due to the fact that the exact input parameters of the calculation model, such as the rolling shear modulus of the CLT or the modulus of elasticity of the concrete are not known precisely. When varying the parameters, however, it becomes apparent that the course can be reproduced fairly accurately. In addition, the γ -method is not optimal for two single loads, since the derivation assumes a sinusoidal load.

5.2. Model – Serviceability Limit Strength

The comparison of the calculation results from the computer model SLS with the measurement results of the sample specimens, which were completely bonded, is shown in the left figure of Figure 6.

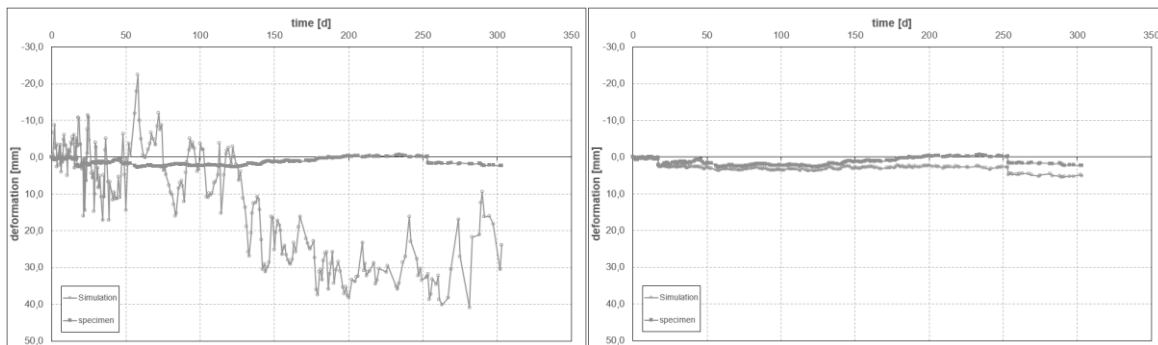


Figure 6: First comparison of results gained by the calculation model and by the experiment (left: without adapted values; right: without mechano-sorptive parts)

First of all, there is a strong deviation between the model and the experiment, and the calculation model does not satisfactorily reflect the deformations of the experiment. The reason is the detection of the mechano-sorptive strain. This is calculated too high with the initially selected model approach and thus falsifies the result. If the mechano-sorptive strain is set to zero and the irreversible strain neglected, the simulation shows a similar, albeit downwardly shifted, deformation curve (see right figure in Figure 6).

Since the deformation curve still has a large deviation, the creep factor of the CLT was set to zero, as the chosen approach is not suitable for a creep calculation of the CLT. This is because the creep number already has the value 1.0 for the first time after a few days and fluctuates very strongly. This approach shows a further improvement of the deflection result, but the reduction of the deformation in the winter months is still not well understood, whereby there is already a certain similarity in the deformation lines between test and simulation. To achieve an even better approximation, the shrinkage deformation of the concrete is multiplied by a factor of 0.5. This can be explained by the addition of additives in concrete production in the precast plants which reduce the shrinkage process by up to 50%. The average deviation between the predicted and the real deformation of the composite is now 126% and the median 51% based on the experiment. These values make clear that the long-term influences with the selected approaches are not suitable for the exact simulation of a long-term test.

However, a better approximation of the deflection is achieved if the long-term behaviour of the concrete - both the shrinkage and the creep - is completely disregarded. This can be justified by the short period of observation, because in this period any creep deformations do not yet occur in size, as the calculation according to the standard suggests. The complete elimination of the deformation due to concrete shrinkage can in turn be attributed to the fact that the precast concrete slab was stored for a certain time until it was connected to the CLT slab. During this period, the shrinkage process of the precast concrete slab was almost completed, as a result of which there was no longer any noticeable shrinkage of the concrete at the composite cross-section.

The course of the deformation at the beginning as well as substantial increases and decreases are now very well reflected by the calculation model. However, the deformation decrease in the period of 130 to 250 days is not detected in the size as it occurs in reality. The deformation increases at the initial load and at the increase of the load will now be almost exactly reproduced in terms of size. Further improvement in the result is possible when the shear modulus of the adhesive is increased. In shear tests, the mean shear modulus was 24 N/mm². In comparative compression tests, a modulus of elasticity of 475 N/mm² was determined, which corresponds to a shear modulus of 170 N/mm² for a transverse expansion coefficient of 0.4. The shear modulus was therefore increased from 24 to finally 97 N/mm². This corresponds to the average of 24 and 170 N/mm². In this final variant (see Figure 7), the average deviation has decreased by 82%. The deviation between

the prediction by the calculation model and the real experiment is now 44% and the median at 8% deviation.

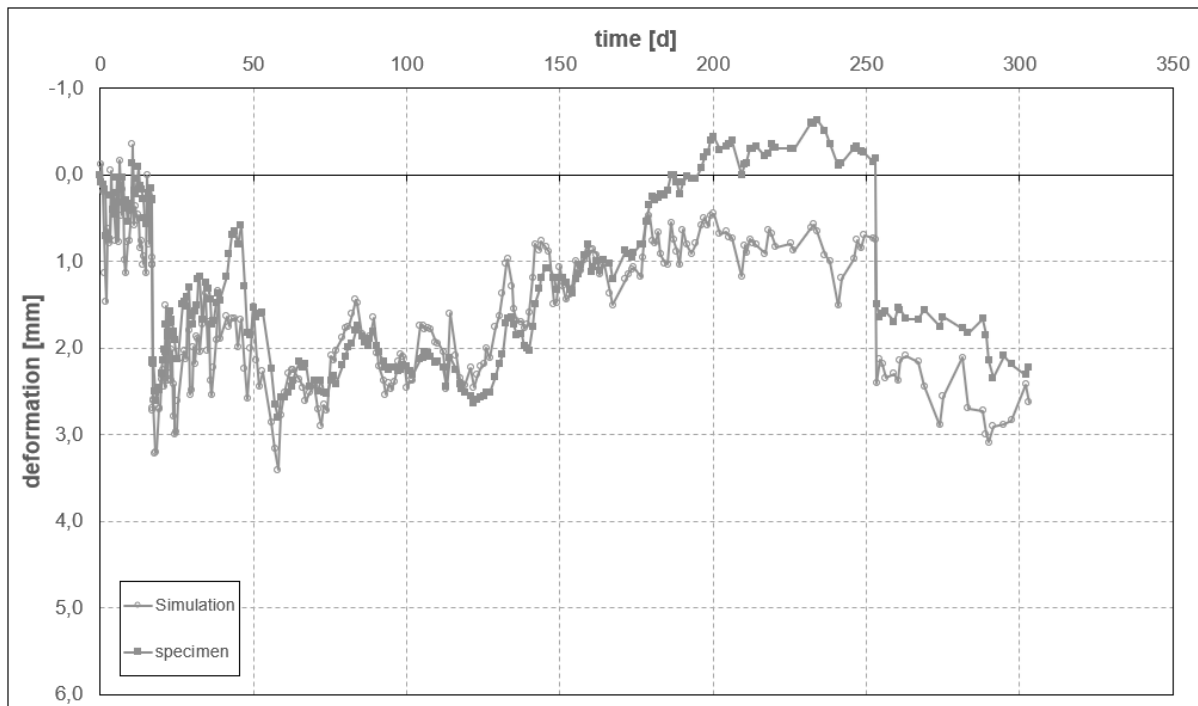


Figure 7: Comparison of experimental and simulation results disregarding the creep of the CLT element and the time-dependent behaviour of the concrete (creep and shrinkage). The shear modulus of the adhesive was increased to 97 N/mm².

In summary, for the model SLS for the bonded composite element, it can be said that the initial deformation is reproduced very well, but the strong reduction in deflection with the model is not yet adequately captured. The reason for this could be that the assumed coefficient of diffusion of Hanhijärvi differs significantly from the value occurring in reality. At the end of the experiment, the difference between measurement and simulation was 0.4 mm, which corresponds to a deviation of 18% (test = 100%).

6. Conclusion

In this work, two calculation models for adhesive CLT-concrete composite elements were presented. The model validation shows that the γ -method with the additional approaches chosen in this work is only conditionally suitable for an exact prediction of the long-term behaviour. It should be noted, however, that the results of the computational model depend very much on the input parameters and that they were not all accurately known or could not be determined from the real experiments. The simulation of the carrying capacity with the γ -method certainly shows potential, but this is also very much dependent on the model input parameters. In general, the variant of the adhesive CLT-concrete composite construction can be classified as very viable and efficient. For the long-term behaviour, longer test periods are necessary in order to be able to make a reliable statement about the creep behaviour and subsequently about the creep factor of the construction. For an adequate calculation model, the most accurate determination of the input parameters is of the utmost importance. Nonetheless, the models presented here are suitable for pre-dimensioning adhesive wood-concrete composite floors, as well as estimating the load and deflection.

7. Literatur

- [1] *Möhler, K.*: Über das Tragverhalten von Biegeträgern und Druckstäben mit zusammengesetzten Querschnitten und nachgiebigen Verbindungsmitteln. TH Karlsruhe, Habilitation, 1956.
- [2] *Fernandez-Cabo, J.L.; Fernandez-Lavandera, J.; Diez-Barra, R. et al.*: The flexibility matrix of timber composite beams with a discrete connection system.
- [3] *Wallner-Novak, M.; Koppelhuber, J.; Pock, K.*: Brettsperrholz Bemessung – Grundlagen für Statik und Konstruktion nach Eurocode, pro:Holz Information,, 2013.
- [4] *Hanhijärvi, A.*: Modelling of creep deformation mechanisms in wood. Espoo, Helsinki University of Technology. Technical Research Centre of Finland., Dissertation, 1995.
- [5] *Fortuin, G.*: Anwendung mathematischer Modelle zur Beschreibung der technischen Konvektionstrocknung von Schnittholz. Hamburg, Universität Hamburg, Dissertation, 2003.
- [6] *Eisenhut, L.*: Geklebter Verbund aus Holz und hochfestem Beton - Untersuchungen zum Langzeitverhalten, Schriftenreihe Bauwerkserhaltung und HolzbauHeft 7, Kassel University Press, Kassel, Hess, 2016.
- [7] *Fortino, S.; Mirianon, F.; Toratti, T.*: A 3D moisture-stress FEM analysis for time dependent problems in timber structures. *In: Mechanics of Time-Dependent Materials* 13 (2009), Heft 4, S. 333-356.
- [8] Georg Erlinger: Rechenmodelle für geklebte Holz-Beton-Verbundkonstruktionen. Wels, University of Applied Sciences Upper Austria, Masterarbeit, 2019.

Investigation of lateral torsional buckling of timber beams subjected to combined bending and axial compression

Nico Köppel
Institute of Structural Design
University of Stuttgart
Stuttgart, Deutschland



Janusch Töpler
Institute of Structural Design
University of Stuttgart
Stuttgart, Deutschland



Prof. Dr.-Ing. Ulrike Kuhlmann
Institute of Structural Design
University of Stuttgart
Stuttgart, Deutschland



Investigation of lateral torsional buckling of timber beams subjected to bending and axial compression

1. Motivation

Due to the increasing demand for long-spanning material-efficient timber structures, the design of slender members is getting more and more important. Trussed beams for example are ideal for big spans because of their low and efficient material consumption (Figure 1). These structures are typically loaded by a combination of normal force, shear force and bending moment. While short beams reach the maximum load bearing capacity due to exceeding of the maximum tensile and compressive strength (cross-section failure), stability failure is usually dominant for slender members. This is characterized by excessive deformations. And the resulting additional internal forces due to imperfections and effects of second-order theory, that may exceed the load bearing capacity. Latest investigations [1] to [4] have shown that the design methods provided by Eurocode 5 [5] for lateral torsional buckling of timber beams subjected to combined bending and compression tend to be conservative and do not allow an economic design.

Eurocode 5 provides two design concepts for slender timber members, where one is the effective length method and the other is one based on calculations of second order theory. In both methods the material specific behaviour of timber is highly simplified. By taking the elasto-plastic material behaviour under compression and the size effect on the tensile strength into account, high reserves of the load-bearing capacity can be activated for slender timber beams.

This material specific behaviour of timber can be considered either in numerical (FEM) or analytical models. The generated results can be used for the verification of the design formulas of EC5 [5]. Analytical models have proven to be very powerful in the past [6],[7] and are also the basis of the effective length method for lateral torsional buckling in current EC5 [8].

However, the mentioned and significant material specific behaviour of timber has not yet been adequately captured with these models.



Figure 1: Trussed beams subjected to bending and compression, Lignotrend Produktions GmbH [9]

In this paper the results of a master thesis at the University of Stuttgart [4], in which an analytical calculation method for the investigation of these effects on slender and especially medium slender timber members was developed, are presented.

Within this newly developed calculation method, stability verification for lateral torsional buckling according to second order theory is combined with approaches, which take into account the plasticizing of timber under compression and the size effect on the tensile resistance.

In this paper it is shown that plasticizing under compression and the size effect have a significant impact on the load bearing resistance of imperfection-sensitive timber structures. With the developed and in this paper presented analytical model it can be shown that the effective length method is partly very conservative, while verifications based on calculations according to second order theory provide good approximations to the load bearing capacity with even potential for optimization.

2. Calculation proceeding

2.1. Material specific behaviour

For modelling the material behaviour of timber, the mechanical models described by *Hörsting* [3] are used. There both, plasticizing of timber under compression and size effect on the tensile strength, are included when calculating the load-bearing capacity of timber beams subjected to bending and axial compression.

Plasticizing under compression

Figure 2 shows the assumed idealized stress-strain behaviour of timber due to axial loading for the analytical calculations. For axial compression an elasto-plastic behaviour is assumed, meaning the cross-section starts plasticizing when the compressive strength is reached. There is no failure criterion implemented for compression. For axial tension, which occurs in this study due to bending and effects of second order theory, the behaviour is assumed to be linear elastic with brittle failure when reaching the tensile strength.

According to *Hörsting* [3] the internal forces N_x , M_y , M_z of a cross-section can be calculated when assuming a perfect elasto-plastic material behaviour (Figure 2) with the help of equations (1) to (3) on the basis of the relations shown in Figure 3.

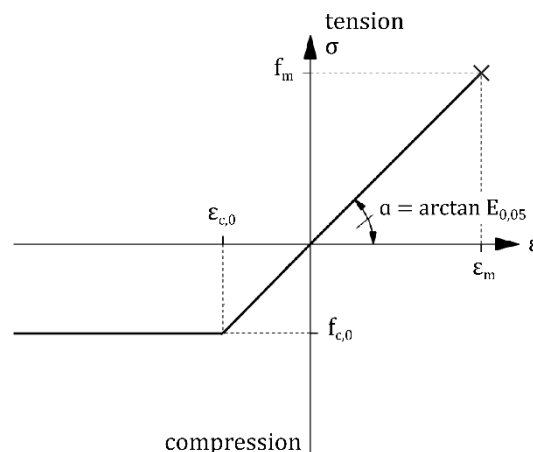


Figure 2: Schematic stress-strain graph of the assumed simplified material behaviour of timber due to axial loading [3]

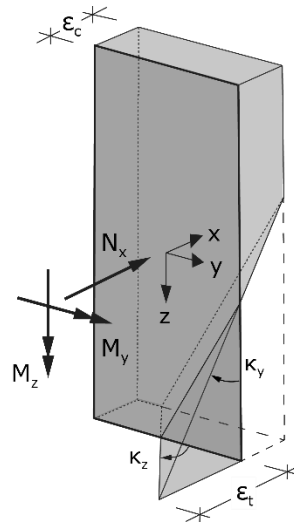


Figure 3: Curvatures (κ_y, κ_z) and elastic strains ($\varepsilon_c, \varepsilon_t$) for a random strain distribution due to combined bending and axial compression (M_y, M_z, N_x)

$$N_x = EA \cdot \left(\varepsilon_t - \kappa_y \frac{h}{2} - \kappa_z \frac{b}{2} \right) + \frac{E}{6\kappa_y \kappa_z} \cdot \left(\begin{array}{l} + \langle -(\varepsilon_t - \varepsilon_c - h\kappa_y - b\kappa_z) \rangle^3 \\ - \langle -(\varepsilon_t - \varepsilon_c - b\kappa_z) \rangle^3 \\ - \langle -(\varepsilon_t - \varepsilon_c - h\kappa_y) \rangle^3 \end{array} \right) \quad (1)$$

$$M_y = EI_y \kappa_y + \frac{E}{24\kappa_y^2 \kappa_z} \cdot \left(\begin{array}{l} - \langle -(\varepsilon_t - \varepsilon_c - h\kappa_y - b\kappa_z) \rangle^3 \cdot (\varepsilon_t - \varepsilon_c - h\kappa_y - b\kappa_z) \\ + \langle -(\varepsilon_t - \varepsilon_c - b\kappa_z) \rangle^3 \cdot (\varepsilon_t - \varepsilon_c - 2h\kappa_y - b\kappa_z) \\ + \langle -(\varepsilon_t - \varepsilon_c - h\kappa_y) \rangle^3 \cdot (\varepsilon_t - \varepsilon_c - h\kappa_y) \end{array} \right) \quad (2)$$

$$M_z = EI_z \kappa_z + \frac{E}{24\kappa_z^2 \kappa_y} \cdot \left(\begin{array}{l} - \langle -(\varepsilon_t - \varepsilon_c - h\kappa_y - b\kappa_z) \rangle^3 \cdot (\varepsilon_t - \varepsilon_c - h\kappa_y - b\kappa_z) \\ + \langle -(\varepsilon_t - \varepsilon_c - b\kappa_z) \rangle^3 \cdot (\varepsilon_t - \varepsilon_c - b\kappa_z) \\ + \langle -(\varepsilon_t - \varepsilon_c - h\kappa_y) \rangle^3 \cdot (\varepsilon_t - \varepsilon_c - h\kappa_y - 2h\kappa_z) \end{array} \right) \quad (3)$$

- with
- b width of cross-section (see Figure 5)
 - h height of cross-section (see Figure 5)
 - A cross-section area ($h \times b$)
 - I_y moment of inertia in direction of y
 - I_z moment of inertia in direction of z
 - E modulus of elasticity in longitudinal direction
 - ε_t elastic tensile strain (see Figure 3)
 - ε_c elastic compressive strain (see Figure 3)
 - κ_y curvature around the strong y -axis (see Figure 3)
 - κ_z curvature around the weak z -axis (see Figure 3)
 - $\langle \rangle$ Föppl-symbol

Size effect on the tensile strength

Timber is subject to a size effect due to its distinctive inhomogeneity like irregularities in growth and defects, which lead to deviations to the ideally straight grain orientation [10]. The more defects there are, the more sensitive timber is to brittle tensile failure; and the larger the stressed timber volume is, the higher the probability of local defects within the stressed volume is. Since the tensile stressed volume of a cross-section in the case of pure bending is smaller than in the case of pure tension, the tensile strength of timber in pure tension is lower due to the size effect. Additionally, the stress distribution within a cross-section plays an important role for the size effect, due to the probability of maximum stress and defects coming together. The size effect is taken into account by modifying the tensile strength throughout an iterative calculation. Here, the Weibull distribution [11] is

used to describe the relation of tensile and bending strength (eq. 4). The distribution parameter k_h of the Weibull distribution can be determined by solving equation (4) for k_h .

$$f_{t,0} = \left(\frac{1}{2 + 2k_h} \right)^{\frac{1}{k_h}} \cdot f_m \quad (4)$$

with $f_{t,0}$ tensile strength parallel to the grain
 f_m bending strength
 k_h distribution parameter

With the parameter k_h a modified maximum elastic tensile strain $\varepsilon_{t,mod}$ on the basis of the size effect can be determined iteratively using the cross-section curvatures and solving the following equation for $\varepsilon_{t,mod}$.

$$\varepsilon_m = \left[2 \cdot \frac{\varepsilon_{t,mod}^{(2+k_h)} - \langle \varepsilon_{t,mod} - \kappa_y h \rangle^{(2+k_h)} - \langle \varepsilon_{t,mod} - \kappa_z b \rangle^{(2+k_h)} + \langle \varepsilon_{t,mod} - \kappa_y h - \kappa_z b \rangle^{(2+k_h)}}{A \cdot (2 + k_h) \cdot \kappa_y \cdot \kappa_z} \right]^{\frac{1}{k_h}} \quad (5)$$

with ε_m elastic bending strain
 $\varepsilon_{t,mod}$ modified elastic tensile strain

Therefore, the modified tensile strength $f_{t,mod}$ can be calculated with

$$f_{t,mod} = \varepsilon_{t,mod} \cdot E \quad (6)$$

2.2. Calculation of internal forces

The following investigations are performed on imperfection-sensitive single span beams with fork bearings under combined bending moment around the strong axis and normal force (see Figure 4).

If it is assumed that the beam shown in Figure 4 is subjected to geometrical imperfections (Figure 5), the stability problem can be translated into a pure stress based mathematical

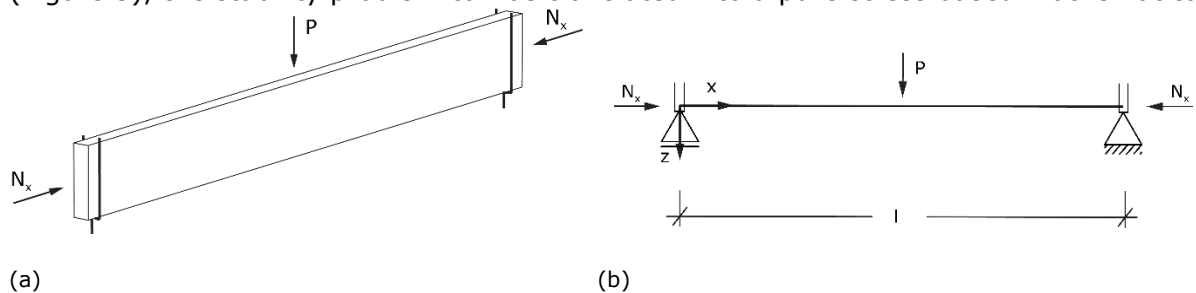


Figure 4: Three-dimensional (a) and two-dimensional (b) structural system of a timber beam with fork bearings, subjected to a compressive force N_x and a bending moment $M_{y,I}$ due to a single force P at midspan

problem. Due to imperfections (initial torsion ϑ and initial curvature in y -direction e_y) an additional internal bending moment around the weak z -axis $M_{z,II}$ occurs. An interaction of the initial curvature in y - and z -direction is neglected hereafter and $e_z = 0$ assumed. Equations (7) and (8) describe the internal forces due to second order effects, noting, that compressive forces are assumed positively.

$$M_{z,II} = \frac{M_{y,I} \cdot \vartheta + (N_x + N_{z,crit} \cdot \alpha_M^2) \cdot e_y}{1 - \alpha_{N,z} - \alpha_M^2} \quad (7)$$

$$M_{y,II} = \frac{M_{y,I} + N_x \cdot e_z}{1 - \alpha_{N,y}} \quad (8)$$

with $M_{y,I}$ external bending moment due to P (see Figure 4)

$M_{y,crit}$	critical bending moment
N_x	axial force (compression positive, see Figure 4)
$N_{y/z,crit}$	critical axial force in direction of y/z
$\alpha_{N,y/z} = N_x/N_{y/z,crit}$	factor of second order amplification for flexural buckling
$\alpha_M = M_{y,I}/M_{y,crit}$	factor of second order amplification for lateral torsional buckling
e_y	initial curvature in y-direction
$e_z = 0$	initial curvature in z-direction (neglected hereafter)
ϑ	initial torsion

2.3. Failure criterion

The following calculations are based on the assumption that a global failure of timber members at risk of lateral torsional buckling generally occurs when the tensile strength is exceeded in the tensile zone (Figure 6). If the compressive stresses reach the compressive strength, the cross-section begins plasticizing.

Equation (9) describes the failure criterion. It is to be noted that the compressive axial load N_x is taken into account with a negative sign in order to consider the favourable impact on the tensile stress verification.

$$-\frac{N_x}{A} + \frac{M_{y,II}}{W_y} + \frac{M_{z,II}}{W_z} \leq f_{t,mod} \quad (9)$$

2.4. Analytical calculations

A flow chart for the stress verification based on an analytical calculation of second order bending moments is shown in Figure 7. With this procedure a maximum bending moment $M_{y,I}$ for a timber beam of specific dimensions and axial loading can be determined.

First, depending on the input data of cross-section dimensions and material parameters, the critical bending moment $M_{y,crit}$ is calculated according to EC5 [5]. Hereby, the assumed structural system and the type of loading are considered by the effective length $l_{ef,m}$. In the next step the magnitude of the axial compression load N_x is specified. With the help of the failure criterion (eq. (9)), the maximum bending moment $M_{y,I}$ can be calculated. Therefore, by taking into account the geometric imperfections e_y , e_z and ϑ , the bending moments $M_{y,II}$ and $M_{z,II}$ can be determined iteratively. As a result, there is a M-N combination with a maximum bending moment for a given axial compression load, which takes into account an elasto-plastic material behaviour under compression and satisfies the failure criterion of equation (9).

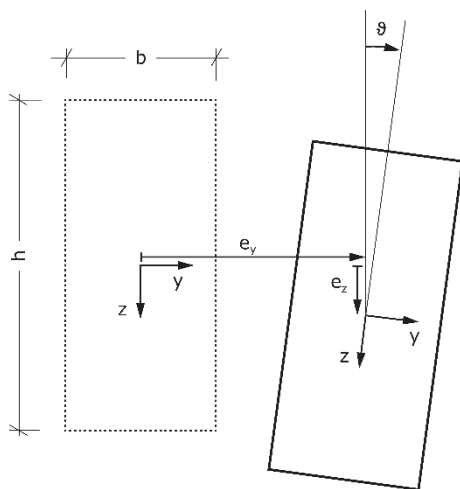


Figure 5: Cross-section of beam shown in Figure 4; imperfections at midspan in form of initial torsion ϑ and initial curvature in y- and z-direction (e_y , e_z)

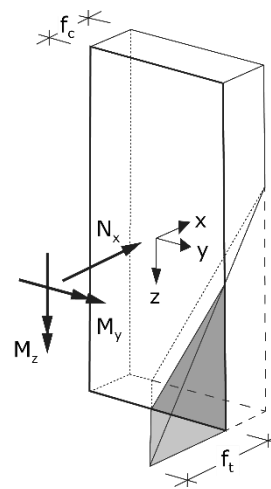


Figure 6: Plot of a random three-dimensional stress distribution due to bending and axial compression

For an additional consideration of the size effect, further steps are necessary. Based on the bending moments $M_{y,II}$ and $M_{z,II}$ the curvatures κ_y and κ_z can be determined. Knowing the curvatures, a modified maximum elastic tensile strain $\varepsilon_{t,mod}$ (eq. (5)) and the modified tensile strength $f_{t,mod}$ (eq. (6)) can be calculated. Now the failure criterion can be reevaluated considering $f_{t,mod}$. The size effect has to be taken into account within an iterative process. The described steps are repeated until an abort criterion is reached and the tensile strength does not increase notably anymore.

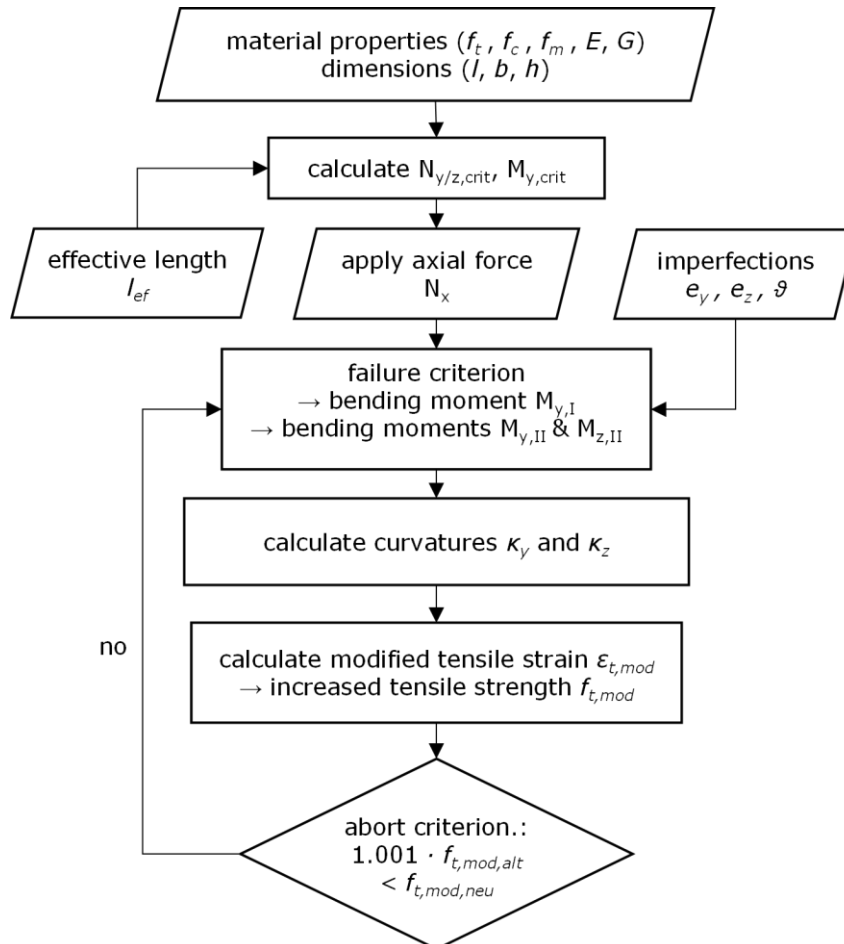


Figure 7: Flowchart for determining the maximum bending moment of a timber beam for a given axial force while considering elasto-plastic behaviour under compression and the size effect

3. Parametric study

3.1. Overview

In general, the parametric study is intended to gain knowledge about the influence of the elasto-plastic material specific behaviour and the size effect on the load-bearing capacity of timber beams at risk of lateral torsional buckling. The following parameters have been investigated:

- Relative slenderness ratio $\lambda_{rel,m}$
- Ratio of axial compression force N_x to bending moment $M_{y,I}$
- Type of timber (glued laminated timber; solid timber)

The cross-sectional dimensions of the investigated timber beams are assumed to be 500 mm x 100 mm ($h \times b$). The slenderness is thus varied via the length of beam. Geometrical imperfections are assumed to be $e_y = l/400$ for initial curvature in direction of the weak axis [5] and $\vartheta_0 = 0.05 \cdot b/h$ for the initial torsion [12]. The structural system and the load application correspond to the system shown in Figure 4, where bending occurs due to a single force applied at midspan. In general, the type of timber is assumed to be glued laminated timber GL 24h according to EN 14080 [13]. Partial factors and modification factors for material parameters are set to 1.0. The assumed material parameters are shown in Table 3.1.

Table 3.1: Assumed material properties for glued laminated timber GL 24h [13] and solid timber C24 [14]

	$E_{0,05}$ [N/mm ²]	$G_{0,05}$ [N/mm ²]	$f_{m,k}$ [N/mm ²]	$f_{t,0,k}$ [N/mm ²]	$f_{c,0,k}$ [N/mm ²]
GL 24h	9600	540	24.0	19.2	24.0
C24	7400	690	24.0	14.5	21.0

3.2. Influence of slenderness

In order to investigate the influence of slenderness on the load-bearing capacity of timber beams at risk of lateral torsional buckling, the interaction between bending moment and axial compression force for glulam GL 24h is investigated. Figure 8 (a) shows the M-N load carrying capacity for a wide range of slenderness. Figure 8 (b), on the other hand, shows especially beams of intermediate length which range from $\lambda_{rel,m} = 0.75$ to $\lambda_{rel,m} = 1.4$. The dashed curve describes the analytical results of the load-bearing capacity with a pure consideration of the elasto-plastic material behaviour, the solid line the load-bearing capacity with an additional implementation of the size effect.

In general, a decrease in load-bearing capacity can be observed with increasing slenderness. For short beams ($\lambda_{rel,m} < 0.75$) a "bump" forms, which partly exceeds the elastic

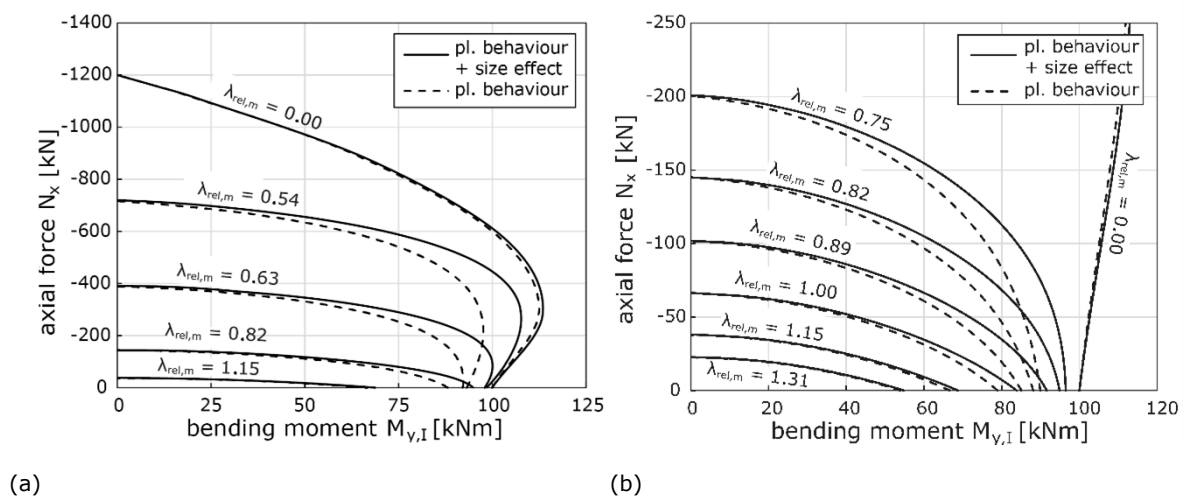


Figure 8: Interaction of bending moment $M_{y,I}$ according to first order theory and axial compression force N_x for timber beams (GL24h) with short (a) and intermediate length (b) depending on the relative slenderness $\lambda_{rel,m}$, based on a verification for stresses of second order theory for lateral torsional buckling

moment carrying capacity of 100 kNm. For beams of intermediate length (Figure 8 (b)), however, the bump flattens out and the impact of plasticizing under compression and the volume effect is decreasing. For $\lambda_{rel,m} = 0.75$, the maximum increase in the bending moment carrying capacity is approximately 8 % due to an additional consideration of the volume effect. With a slenderness ratio of $\lambda_{rel,m} = 1.31$, however, the maximum increase is only about 1 %.

3.3. Influence of axial compression force

Figure 9 shows the load-bearing capacity with regard to the bending moment as a function of the slenderness $\lambda_{rel,m}$. Depending on the ratio of compression force N_x/N_0 , where N_0 represents the maximum elastic load-bearing capacity ($N_0 = f_{c,0,k} \cdot A$). In addition, the maximum elastic bending moment capacity of the given cross-section ($M_{y,0} = f_{m,k} \cdot W_y$) is shown for comparison (dotted line). The dashed curves again describe the analytical results of the load-bearing capacity with a pure consideration of the elasto-plastic material behaviour, the solid lines the load-bearing capacity with an additional implementation of the size effect.

As the compression force increases, the curves generally drop more steeply achieving a specific maximum slenderness for a specific compressive load. For a pure bending ($N_x/N_0 = 0$), the graph is always below the dotted line of the elastic bending moment capacity. If, however, a compression force is applied, a "hump" forms due to the material specific behaviour of plasticizing under pressure and the size effect. Especially in the range of short beams and beams of intermediate length, the possible moment carrying capacity $M_{y,0}$ according to the linear elastic stress criterion is exceeded.

3.4. Influence of solid and glued laminated timber

The load-bearing capacity of glued laminated timber GL 24h according to EN 14080 [13] is compared to solid timber C24 according to EN 388 [14]. Depending on the type of timber, there are differences in

- Stiffness properties (modulus of elasticity E , shear modulus G)
- Strength properties (tensile, compressive strength)
- Ratio of strength to stiffness (f_t / E)
- Ratio of compressive to tensile to bending strength ($f_c / f_t / f_m$)

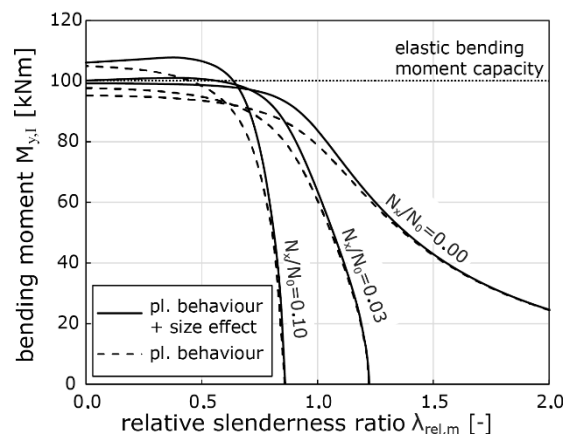


Figure 9: Maximum load bearing capacity with regard to the bending moment capacity as a function of the slenderness depending on different axial compression loadings for glued laminated timber GL 24h with $\lambda_{rel,m}$ relative slenderness of lateral torsional buckling, $M_{y,1}$ maximum bending moment according to first order theory, N_x compression force, $N_0 = f_{c,0,k} \cdot A$ maximum compression force

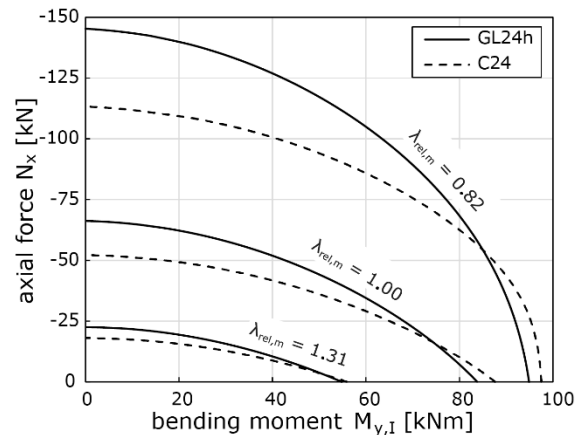


Figure 10: Interaction of bending moment $M_{y,I}$ according to first order theory and axial compression force N_x for glued laminated timber GL 24h in comparison to solid timber C24 depending on the relative slenderness $\lambda_{rel,m}$, based on a verification for stresses of second order theory for lateral torsional buckling

The stiffness properties have a direct effect on the critical bending moment $M_{y,crit}$ and the critical axial force $N_{y/z,crit}$. Therefore, members with low stiffness tend to fail due to excessive deformation and the resulting additional internal forces more easily.

The ratio of tensile strength to bending strength f_t/f_m essentially determines the influence of size effect [15]. For a smaller f_t/f_m ratio, the size effect is therefore bigger. The compressive strength, on the other hand, has an influence on the axial load bearing capacity in compression because a lower compressive strength results in earlier plasticizing of the cross-section.

Figure 10 shows the load bearing capacity of timber beams with an interaction of bending moment and axial compression force of glued laminated timber GL 24h (solid line) compared to solid timber C24 (dotted line). Three different slenderness ratios ($\lambda_{rel,m} = 0.81, 1.00, 1.31$) within the range of intermediate slenderness are considered. With the same bending strength ($f_m = 24 \text{ N/mm}^2$) glulam provides higher stiffness properties and a higher tensile and compressive strength than solid timber.

Across all examined slenderness ratios, gluelam shows a higher axial load bearing capacity compared to solid timber, which results from the higher compressive strength $f_{c,0,k}$. In the case of pure bending, however, solid timber achieves a higher bending moment capacity. Thus, the bending moment capacity of solid timber beams for $\lambda_{rel,m} = 0.81$ is approx. 3 % higher than for the glued laminated timber beams. With higher slenderness the difference is decreasing. For a slenderness ratio of $\lambda_{rel,m} = 1.31$ the difference regarding the bending moment capacity is reduced to approx. 1.5 %. The higher bending moment capacity can be explained by the higher influence of the size effect for solid timber with two axis bending $M_{y,II}$ and $M_{z,II}$, because of the smaller f_t/f_m ratio.

4. Comparison with the literature

Presently there are two common design concepts for timber beams at risk of lateral torsional buckling which are both covered in EC5 [5] - the effective length method and design based on calculations of second order theory (see Figure 11). For the described investigations the interaction formula for the effective length method is taken from DIN 1052:2004 [16] due to shortcomings of the formula in current EC5 [1],[18].

The effective length method for lateral torsional buckling of timber beams subjected to both bending and axial compression represents a combination of the two separate effective length methods for pure axial loading (k_c -method) and for pure bending (k_m -method).

	effective length method	second order theory	
elastic behaviour	$\frac{N_x}{k_{c,y}A f_c} + \frac{M_y}{k_m W_y f_m} \leq 1,0$	$\frac{N_x}{A f_c} + \frac{M_{y,II}}{W_y f_m} + \frac{M_{z,II}}{W_z f_m} \leq 1,0$ (12)	
plastic behaviour	$\frac{N_x}{k_{c,z}A f_c} + \frac{M_y}{k_m W_y f_m} \leq 1,0$ (10)	according to EC5: $\left(\frac{N_x}{A f_c}\right)^2 + \frac{M_{y,II}}{W_y f_m} + \frac{M_{z,II}}{W_z f_m} \leq 1,0$ (13)	according to equation (9): $\frac{-N_x}{A f_m} + \frac{M_{y,II}}{W_y f_m} + \frac{M_{z,II}}{W_z f_m} \leq 1,0$ (15)
plastic behaviour + size effect	$\frac{N_x}{k_{c,y}A f_c} + \frac{M_y}{k_m W_y f_m} \leq 1,0$ $\frac{N_x}{k_{c,z}A f_c} + k_{red} \frac{M_y}{k_m W_y f_m} \leq 1,0$ (11)	$\left(\frac{N_x}{A f_c}\right)^2 + k_{red} \frac{M_{y,II}}{W_y f_m} + \frac{M_{z,II}}{W_z f_m} \leq 1,0$ $\left(\frac{N_x}{A f_c}\right)^2 + \frac{M_{y,II}}{W_y f_m} + k_{red} \frac{M_{z,II}}{W_z f_m} \leq 1,0$ (14)	$\frac{-N_x}{A f_t} + \frac{M_{y,II}}{W_y f_t} + \frac{M_{z,II}}{W_z f_t} \leq 1,0$ $\frac{-N_x}{A f_t} + \frac{M_{y,II}}{W_y f_t} + \frac{M_{z,II}}{W_z f_t} \leq 1,0$ (16)

Figure 11: Overview of the investigated design methods and their consideration of plasticizing under compression and the size effect

Especially in the k_m -method the material specific behaviour is highly simplified. For including the size effect, the coefficient k_{red} is introduced, which increases the bending strength for multiaxial bending. For implementing the elasto-plastic material behaviour under compression in the k_c -method the k_c -factor is adapted accordingly.

For design based on calculations of second order theory the size effect is as well considered with k_{red} . The elasto-plastic material under compression, on the other hand, is taken into account by squaring the compression term.

In order to get an understanding of how the material specific behaviour affects the load-bearing capacity of timber beams at risk of lateral torsional buckling, the analytical results of both effects (eq. (15) and (16) in Figure 11) are compared with the results of purely elastic second order theory calculations (eq. (12) in Figure 11), see diagram in Figure 12. For glued laminated timber (GL 24h), an impact of plastic behaviour under compression can be shown up to a slenderness of $\lambda_{rel,m} = 1.00$. The size effect, on the other hand, has an influence up to a slenderness of $\lambda_{rel,m} = 1.15$. For $\lambda_{rel,m} = 0.75$ there is an increase in the load bearing capacity of about 30 % in comparison to verifications based on purely elastic material behaviour.

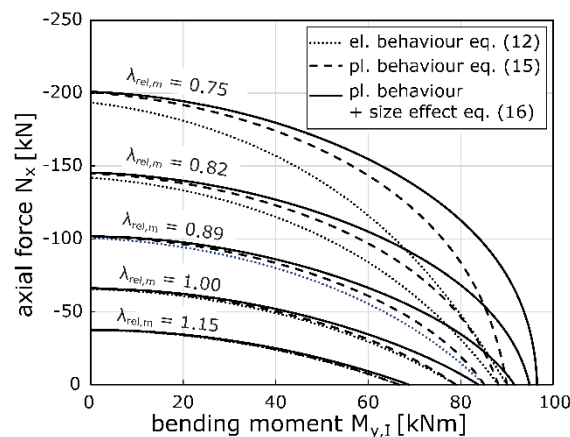


Figure 12: Interaction of bending moment $M_{y,I}$ according to first order theory and axial compression force N_x considering plasticizing (dashed) and additionally the size effect (solid), compared to calculations of linear-elastic second order theory (dotted), depending on the relative slenderness $\lambda_{rel,m}$, based on a verification for stresses of second order theory for lateral torsional buckling

Figure 13 shows the calculation results of the two existing design concepts according to EC5 [5] in comparison to presented verifications based on analytical calculations for three different intermediate slenderness ratios. The curve according to the developed analytical design method shows the highest load-bearing capacity in total. For $\lambda_{rel,m} = 0.75$, verifications based on second order theory according to EC5 result in a similar graph, however, with a slightly lower load-bearing capacity. Verifications based on calculations of second order theory and on analytical calculations due to the developed design concept result in nearly identical outcome for a slenderness of $\lambda_{rel,m} = 1.15$.

For combined bending and axial compression, the effective length method generally provides results with a lower load-bearing capacity. However, for pure bending or pure axial compression the maximum bending moment and axial compression force are higher compared to the other two approaches. Also, the graph resulting from the effective length method shows a characteristic kink, where there is a switch in the decisive design equation. Here, the effective length method comes to a higher load-bearing capacity than the other two verification methods.

The higher load-bearing capacity for pure bending and pure axial compression might be explained by the deviation in the assumption of imperfections [17]. The coefficient k_c , which represents the flexural buckling coefficient of the effective length method, implies more favourable imperfections for glued laminated timber (L/1100) than assumed in the other two calculation methods (L/400). Additionally the effective length method for lateral torsional buckling with the coefficient k_m generally neglects the initial torsion of the cross-section.

The kink in the curve of the results of the effective length method occurs due to a switch of the decisive design formula according to DIN 1052 (see Figure 11 – eq. (11a) to (11b)). The cross-section verification of an imperfection-sensitive member is based on a defined Eigenform with the maximum imperfections e_y , e_z and ϑ . According to EC5 [5] and DIN 1052 [16] influences from imperfections in y- and z-direction do not have to be superimposed. Considering e_z (and ϑ), and hence neglecting e_y , bending will cause lateral torsional buckling and an axial compression force will cause flexural buckling around the weak axis. This interaction is represented by equation (11b). Considering e_y , and hence neglecting e_z (and ϑ), buckling around the strong axis is caused by an axial compression force. Here the second order effects due to a bending moment $M_{y,I}$ and e_y are usually negligibly small. A lateral torsional buckling does not occur in this case, since there are no corresponding imperfections (e_z and ϑ).

Equation (11a) thus does not appear to be mechanically justifiable, since combined imperfections e_y , e_z and ϑ are assumed here, but neglecting the proportion of the flexural buckling around the weak axis [1]. In the current revision of EC5 $k_{c,y}$ is replaced by $k_{c,z}$ in equation (11a) [18]. When doing so the effective length method is clearly on the safe side for combined bending and axial compression force but mechanically correct.

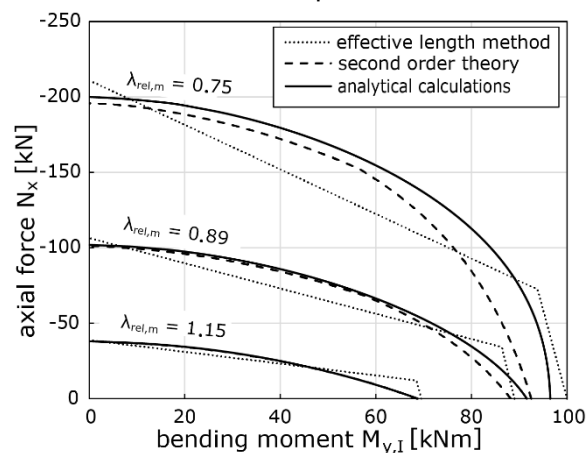


Figure 13: Interaction of bending moment $M_{y,I}$ according to first order theory and axial compression force N_x for verifications based on analytical calculations compared to the effective length method and verifications based on calculations of the second order theory according to EC5 [5], depending on the relative slenderness $\lambda_{rel,m}$

5. Summary

In this paper the results of an investigation of lateral torsional buckling of timber beams subjected to combined bending and axial compression are presented, which was part of a master thesis at the Institute of Structural Design at the University of Stuttgart [4].

For the analytical calculations, approaches for a calculation of internal forces according to second order theory and for an elasto-plastic cross-section failure are combined. Imperfection-sensitive behaviour is described by known solutions of the lateral torsional buckling problem according to second order theory. The cross-sectional failure for combined bending and axial compression is taken into account by a mechanical model developed by *Hörsting* [3], which integrates plasticizing under compression and the size effects on the tensile strength of wood. By combining the two approaches the material specific behaviour of imperfection-sensitive wooden members can be successfully implemented into the analytical calculations.

According to the parametric study, the positive influence of plasticizing under compression and the size effect decreases with increasing slenderness, approaching the ideal-elastic solution according to the calculation of second order theory. For beams of intermediate length, however, there is a notable increase in the load-bearing capacity compared to the design methods of EC5. For $\lambda_{rel,m} = 0.75$ there is an increase in the load bearing capacity of approximately 30 % in comparison to calculations with purely elastic material behaviour. Overall, an impact of the material specific behaviour can be observed up to a slenderness ratio of approximately $\lambda_{rel,m} = 1.00$ to 1.15.

In comparison to the verification based on calculation of second order theory provided by EC5, the own approach based on analytical calculations shows higher load bearing capacities especially for beams of intermediate length. For $\lambda_{rel,m} = 0.75$ there is an increase in the bending moment capacity of approx. 5 %. With increasing slenderness, the interaction curves appear to be nearly identical so that the simplified material behaviour can be seen as a good assumption.

The effective length method generally provides lower load bearing capacities than the results derived by the presented analytical approach, but in some cases the load-bearing capacity of the effective length method is higher. This is due to different assumptions of the equivalent imperfections according to EC5 and shortcomings of the interaction formula [1]. In the 2nd draft of the current revision of the EC5 these deficits are resolved [18]. With these new interaction formulas the results of the equivalent length method for combined bending and compression are far on the safe side compared to verifications based on the presented analytical approach.

When comparing the results for glued laminated timber (GL 24h) to solid timber (C24), higher load bearing capacities could be reached for solid timber, which contradicts practical engineer's understanding. Thus, further investigations are necessary to verify if the implementation of the size effect on the basis of the *Weibull* distribution is satisfying.

Presently there are only very little data regarding experimental tests of imperfection-sensitive timber beams subjected to both bending and axial compression available. For a verification of the analytical model experimental investigations true to scale are necessary. The calculation of internal forces according to second order theory assumes a purely elastic behaviour while the mechanical model according to *Hörsting* [3] describes an elasto-plastic material-behaviour. For coherent results for the verifications based on analytical calculations, the elasto-plastic behaviour should be implemented equally in the second order theory calculations.

Additionally, the assumed failure criterion (eq. 9) only takes into account elastic behaviour on the resisting side as well. Including the elasto-plastic behaviour for calculating plastic moments of resistance ($W_{y,pl}$, $W_{z,pl}$), even bigger load-bearing capacities may be reached.

Regarding the present design methods of EC5, the approach based on the calculation according to second order theory represents a solid simplified method to design slender timber beams subjected to combined bending and axial compression with even a small potential for optimization. For the effective length method further investigations are necessary especially regarding the interaction formula for compression force and bending

moment. According to the current revision of EC5 [18] it is suggested to replace the coefficient $k_{c,y}$ by $k_{c,z}$ in equation (11a), so the results may be conservative but mechanically correct and on the safe side.

6. References

- [1] Brüninghoff, H.: Klapp, H.: *Stabilitätsnachweis im Holzbau – Biegedrillknicken mit Normalkraft*. Bauen mit Holz 107, pp. 27-33, 2005
- [2] Eggen, T. E.: *Buckling and geometrical nonlinear beam-type analyses of timber structures*. University of Science and Technology Trondheim, Dissertation, 2000
- [3] Hörsting, O.-P.: *Zum Tragverhalten druck- und biegebeanspruchter Holzbauteile*. Technical University Braunschweig, Dissertation, 2008
- [4] Köppel, N.: *Untersuchungen zur Momenten-Normalkraft-Interaktion biegedrillknickgefährdeter Holzbauteile*. University of Stuttgart, Institute of Structural Design, No. 2019-32X, Master Thesis, 2019
- [5] EN 1995-1-1: *Eurocode 5: Design of timber structures – Part 1-1: General – Common rules and rules for buildings*. European Committee for Standardization (CEN), Brussels, 2004
- [6] Kuhlmann, U.; Hofmann, R.: *Simplified method to determine the torsional moment due to lateral torsional buckling*. Proceedings of 3rd meeting of International Network on Timber Engineering Research (INTER), Graz, Austria, 2016
- [7] Kuhlmann, U.; Hofmann, R.: *Vereinfachte Bemessung von Brettschichtholzträgern variabler Höhe für das Torsionsmoment aus Kippstabilisierung*. AiF/IGF-Project No. 17398 N; Institute of Structural Design, University of Stuttgart, 2013
- [8] Heimeshoff, B.: *Berechnung und Ausführung von Holzbauwerken*. Ingenieur-Holzbau 86, p. 1-44, 1986
- [9] Roof structure swimming pool
<https://www.lignotrend.de/referenzen/schwimmhalle-in-leipzig/>
Accessed on: 23.11.2018
- [10] Buchanan, A. H.: *Strength model and design methods for bending and axial load interaction in timber members*. University of British Columbia, Dissertation, Vancouver, 1984
- [11] Weibull, W.: *A Statistical theory of the strength of materials*. Generalstabens Lito-grafiska Anstalts Förlag, Stockholm, 1939
- [12] Larsen, H. J.; Theilgaard, E.: *Laterally loaded timber columns*. Journal of the Structural Division ST7 105, pp. 1347-1363, 1979
- [13] EN 14080: *Timber structures – Glued laminated timber and glued solid timber – Requirements*. European Committee for Standardization (CEN), Brussels, 2013
- [14] EN 338: *Structural timber – Strength classes*. European Committee for Standardization (CEN), Brussels, 2016
- [15] Burger, N; Glos, P.: *Verhältnis von Zug- zu Biegefestigkeit bei Vollholz*. Holz als Roh- und Werkstoff 55, pp. 345-350, 1997
- [16] DIN 1052: *Entwurf, Berechnung und Bemessung von Holzbauwerken – Allgemeine Bemessungsregeln und Bemessungsregeln für den Hochbau*. Deutsches Institut für Normung (DIN), Berlin, 2004
- [17] Blaß, H. J.: *Design of timber columns*. International council for building research studies and documentation - working commission W18A -timber structures (CIB-W18A/20-2-2), Dublin, September 1987
- [18] NA 005-04-01-01 AK N 1660: *CEN/TC 250/SC 5 N 1011 PT SC 5 T3 2ND DOC EN 1995-1-1 subtask 3-1 Stability and bracing*. 28.05.2019

Mechanical behaviour of beech glued laminated timber columns subjected to compression loading

Monika Zeilhofer
Technical University Munich, Chair of Wood Science, Professorship of Wood Technology
Munich, Germany



Mechanical behaviour of beech glued laminated timber columns subjected to compression loading

1. Introduction and relevance of the topic

The high compression strength of beech glued laminated timber may allow an efficient application of this hardwood species in building components stressed in compression, like columns or compression members in a truss system. Compression loading causes either stress or stability failure. Exceeding the material strength provokes stress failure while disproportionate horizontal deformations in combination with a high decrease of load carrying capacity lead to stability failure.

The design code DIN EN 1995-1-1:2010 [1] offers two approaches to determine the load carrying capacity of slender timber members under compression loading, namely the equivalent member method and a second order theory analysis. The equivalent member method was derived from a strain-based modelling on spruce glued laminated timber columns and considers stability issues by a reduction of the material strength. An increase of the load due to horizontal deformations of the column is accounted for in the second order theory analysis. Theiler [2] found a good accordance between calculated load carrying capacities by means of the equivalent member method with experimentally tested as well as simulated spruce glued laminated timber columns under compression loading. He suggested improvements in the design of spruce glued laminated timber columns under compression loading with second order theory analysis regarding the stiffness and imperfection parameters [2]. For high quality beech glued laminated timber under compression loading, the DIN EN 1995-1-1:2010 [1] equivalent member method design seems to overestimate the load carrying capacity of simulated and experimentally tested columns according to Ehrhart et al. [3] due to a different strength to stiffness ratio for hardwoods than for softwoods. In the work of Ehrhart et al. [3] big cross sections were tested experimentally, which is not representative for applications in truss systems. This indicates the necessity to examine the DIN EN 1995-1-1:2010 [1] calculation methods for beech glued laminated timber columns employing material from low to high quality with small cross sections.

In this study compression tests on beech glued laminated timber columns of different slenderness ratios with small cross sections were performed. The measured load carrying capacities are compared with calculation approaches given in DIN EN 1995-1-1:2010 [1]. A strain-based modelling is implemented and verified by the testing outcomes. This work summarizes the Master's Thesis 'Mechanical behaviour of beech glued laminated timber columns subjected to compression loading' [4] written at Technical University Munich, Chair of Wood Science, Professorship of Wood Technology under the supervision of Maximilian Westermayr and Jan-Willem van de Kuilen within the frame of the research project "Beech Connect".

2. Materials and methods

2.1. Material

The origin of the raw beech lamellas was Central Germany. Half of the lamellas were provided from the sawmill *Pollmeier* with the trade name *Common Shop*, consisting of timber of the lowest sorting class specifically defined by the producer with visual grading. It contained a high number of growth defects, like knots, fibre deviation, cracks, discolouration and pith. This sorting process did not correspond with the strength grading criteria in DIN

EN 408:2012 [5]. The other half of the boards were available at TU Munich, Chair of Wood Science, including wood with middle or high quality that was free of remarkable fibre deviation and had a low number of wood defects.

The moisture content, the density and the dynamic Modulus of Elasticity (MoE) were measured on the original board length of approximately 3100 mm for all lamellas. The raw lamellas had a mean moisture content of 10 % with a COV of 12 %, a mean density of 720 kg/m³ with a COV of 5 % and a mean dynamic MoE of 13300 N/mm² with a COV of 17 %. The dynamic MoE, with values between 8500 N/mm² and 19000 N/mm², represents a natural spread of properties for beech wood of low to high quality.

No visual grading of the raw lamellas according to DIN EN 408:2012 [5] was performed in order to cover the full range of wood qualities. The lamellas were only sorted by their dynamic MoE to estimate the quality of the material. Similar to the work of Westermayr et al. [6], two glulam specimen setups were generated. In the homogeneous setup, all four lamellas within one specimen had a similar dynamic MoE including low as well as high values (Figure 1). In the combined setup, the dynamic MoE of the two outer lamellas outraged the dynamic MoE of the two inner lamellas with increasing ratios between the dynamic MoE of the outer lamellas and the dynamic MoE of the inner lamellas (Figure 2). With the applied sorting process of the lamellas, the predictability of the load carrying capacities of the specimens by the dynamic MoE should be assessed. The lamellas, sorted by their dynamic MoEs and planed to a thickness of 20 mm, were bonded to one glued laminated timber member with the MUF adhesive system *Kauramin 683+688* from *BASF* by *Schaffitzel Holzindustrie*.

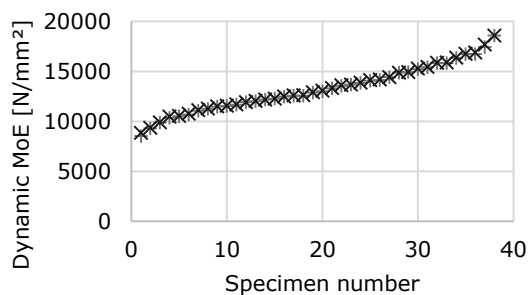


Figure 1: Homogeneous specimens - Dynamic MoEs of the inner and outer lamellas

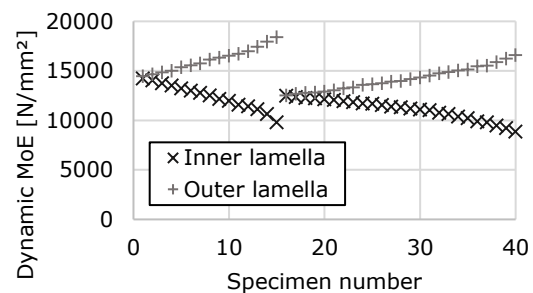


Figure 2: Combined specimens - Dynamic MoEs of the inner and outer lamellas

The dynamic MoE of the entire specimen was determined on the final length of the specimens. The homogeneous setup results in a high scatter of dynamic MoEs of the entire specimens. On the contrary, the dynamic MoEs of the entire combined specimens exhibit a low scatter similar to the findings in Westermayr et al. [6]. For the homogeneous specimens, the mean dynamic MoEs of the raw lamellas within one specimen achieve a correlation $R^2 = 0.96$ with the dynamic MoEs of the entire specimen as already illustrated in Westermayr et al. [6].

In total, 57 specimens were available for testing with two different slenderness ratios. The specimens had a length of 1040 mm ($\lambda = 45$) as well as 1850 mm ($\lambda = 80$) and a cross section of 80 x 80 mm². 19 specimens of slenderness ratio $\lambda = 45$ were tested for buckling around the y-axis, which defines a horizontal movement of the specimen perpendicular to the adhesive layer. 18 specimens with $\lambda = 45$ were subjected to buckling around the z-axis, which corresponds with a horizontal movement of the specimen parallel to the adhesive layer. Both directions were assessed to investigate an influence of the orientation of the adhesive layer to the buckling direction on the load carrying capacity of the specimens. The specimens with slenderness ratio $\lambda = 80$ were all assessed for buckling around the y-axis. In every slenderness ratio/buckling direction subset, the amounts of homogeneous and combined specimens were approximately equal (Table 1).

Table 1: Number (n) of specimens for the different slenderness ratios and buckling directions as well as distinction into homogeneous and combined specimens.

Slenderness	Length [mm]	Buckling direction	n _{total}	n _{homogeneous}	n _{combined}
45	1040	y	19	10	9
45	1040	z	18	8	10
80	1850	y	20	10	10
<i>TOTAL</i>			57	28	29

2.2. Methods

Destructive and non-destructive measurements

Before performing the destructive compression tests, the dynamic MoE, the density and the moisture content of the raw lamellas as well as of the entire specimens were determined. The dynamic MoE was calculated by means of Eigenfrequency and adjusted to 12 % moisture content according to Unterwieser & Schickhofer [7]. The initial deformation was measured as the deviation of the beech glued laminated timber column from an ideal straight line.

During the experimental testing, the beech glued laminated timber columns were mounted on bearings flexible in solely one direction. The load was applied with a hydraulic testing machine depicted in Figure 3.

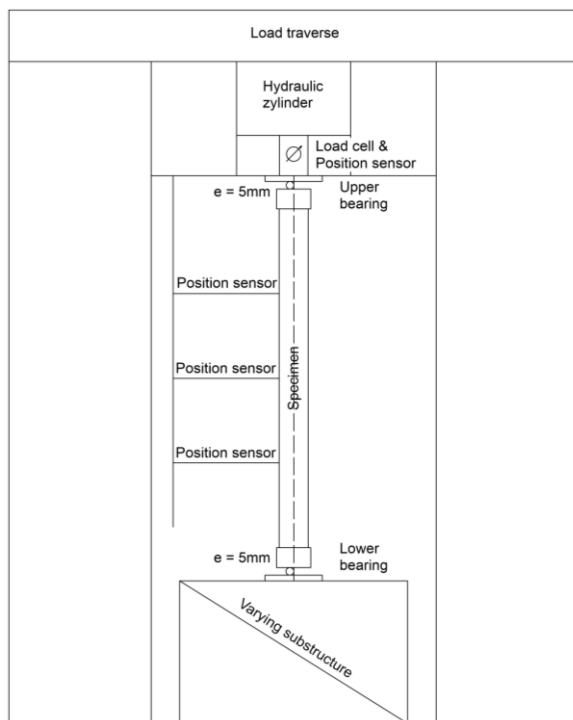


Figure 3: Sketch of the testing machine.

The experiments were performed path-controlled until a decrease in the load was visible. One experiment took between five and fifteen minutes. An eccentricity $e = 5\text{ mm}$ was applied to control the buckling direction of the specimens and prohibit damage to the measurement equipment. The horizontal displacements in buckling direction were assessed in the middle and both quarter points of the specimens.

Strain-based modelling

The equivalent member method in DIN EN 1995-1-1:2010 [1] was derived from a strain-based modelling on spruce glued laminated timber columns with stochastically simulated material properties [8]. A material model was used, which was specifically developed for spruce glued laminated timber [9]. It considers linear elastic material behaviour under tensile loading and a non-linear plastic material behaviour under compression loading. The load carrying capacity was investigated for different slenderness ratios and the factor k_c was defined (Equation 10). In contrast to spruce wood, beech glued laminated timber from similar cross section, origin and setup, regarding the dynamic MoE like the tested material in this work, gains a higher strength to stiffness ratio [6]. A strain-based modelling with a material model for beech glued laminated timber is introduced to review the DIN EN 1995-1-1:2010 [1] buckling curve.

Glos et al. [10] developed a material model for high-strength beech glued laminated timber from the material model for spruce glued laminated timber [9]. Equation 1 [10] describes the material behaviour under compression loading.

$$\sigma_c = \frac{\epsilon + k_1 * \epsilon^4}{k_2 + k_3 * \epsilon + k_4 * \epsilon^4} \quad 1$$

The stress σ_c results from the strain ϵ across the cross section and the parameters k_i (equations 2 - 5), which depend on the MoE for compression $E_{c,0}$, the compression strength $f_{c,0}$, the remaining compression strength after reaching maximum compression strength $f_{c,u,0}$ and the strain at maximum compression strength $\epsilon_{c,0}$.

$$k_1 = \frac{f_{c,u,0}}{3 * E_{c,0} * \epsilon_c^4 * (1 - \frac{f_{c,u,0}}{f_{c,0}})} \quad 2 \quad k_3 = \frac{1}{f_{c,0}} - \frac{4}{3} * \frac{1}{E_{c,0} * \epsilon_{c,0}} \quad 3$$

$$k_2 = \frac{1}{E_{c,0}} \quad 4 \quad k_4 = \frac{1}{3 * E_{c,0} * \epsilon_c^4 * (1 - \frac{f_{c,u,0}}{f_{c,0}})} \quad 5$$

Ehrhart et al. [3] and Theiler [2] employed equation 6 to calculate the remaining compression strength $f_{c,u,0}$, which was determined for spruce glued laminated timber [11].

$$f_{c,u,0} = 0.85 * f_{c,0} \quad 6$$

Equation 6 is also applied in this work for beech glued laminated timber as no own experimental data was available to determine the remaining compression strength $f_{c,u,0}$. The limit for the strain at maximum compression strength $\epsilon_{c,0}$ is given by equation 7 [10].

$$\epsilon_{c,0} \geq \frac{4}{3} * \frac{f_{c,0}}{E_{c,0}} \quad 7$$

O'Halloran [12] found, by means of experimental investigations, equation 8 for the strain at maximum compression strength $\epsilon_{c,0}$. Equation 8 was approved by Glos [11] and Frese et al. [13] for spruce glued laminated timber.

$$\epsilon_{c,0} = 1.25 * \frac{f_{c,0}}{E_{c,0}} \quad 8$$

Equation 8 does not fulfil the criterion 7 [10]. Ehrhart et al. [3], however, used equation 8. In this work, equation 9 was developed representing the closest solution to both the criterion 7 and equation 8.

$$\epsilon_{c,0} = 1.34 * \frac{f_{c,0}}{E_{c,0}} \quad 9$$

The strain-based modelling is performed according to Glos [9] with a fixed assumed shape of the buckling curve. A Visual Basic Script Application with Microsoft Excel 2016 is implemented to execute the strain-based modelling.

3. Results and Discussion

3.1. Experimental investigation

Influence of specimen setup on the load carrying capacity

The buckling strength $f_{crit,0}$ is defined as the load carrying capacity of the specimen divided by the specimen cross section. The buckling strength $f_{crit,0}$ decreases with increasing specimen length while the COV increases as visible in Table 2. The growth in scatter may arise from a wider range of properties with higher specimen length.

The mean buckling strengths $f_{crit,0}$ for homogeneous (H) and combined (C) specimens do not differ significantly. The minimum and maximum buckling strength $f_{crit,0}$ of the homogeneous specimens are lower and higher respectively than the minimum and maximum buckling strength $f_{crit,0}$ of the combined specimens. This indicates that a combination of lamellas with low and high dynamic MoEs offers the possibility to reduce the spread in buckling strengths $f_{crit,0}$ in comparison to a homogeneous specimen setup. A quantification of the effect of different ratios of dynamic MoEs between outer and inner lamellas on the buckling strength $f_{crit,0}$ was not possible.

Table 2: Mean buckling strength $f_{crit,0}$ of the specimens for different slenderness ratios, specimen setups and buckling directions.

Slenderness	Setup	n	Mean $f_{crit,0}$ [N/mm ²]	Min $f_{crit,0}$ [N/mm ²]	Max $f_{crit,0}$ [N/mm ²]	COV F
45y	H	10	46	31	53	0.14
	C	9	41	36	48	0.11
45z	H	8	38	27	48	0.16
	C	10	41	37	48	0.08
80y	H	10	28	17	43	0.26
	C	10	30	23	38	0.16

Taking particularly the homogeneous specimens into account, a correlation between the mean dynamic MoE of the lamellas within one specimen and the buckling strength $f_{crit,0}$ of $R^2 = 0.51$ and a $R^2 = 0.74$ can be found for specimens of slenderness ratio $\lambda = 45$ and $\lambda = 80$, respectively. Similar correlations can be achieved between the dynamic MoE of the entire specimens and the buckling strengths $f_{crit,0}$. The correlation between dynamic MoE and buckling strength $f_{crit,0}$ may be traced back to the correlation between dynamic and static MoE for beech glued laminated timber [6]. The improvement of the correlation between dynamic MoE and buckling strength $f_{crit,0}$ with increasing specimen length may be explained with the measurement of the dynamic MoE on the original board length of 3100 mm. The properties of a specimen with 1850 mm may be represented more appropriately by the dynamic MoE measured on the original board length than of the shorter specimens with a length of 1050 mm. The increasing correlation between the dynamic MoE and the buckling strength $f_{crit,0}$ with increasing slenderness ratio may also result from the increasing effect of the stiffness on the buckling behaviour for higher slenderness ratios.

The buckling strengths $f_{crit,0}$ of specimens buckling around the y- and the z-axis are not significantly different as visible in Table 2. The specimens buckling around the z-axis exhibit a slightly lower scatter in their buckling strengths $f_{crit,0}$ than the specimens buckling around the y-axis probably deriving from a lower scatter in dynamic MoE.

Test results in comparison to DIN EN 1995-1-1:2010 [1] design methods

DIN EN 1995-1-1:2010 [1] describes the relationship between slenderness and load carrying capacity in the buckling curve. The equivalent member method and the second order theory analysis require strength and stiffness values to calculate the load carrying capacity. Table 3 provides an overview of the applied strength and stiffness features from

Westermayr et al. [6], investigated for beech glued laminated timber of the same cross section, origin and similar specimen setup regarding the dynamic MoE, like the specimens in this work.

Table 3: Applied strength and stiffness properties [6].

Characteristic compression strength $f_{c,0,k}$ [N/mm ²]	53
Characteristic bending strength $f_{m,k}$ [N/mm ²]	53
Characteristic tensile strength $f_{t,0,k}$ [N/mm ²]	39
Characteristic compression stiffness $E_{c,0,05}$ [N/mm ²]	11000
Mean compression stiffness $E_{c,mean}$ [N/mm ²]	13670
Characteristic tensile stiffness $E_{t,0,k}$ [N/mm ²]	10870

To estimate the buckling strength $f_{crit,0}$, intended and unintended eccentricities of the applied load must be assessed besides the strength and stiffness properties. The intended eccentricity of load application during the experiments was $e = 5$ mm. The unintended eccentricities consist solely of an initial deformation of the specimens, as geometrical imperfections, such as a tilting of the specimen or an unintended eccentricity of loading, can be excluded due to the testing setup. Structural imperfections, resulting from an asymmetrical distribution of strength and stiffness properties across the cross section, can be neglected due to the symmetrical specimen setup. Section 10 of DIN EN 1995-1-1:2010 [1] limits the eccentricity considered in the design of slender compression members to $l/500$, which seems to apply to the equivalent member method calculation. In the second order theory analysis, structural and geometrical imperfections are accounted for with $w_0 = l/400$. Considering additional bending stresses caused by the eccentricity $e = 5$ mm, the calculated buckling strengths $f_{crit,0}$ by DIN EN 1995-1-1:2010 [1] methods employing strength and stiffness properties from Westermayr et al. [6] (Table 3) are discussed with the measured buckling strengths $f_{crit,0}$ in Figure 4.

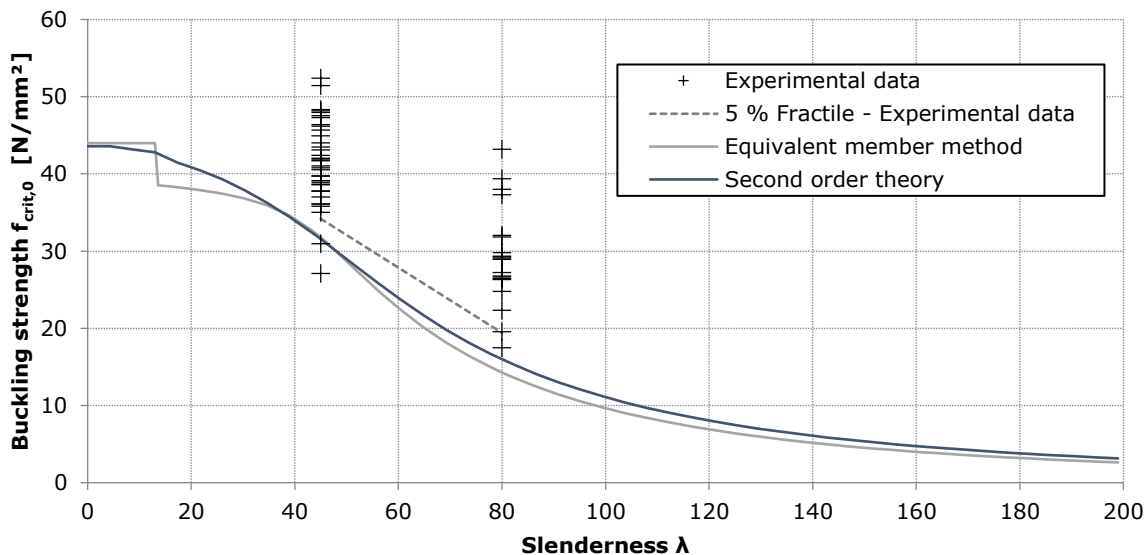


Figure 4: Measured buckling strengths $f_{crit,0}$ (crosses) and 5% fractiles (dotted line) in comparison to calculated buckling strengths $f_{crit,0}$ by DIN EN 1995-1-1:2010 [1] (solid lines) with strength and stiffness properties from Westermayr et al. [6] (Table 3) and eccentricity $e = 5$ mm.

The buckling curves according to DIN EN 1995-1-1:2010 [1] equivalent member method and second order theory analysis exhibit only small differences. The unsteadiness in the equivalent member method curve at a slenderness ratio λ of approximately 13 derives from a change of quadratic to a linear relationship between compression loading and compression strength.

The measured buckling strengths $f_{crit,0}$ are underestimated with DIN EN 1995-1-1:2010 [1] calculation methods. The underestimation of the measured buckling strengths $f_{crit,0}$ by DIN EN 1995-1-1:2010 [1] is more pronounced for slenderness ratio $\lambda = 80$ than $\lambda = 45$. For slenderness ratio $\lambda = 45$, equivalent member method and second order theory analysis yield similar results, while for slenderness ratio $\lambda = 80$, the second order theory analysis determines buckling strengths $f_{crit,0}$ closer to the experimental data.

A reason for the underestimation of the measured buckling strengths $f_{crit,0}$ by DIN EN 1995-1-1:2010 [1] design can be found in the consideration of the applied eccentricity $e = 5$ mm and the initial deformation of the specimens. The initial deformation of the specimens - $w_{0,measured,mean} = l/2500$, $w_{0,measured,0.95} = l/770$, $w_{0,measured,max} = l/625$ - are smaller than the imperfections suggested by DIN EN 1995-1-1:2010 [1], probably due to the storage in normal climate after planing. In a realistic situation, the initial deformations may reach higher values due to the influence of moisture changes during transportation and storage at a construction site, as well as a tilted installation. In similar experiments, Ehrhart et al. (2019) who applies eccentricities of $l/380$ and $l/570$ neglects the eccentricity in the calculation. The eccentricity of $e = 5$ mm in this work equals values of $l/208$ and $l/360$. A comparison of the calculated buckling strengths $f_{crit,0}$ with eccentricities of $e = 5$ mm and $e = 0$ mm with the measured buckling strengths $f_{crit,0}$ is shown in Figure 5.

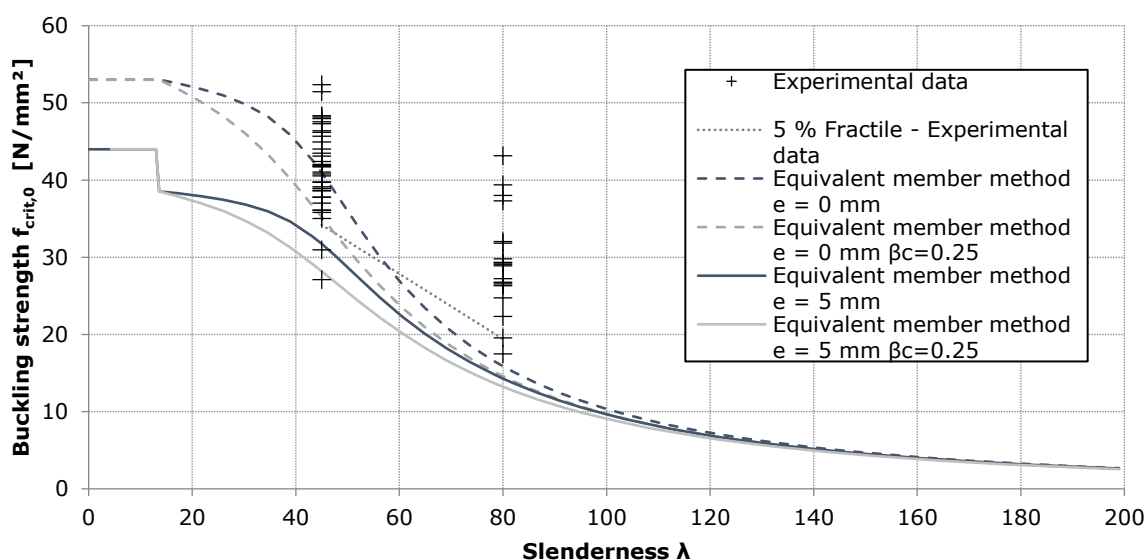


Figure 5: Measured buckling strengths in comparison to calculated buckling strengths $f_{crit,0}$ with equivalent member method according to DIN EN 1995-1-1:2010 [1]. Eccentricities of $e = 5$ mm (solid lines) and $e = 0$ mm (dashed lines), imperfection parameter $\beta_c = 0.1$ and $\beta_c = 0.25$.

Calculating the buckling strengths $f_{crit,0}$ by neglecting the eccentricity leads to an overestimation of the measured buckling strengths $f_{crit,0}$ for slenderness ratio $\lambda = 45$. On the contrary, hardly any change in the calculated buckling strengths $f_{crit,0}$ by neglecting the eccentricity is visible for slenderness ratio $\lambda = 80$. A reasonable compromise between an eccentricity of $e = 5$ mm and $e = 0$ mm may be found by considering an eccentricity of $e = 5$ mm - $(l/500 - l/770)$ in the calculation. This equals the eccentricity $e = 5$ mm minus the difference between the initial deformation considered in the equivalent member method calculation reduced by the 95 % fractile of the measured initial deformations. The 5 % fractiles of the measured buckling strengths $f_{crit,0}$ show a high accordance with these calculated buckling strengths $f_{crit,0}$ with the reduced eccentricity of $e = 5$ mm - $(l/500 - l/770)$ for slenderness ratio $\lambda = 45$.

The small initial deformations of the columns may also be a reason for the underestimation of the measured buckling strengths $f_{crit,0}$ by the second order theory analysis. The modification of the initial deformation in the design code from $w_0 = l/400$ to the measured 95 % fractile of the initial deformation of the specimens of $w_0 = l/770$ contributes to a better accordance between the measured and calculated buckling strengths $f_{crit,0}$ for specimens of slenderness ratio $\lambda = 45$. A slight overestimation of the measured buckling strengths

$f_{crit,0}$ occurs using the mean initial deformation for slenderness ratio $\lambda = 45$. For slenderness ratio $\lambda = 80$, the calculated buckling strength $f_{crit,0}$ is hardly changed by employing different initial deformations.

The DIN EN 1995-1-1:2010 [1] buckling curves have a higher gradient than the slope of the 5 % fractiles of the measured buckling strengths $f_{crit,0}$. The equivalent member method was derived from a strain-based modelling on spruce glued laminated timber [8]. Spruce glued laminated timber shows a strength to stiffness ratio of 1/420 to 1/370 while beech glued laminated timber in this project [6], exhibits a strength to stiffness ratio of 1/208. Ehrhart et al. [14] found a strength to stiffness ratio of approximately 1/250 for high-quality beech glued laminated timber. An increase of the strength to stiffness ratio results in a decrease of the slope of the buckling curve [15]. The factor k_c (Equation 10) defines the shape of the buckling curve and depends on strength and stiffness properties, as well as geometry features of the specimens, but also on the critical relative slenderness $\lambda_{rel,0}$ and the imperfection parameter β_c .

$$k_c = \frac{1}{k + \sqrt{k^2 - \lambda_{rel}^2}} \quad 10$$

$$\lambda_{rel} = \frac{\lambda}{\pi} \sqrt{\frac{f_{c,0,k}}{E_{0,05}}} \quad 11$$

$$k = 0,5 * [1 + \beta_c * (\lambda_{rel} - \lambda_{rel,0}) + \lambda_{rel}^2] \quad 12$$

A decrease of the slope of the buckling curve can be realised in the equivalent member method by an enlargement of the imperfection parameter β_c . Applying the imperfection parameter $\beta_c = 0.25$ leads to a good accordance between the slope of the calculated and measured 5 % fractile buckling strengths $f_{crit,0}$ as visible in Figure 5. The change of β_c affects the buckling strength $f_{crit,0}$ of specimens with slenderness ratio $\lambda = 45$ much more than the buckling strengths $f_{crit,0}$ of specimens with slenderness ratio $\lambda = 80$.

3.2. Comparison of the modelling results with experimental data and DIN EN 1995-1-1:2010 [1]

Blaß [16] and Theiler [2] proved that strain-based modelling can reproduce buckling experiments on spruce glued laminated timber appropriately. Ehrhart et al. [3] confirmed those findings for beech glued laminated timber columns.

In Figure 6, the buckling strengths $f_{crit,0}$ for different slenderness ratios, obtained from strain-based modelling are compared with the experimental data as well as the calculated buckling strengths $f_{crit,0}$ according to DIN EN 1995-1-1:2010 [1] equivalent member method with $\beta_c = 0.1$ and $\beta_c = 0.25$. An eccentricity of $e = 5$ mm is considered in the calculated buckling strengths $f_{crit,0}$. Strength and stiffness values from Table 2 [6] are employed.

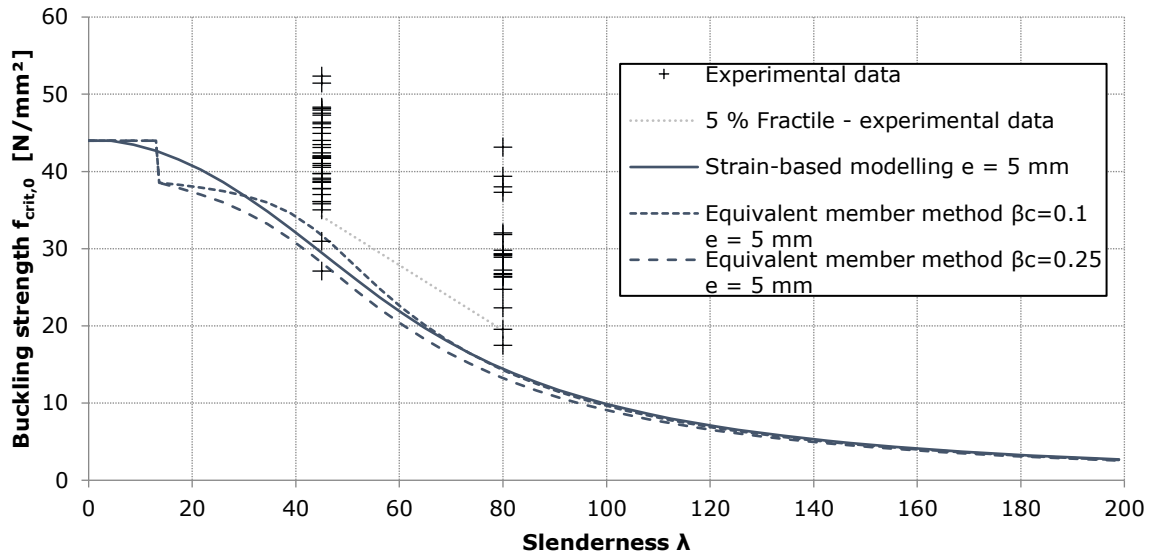


Figure 6: Comparison of the measured and calculated buckling strengths $f_{crit,0}$ by DIN EN 1995-1-1:2010 [1] equivalent member method with $\beta_c = 0.1$ (small dashed lines) and $\beta_c = 0.25$ (big dashed lines) as well as strain-based modelling (solid lines) with an eccentricity of $e = 5$ mm.

The strain-based modelling underestimates the buckling strengths $f_{crit,0}$ of the specimens. The strain-based modelling buckling curve matches more appropriate with the equivalent member method curve with $\beta_c = 0.25$ than with $\beta_c = 0.1$ for an eccentricity $e = 5$ mm. All calculated buckling curves yield higher slopes than the 5 % fractiles of the measured buckling strengths $f_{crit,0}$ where the DIN EN 1995-1-1:2010 [1] equivalent member method with $\beta_c = 0.25$ shows the closest gradient followed by the strain-based modelling.

4. Summary and conclusions

The load carrying capacities measured on beech glued laminated timber lay on the safe side of the calculated load carrying capacities by means of DIN EN 1995-1-1:2010 [1]. Due to the different strength to stiffness ratio of beech wood compared to spruce wood, an adjustment of the imperfection parameter β_c in DIN EN 1995-1-1:2010 [1] equivalent member may lead to a better accordance between calculated and measured buckling curve. The suggested revisions in the equivalent member method can be verified by a strain-based modelling applying a material model for beech glued laminated timber [10]. The tested material shows small geometrical imperfections. In practical cases, larger eccentricities or imperfections can affect the load carrying capacity.

The dynamic MoEs of glued laminated timber members with similar dynamic MoEs of the lamellas exhibit a good correlation with their measured load carrying capacity. A combination of outer lamellas with higher dynamic MoEs than the inner lamellas leads to a reduction in the scatter of load carrying capacities of the specimens.

5. Outlook

More tests on columns with different slenderness ratios should be performed to encourage the suggested adjustment of the imperfection parameter β_c in DIN EN 1995-1-1:2010 [1] equivalent member method. The scientific lamella arrangement within the glued laminated timber members by means of the dynamic MoE in this study should be complemented with an industrial lamella arrangement where the single lamellas are chosen from strength classes with scattering dynamic MoE. Additional buckling tests could be performed where the raw lamellas are graded and sorted into strength classes in order to achieve a testing setup representative for practical cases.

In practical cases, members of a truss system and columns are subjected to long term loading, creep and moisture changes. An increase of the moisture content of beech glued laminated timber columns yields a significant decrease in strength and stiffness properties

([17] and [16]). Thus, the effects of moisture changes, creep behaviour and long-term loading on the load carrying capacity of beech glued laminated timber columns need to be examined by further research.

6. References

- [1] DIN EN 1995-1-1, Design of timber structures – Part 1-1: General – Common Rules, 2010.
- [2] M. Theiler, "Stabilität von axial auf Druck beanspruchten Bauteilen aus Vollholz und Brettschichtholz. In German. Dissertation. ETH Zürich," 2014.
- [3] T. Ehrhart, R. Steiger, P. Palma, E. Gehri and A. Frangi, "Compressive strength and buckling resistance of GLT columns made of European beech (*Fagus sylvatica*)," *INTER Conference 52, Tacoma, USA, Paper 52-12-1*, 2019.
- [4] M. Zeilhofer, Mechanical behaviour of beech glued laminated timber columns subjected to compression loading. Master's Thesis. Technical University Munich, München, 2019.
- [5] DIN EN 408:2012, Strength grading of wood - Part 5: Sawn hard wood, 2012.
- [6] M. Westermayr, P. Stapel and J.-W. van de Kuilen, "Tensile and Compression Strength of Small Cross Section Beech Glulam Members," *INTER Conference 51, Tallinn, Estonia, Paper No. 51-12-2*, 2018.
- [7] H. Unterwieser and G. Schickenhofer, "Influence of moisture content of wood on sound velocity and dynamic MoE of natural frequency- and ultrasonic runtime measurement," *European Journal of Wood and Wood Products*. (69), pp. 171-181, 2011.
- [8] H. Blaß, "Design of columns," *Proceeding of the 1991 International Timber Engineering Conference, London, United Kingdom*, 1991.
- [9] P. Glos, "Zur Bestimmung des Festigkeitsverhalten von Brettschichtholz bei Druckbeanspruchung aus Werkstoff- und Einwirkungskenngrößen. In German. Dissertation," *Laboratorium für den konstruktiven Ingenieurbau (LKI) Technische Universität München*, 1978.
- [10] P. Glos, J. Denzler and P. Linsemann, "Strength and stiffness behaviour of beech laminations for high strength glulam," *CIB-W18 Proceedings 37, Paper No. 37-6-3, Edingburgh, Ireland*, 2004.
- [11] P. Glos, "Zur Modellierung des Festigkeitsverhaltens von Bauholz bei Druck-, Zug- und Biegebeanspruchung. In German," *Laboratorium für den konstruktiven Ingenieurbau (LKI) Technische Universität München*, 1981.
- [12] M. O'Halloran, Curvilinear stress-strain relationship for wood in compression. Dissertation. Colorado State University., Fort Collins, 1973.
- [13] M. Frese, M. Enders-Comberg, H. Blaß and P. Glos, "Compressive strength of spruce glulam," *European Journal of Wood Products*. 70., pp. 801-809, 2012.
- [14] T. Ehrhart, R. Steiger, P. Palma and A. Frangi, "Mechanical properties of European beech glued laminated timber," *INTER Conference 51, Tallinn, Estonia, Paper 51-12-4*, 2018.
- [15] H. Blaß, "Design of timber columns," *CIB-W18 Meeting 20, Paper No. 20-2-2, Dublin, Ireland*, 1987a.
- [16] H. Blaß, "Tragfähigkeit von Druckstäben aus Brettschichtholz unter Berücksichtigung streuender Einflussgrößen. In German. Dissertation. Karlsruher Institut für Technologie," 1987b.
- [17] A. Ehret, "Mechanisches Verhalten von Buchen Brettschichtholz unter Zug- und Druckbelastung. In German. Master's Thesis. Technical University Munich," 2018.
- [18] Z-9.1-679, BS-Holz aus Buche und BS-Holz Buche-Hybridträger – Allgemeine bauaufsichtliche Zulassung, 2014.